ACOUSTIC EMISSION MAPPING OF DISCHARGES IN SPARK EROSION MACHINING

ACOUSTIC EMISSION MAPPING OF DISCHARGES IN SPARK EROSION MACHINING

By

CRAIG R. SMITH, B.ENG.

A Thesis

Submitted to the School of Graduate Studies

In Partial Fulfillment of the Requirements

For the Degree

Master of Applied Science

McMaster University

MASTER OF APPLIED SCIENCE (2012)	McMaster University
(Department of Mechanical Engineering)	Hamilton, Ontario

TITLE:	Acoustic Emission Mapping of Discharges in Spark Erosion Machining
AUTHOR:	Craig R. Smith, B.Eng. (McMaster University)
SUPERVISOR:	Dr. Philip Koshy
NUMBER OF PAGES:	xi, 122

Abstract

Electrical discharge machining (EDM) is a non-conventional machining process utilizing a series of electrical discharges to melt and vaporize workpiece material. In a wire EDM configuration wire breakage is a limiting factor in the machining productivity during the machining of workpieces with varying heights. Present methods of estimating workpiece height on-line in an effort to optimize machining parameters monitor the electrical signals for changes which may not be completely indicative of a change in workpiece height. This thesis intends to utilize acoustic emission (AE) sensors as a method for mapping the discharge location in order to estimate the workpiece height. This represents a novel approach as acoustic emission testing, while prevalent in the process monitoring of numerous conventional machining processes has yet to be significantly studied in combination with EDM.

Another useful application of AE sensors with the EDM process under consideration is during the fast hole EDM process, where excessive wear is seen in the electrode causing true electrode length to remain uncertain. By using acoustic emission sensors to determine the true length of the electrode it could be possible to aid in the breakout detection of the electrode.

Acknowledgements

Firstly, I would like to thank my supervisor Dr. Philip Koshy. With his support I was given free reign of this research project and that has made it a truly fulfilling experience. These past two years have been filled with many ups and downs, and Dr. Koshy was always there to provide guidance and a new perspective when a roadblock had been hit. Through my many years working with Dr. Koshy (dating back to undergraduate summer research assistantships!) I have had the fortunate opportunity to see the best side of academia, as his research groups have always put a premium on fostering creative thought. I couldn’t have asked for more.

Thank you to Mark MacKenzie and Ron Lodewyks for helping to purchase the materials needed to complete this research.

I would also like to thank my family and friends who have been supportive of me throughout this whole process. Even though we didn’t win much, the Deep Homers always provided a fun evening out.

If I failed to mention you, yet you are still taking the time to read the acknowledgements page of my thesis then I would like to thank you as well.

Table of Contents

List of Figures

List of Tables

Chapter 1

Introduction

Process monitoring plays a crucial role in present machining practices as a means for ensuring productive machining and maintaining surface quality of the machined part. In conventional machining (broaching, milling, turning etc.) a variety of monitoring techniques have been extensively researched and developed. However in the non-conventional electrical discharge machining (EDM) process, monitoring techniques are limited, with the most prevalent method being the examination of electrical signals (current, voltage) obtained during machining. The electrical signals can be used to determine the quality of discharges to monitor process stability, however they do not provide enough information to determine the spatial location of each discharge, which is beneficial for further improvement of the process.

This thesis explores the use of acoustic emission (AE) sensors as a means to map the location of individual discharges in EDM. By mapping the discharge locations it is possible to monitor for unwanted localization of discharges, or to optimize machining parameters with respect to instantaneous machining area. In order to develop a method for discharge mapping using AE signals, a variety of data processing techniques are also explored. Necessary background information on electrical discharge machining and acoustic emission sensing is presented in this chapter in order to provide a better understanding as to the scope of this thesis.

1.1 Electrical Discharge Machining (EDM)

Electrical discharge machining (EDM) is a non-conventional machining process which does not utilize a traditional cutting edge to remove material. Instead the cutting tool or “electrode” can be made from any electrically conductive material, with copper and graphite being popular choices due to their ability to withstand wear during the process. Machining occurs fully submerged in a tank of dielectric fluid which acts as an insulator surrounding the oppositely charged workpiece and electrode as shown in Figure 1.1a. As the distance between the electrode and workpiece decreases the electric field between the two intensifies. When the gap width is on the order of 10-100 μm [1], the dielectric fluid begins to break down (Figure 1.1b). This breakdown creates a favourable pathway or “plasma channel” for the current to flow between electrode and workpiece to complete the electrical circuit. The heat generated from this electrical discharge melts both the workpiece and electrode (Figure 1.1c). The plasma channel diameter increases with time, until a set time has elapsed ending the current flow. An implosion of the plasma channel follows and the solidification of the molten metal debris occurs which can now be flushed away (Figure 1.1d).

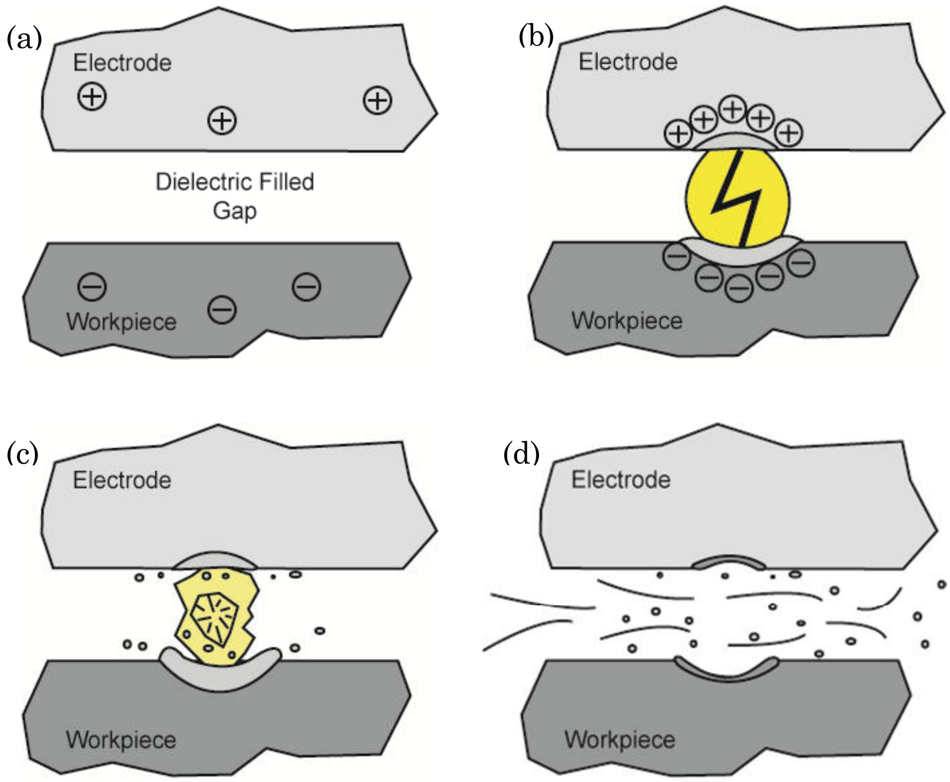

Figure 1.1: Material removal mechanism of EDM process.
a) Schematic b) Dielectric Breakdown, c) Plasma growth d) Flushing.

The electrode material and EDM parameters are selected such that the wear on the electrode is minimized while maximizing the amount of material removed from the workpiece. Each discharge removes 1 – 1000 μm^3 of workpiece material depending on the machining configuration [2], while less than 5% of this volume is removed from the electrode [3]. Performing this process at frequencies as high as 10^5 Hz can generate material removal rates on the order of 100 mm^3/min [4]. While this is a slow process compared to other conventional machining techniques, EDM has the advantage of being able to machine otherwise hard to machine materials as long as they are electrically conductive. As such EDM is often used in the aerospace industry and in mold manufacturing where high tolerances of hard to machine metals are required.

There are multiple configurations of EDM that are commonly used, and while the fundamental process is as described above, each are suited for different machining operations. One configuration is the sink or ram type EDM. In this configuration the electrode is driven into the workpiece to leave a negative impression of the electrode. This is beneficial in the construction of complex concave geometries such as molds and dies. The electrode can also travel along a path to create an EDM milling process. This research project focuses on two other EDM configurations; the wire EDM and fast hole EDM processes which will be now be discussed.

1.1.1 Wire EDM

Wire EDM utilizes a thin 0.02-0.33 mm [1] wire as the electrode. The wires are often plain brass or brass with a zinc/steel coating to allow for faster machining speeds [5]. The wire EDM configuration can be seen in Figure 1.2, where the wire is used be used to cut out complex shapes. The wire is held in tension to reduce deflection and vibrations which can affect accuracy and surface finish. The wire is continuously fed between two wire guides to provide a constantly renewed section of wire to machine with. This helps ensure surface finish to be consistent and prevents wire breakage. Wire breakage is a major concern in wire EDM, as these machines are often left unattended and used on parts that have already had significant investment made to their manufacture. Wire breakage reduces the productivity of the operation, costing money in scrapped parts and lost machining time.

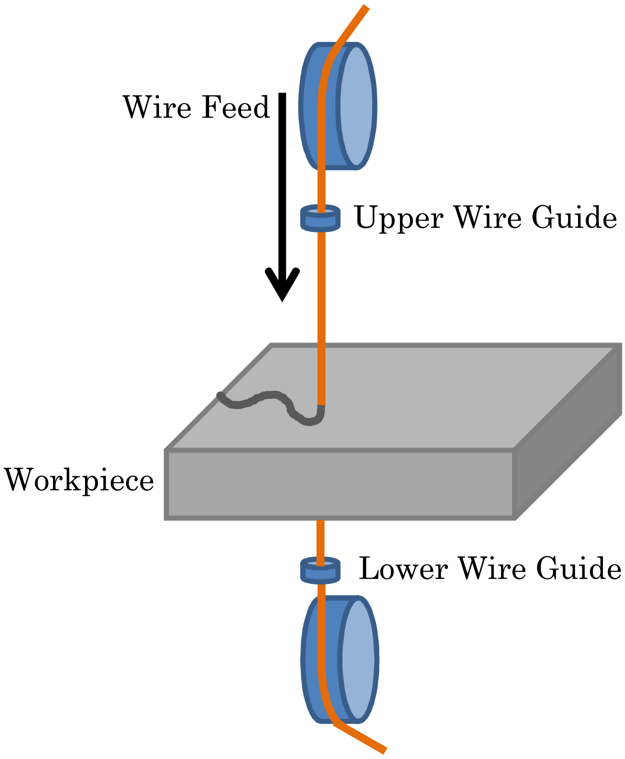

Figure 1.2: Wire EDM configuration.

1.1.2 Fast Hole EDM

The fast hole EDM configuration is characterized by using a very thin electrode (0.2 – 3 mm) in diameter, and for this reason is also referred to as small hole EDM. The electrode is a brass or copper tube that can have one or more channels for increased stiffness to prevent against deflection, and also to provide through flushing during machining. The fast hole electrode is rotated as it is plunged into the surface to ensure uniform wear on the electrode. A major issue with fast hole EDM is that due to the size of the electrode, it is affected by tool wear much more than other EDM configurations. This can make true electrode length as well as electrode breakout difficult to determine.

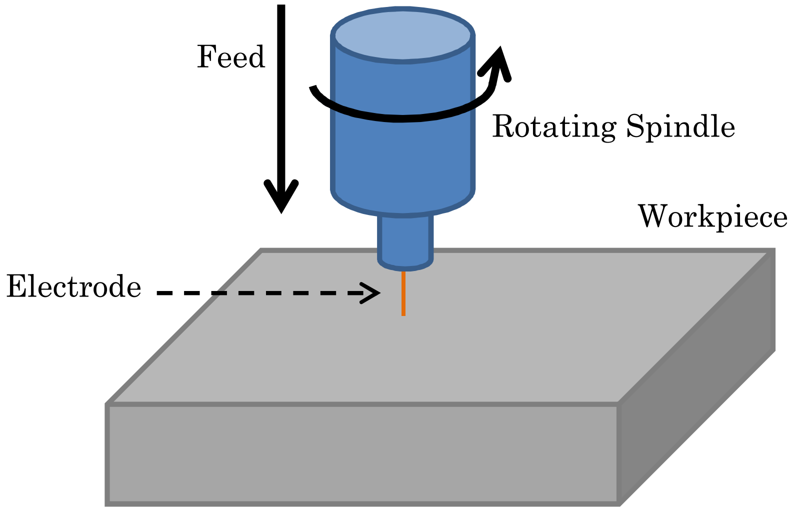

Figure 1.3: Fast hole EDM configuration.

1.2 Acoustic Emission (AE)

This research project intends to utilize acoustic emission waves created by discharges in order to monitor the EDM process. Acoustic emissions refer to elastic waves that propagate throughout a medium in the frequency range of “20 kHz up to several megahertz” [6]. These elastic waves are produced through the release of energy causing; crack growth, phase transformation due to heat, and melting among numerous other potential sources [7]. This lends itself well to the EDM process where the heat generated releases energy into the workpiece material acting as a source for elastic waves. Sound is often associated with monitoring the EDM process, with experienced operators often judging the stability of the process by the sound caused by machining. It is a natural progression to monitor the process via non-destructive acoustic emission testing, despite some implementation issues that may exist.

1.2.1 Acoustic Wave Modes

The two simplest acoustic wave modes that are used in non-destructive testing are the longitudinal "P" wave and the shear "S" wave. The longitudinal wave is characterized by a wave front travelling parallel to the surface, while the shear wave travels perpendicular to the surface. As parallel and perpendicular motion compound, more complex motions such as Rayleigh and Lamb waves are created. The Rayleigh wave is a surface wave characterized as a rolling movement along the surface shown in Figure 1.4.

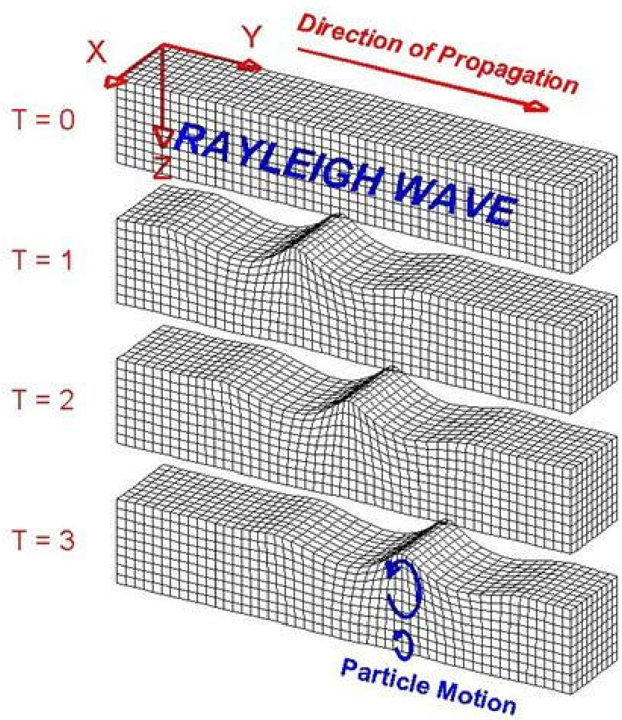

Figure 1.4: Motion of Rayleigh wave [8].

In the special case of a very thin surface, the propagation of Lamb waves occurs. The Lamb wave follows an elliptical motion similar to the Rayleigh wave and since the plate is very thin the wave occurs on both plate surfaces, as opposed to the Rayleigh wave which only occurs on one surface. The relative motion of the wave at the two surfaces can be characterized as either being asymmetric or symmetric as seen in Figure 1.5.

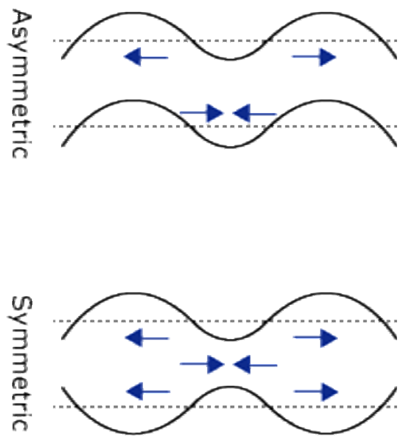

Figure 1.5: Lamb wave types [9].

The wave modes can be differentiated through wave speed which aids in interpreting a typical acoustic emission sensor output. In considering the 4 types of waves previously discussed (longitudinal, shear, Rayleigh, Lamb) the longitudinal wave is the fastest of the three waves [10]. The second fastest is the shear wave, and the Rayleigh wave is the slowest at 0.87-0.95 of the shear wave speed depending on Poisson's ratio [9]. The Lamb wave is essentially a composite of the other three wave types and as such the speed of a Lamb wave is between longitudinal and shear [10]. Specifically in the case of this wave propagation in a thin rod this sound velocity is termed the 'thin rod velocity' [10]. The Rayleigh wave carries approximately 67% [10] of the total energy associated with the acoustic emission and is the most dominant wave seen in acoustic emission signals.

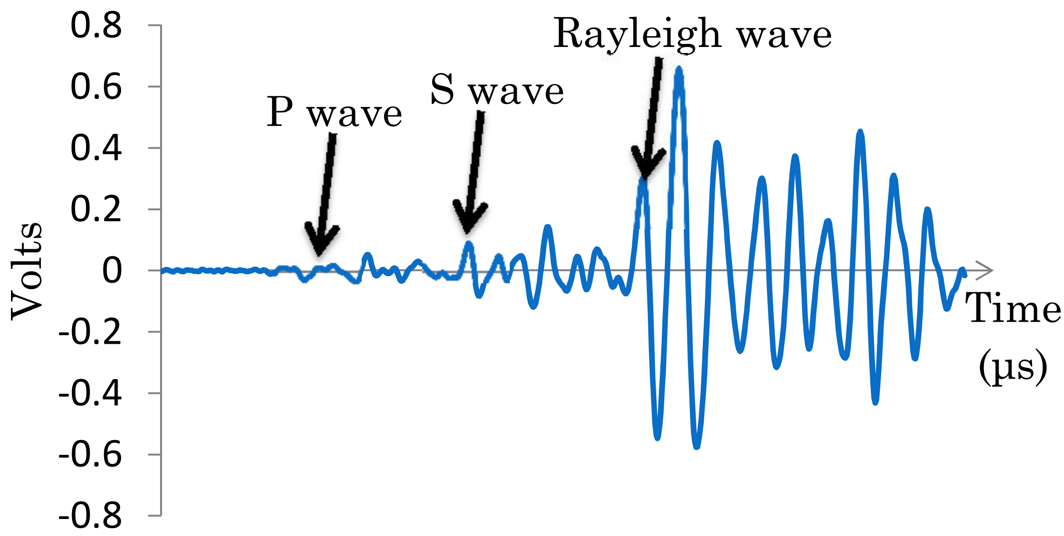

Figure 1.6: Typical acoustic emission signal [10].

An important aspect of acoustic wave propagation that must be taken into account during AE testing is that of attenuation. Attenuation refers to the decrease in acoustic emission amplititude with respect to distance travelled of the acoustic wave. The equation for acoustic wave amplitude A at a propogation distance z can be described as follows [9]:

$$A(z) = A_0 e^{-\alpha z} \tag{1.1}$$

Where A_0 refers to the initial amplitude of the acoustic wave at the source location. The attenuation constant α is dependent on the material and is determined experimentally.

1.2.2 Electromagnetic Interference (EMI)

Due to the frequency range of acoustic emissions, AE transducers are not sensitive to low frequency electrical noise, however there is a phenomenon in EDM which causes very high frequency electromagnetic interference (EMI) in the acoustic emission signal at the instance of discharge.

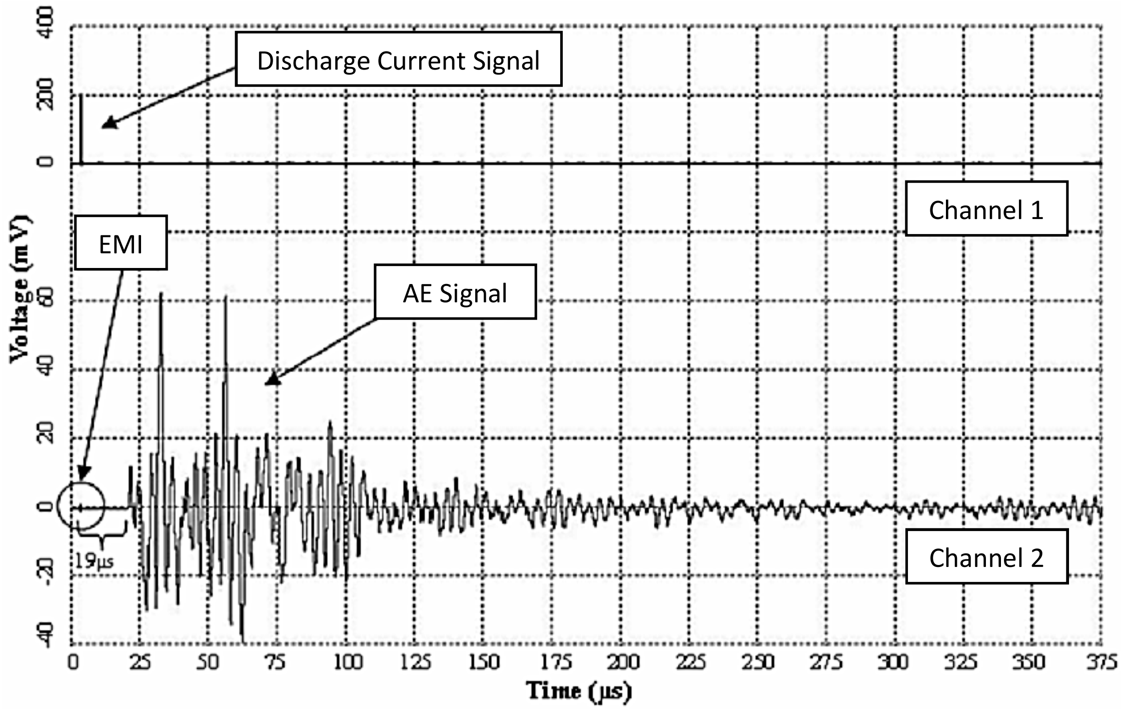

Figure 1.7: EMI in acoustic emission signal [11].

This phenomenon is known as ringing and occurs during the rise of high frequency flow of current. As the current begins to flow, a parasitic capacitance and current leakage is present which causes oscillations in the current as it tries to stay at its set value. A parasitic capacitance is an unwanted capacitance between two charged surfaces that are in close proximity to each other. This is exactly what is seen with the EDM electrode and workpiece interaction. The current leakage occurs between the electrode and workpiece in an attempt to eliminate this capacitance. This high frequency current oscillation causes a high frequency EMI to occur in the acoustic emission signal [12]. In some cases of a low amplitude acoustic emission signal, the EMI can overwhelm the wanted signal causing issues with data processing.

1.3 Scope of Thesis

The intent of this research was to provide a method for monitoring the EDM process through non-destructive testing with acoustic emission sensors. Much can be gained by analyzing the current and voltage signals during machining. With this information it is possible to determine the types of discharges that are occurring during machining such as normal sparks or harmful arcs and shorts [13].

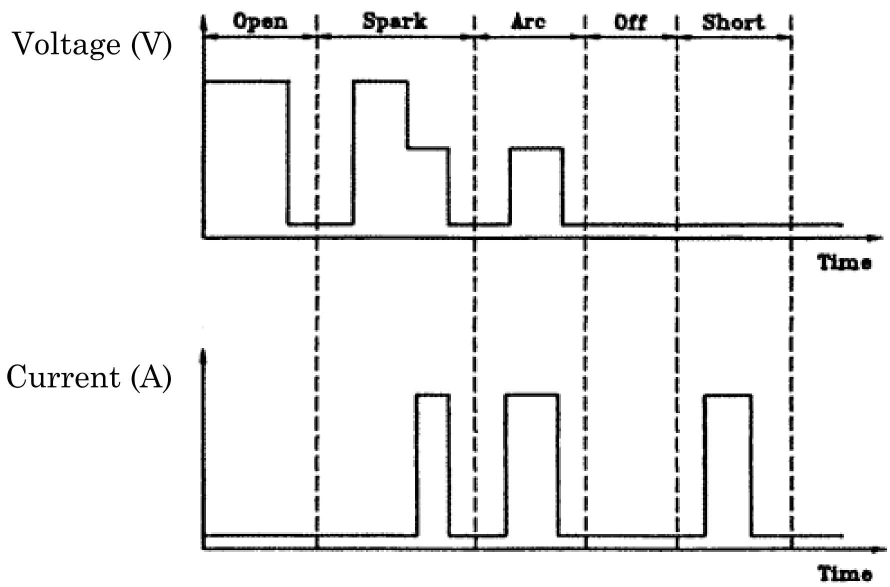

Figure 1.8: Current and voltage waveforms [13].

This knowledge gives us a basic overview of the process, allowing for the detection of machining instability due to harmful spark and arc discharges. However, it does not give a specific location as to where the machining is taking place which can lead to even further process improvement. This is an area which has been explored very minimally, though the use of acoustic emission in the monitoring of conventional machining processes as well as the monitoring of electrical transformers has shown that it is an area worth investigating. Of particular interest is the development of a method for mapping the location of discharges in real time. This could prove extremely beneficial as it would provide a technique for monitoring the wire EDM process to prevent against wire breakage and to optimize process parameters. It would also allow for the detection of engaged fast hole electrodes in order to determine true hole depth. The goals of this research were to sense spark location in wire and fast hole EDM to within 1 mm accuracy under real machining parameters. Ultimately this technique could also be used to detect certain abnormalities such as improper flushing in the sink EDM process, so that adaptive flushing strategies could be utilized to ensure process stability and surface quality.

Chapter 2

Literature Review

A review of the state of the art follows. This expands upon the above introduction to show present discharge mapping methods and the use of acoustic emission sensors in analogous situations.

2.1 Source Location in EDM

There currently exists several discharge mapping methods providing various degrees of accuracy. These are mostly based upon the electrical nature of the process which is often accompanied by several implementation issues.

2.1.1 Divided Electrode Method

The divided electrode method for discharge mapping is the simplest of all mapping techniques. An electrode is divided into multiple parts as seen in Figure 2.1, with each electrode division being insulated from one another [14].

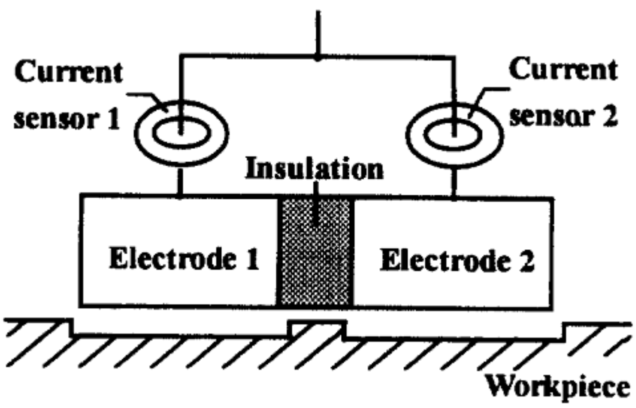

Figure 2.1: Divided electrode method [14].

The incoming current is branched to each electrode division, such that the sum of the parts acts as a single electrode. A current sensor attached to each branch is used to sense the electrode segment through which the current is flowing. The resolution of this method is dependent on the size of each individual electrode. The complexity of manufacturing intricate electrodes with many small individual parts renders this method to be quite unfeasible.

2.1.2 Branched Current Method

In the branched current method, the discharge location is determined using the principle of resistivity. The resistance of a conductor is a function of the specific resistivity of the material and the cross sectional area and length of the conductor. When branching the current at two opposite ends of the electrode as shown in Figure 2.2, the difference in current can be correlated to a difference in resistance.

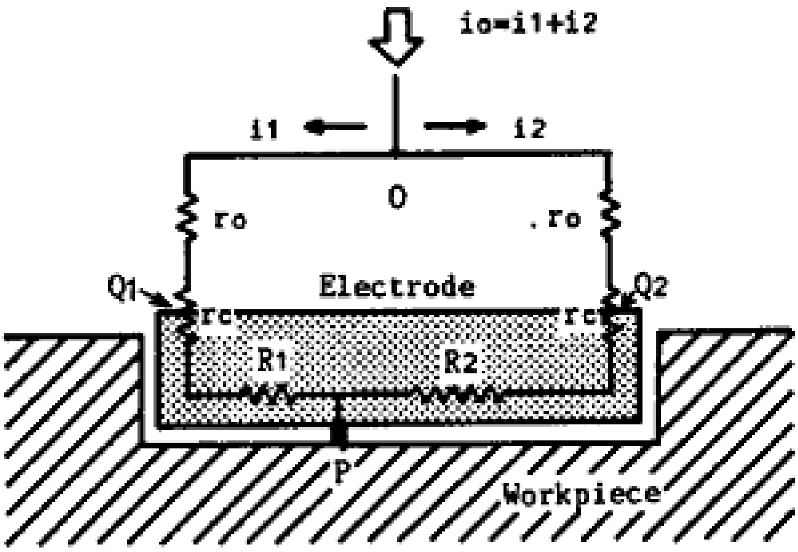

Figure 2.2: Branched current method [15].

The current in each branch can be calculated from Equation 2.1 [15] :

$$i_1 = \frac{i_0[R_2 + (r_0 + r_c)]}{[R_1 + R_2 + 2(r_0 + r_c)]}$$
$$i_2 = \frac{i_0[R_1 + (r_0 + r_c)]}{[R_1 + R_2 + 2(r_0 + r_c)]} \tag{2.1}$$

Since the resistance in the wire branches r_0 as well as the contact resistances r_c are not dependent on spark location, the measurement of i_1 and i_2 leads to the calculation of resistances R_1 and R_2. The spark location can be calculated through knowledge of the cross sectional area (A) of the electrode as well as the resistivity (ρ) as follows:

$$PQ_1 = \frac{AR_1}{\rho}$$
$$PQ_2 = \frac{AR_2}{\rho} \tag{2.2}$$

An implementation issue with the branched current method is in the relative magnitude of the resistances between the electrode and the branches. Resolution of the branched current method is best when the electrode resistances are significantly higher than the resistance in the wire branches. "Therefore, a graphite material was used for the tool electrode, since its specific resistance is larger than that of copper." [15] This poses a significant problem with using the branched current method in wire EDM as the wire used is most commonly brass. The resistivity of brass is an order of magnitude lower than graphite, and is comparable to that of the the copper branch wires [16]. The branched current method is more suitable for the sink EDM configuration where a graphite electrode can be used.

The literature remains unclear on the range limitations of this method, merely stating that the current branches must be separated by a 'sufficient' distance while noting that minimizing the loop OQ_1PQ_2O (See Figure 2.2) is an important way to reduce the self-inductance in the loop which causes variation in the current measurement [15]. This also helps to ensure that the wire resistance remains negligible. The researchers also recommend delaying the sampling to disregard the transient component of the current signal. This could prove difficult with smaller pulse on-times which can reach 1 µs as compared to the 200 µs pulse on-time used to test this method [15,16]. Exact resolution remains unknown, however Li notes that "the error is several millimetres when the length of the electrode is 100 mm" [14].

2.1.3 Potential Difference Method

The potential difference method, developed by Kunieda et al. [14] is similar in method to the branched current method discussed in Section 2.1.2.

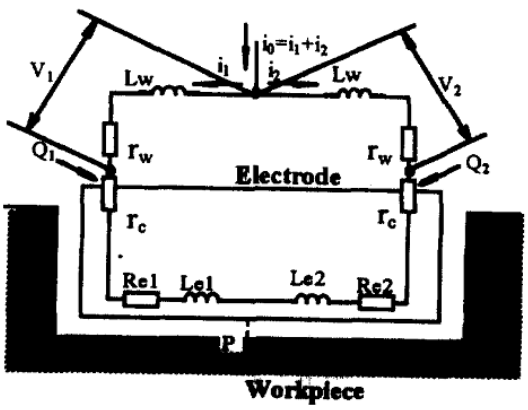

Figure 2.3: Potential current method [14].

The current is branched in the same way as discussed previously, however the potential difference between the points Q_1 and Q_2 can be determined to be a function of the inductance in the loop and not of resistance:

$$V_1 - V_2 = \frac{di_0}{dt} L_w \left(\frac{L_{e2} - L_{e1}}{L} \right) \tag{2.3}$$

With this relationship, the specific resistivity of the electrode is not a factor, meaning that the electrode is not limited to being graphite as with the branched current method.

Han et al. [17] examined ways to improve this accuracy and determined that the voltage readings vary greatly along the duration of the signal. "Because of the noise of the discharge, good sensitivity for detecting discharge locations is still difficult to obtain" [17]. The noise at the beginning and end of the signal affect the peak voltage and subsequently the accuracy of the spark location. A wide degree of error is present when using the measurements from the beginning of the voltage wave as seen in Figure 2.4.

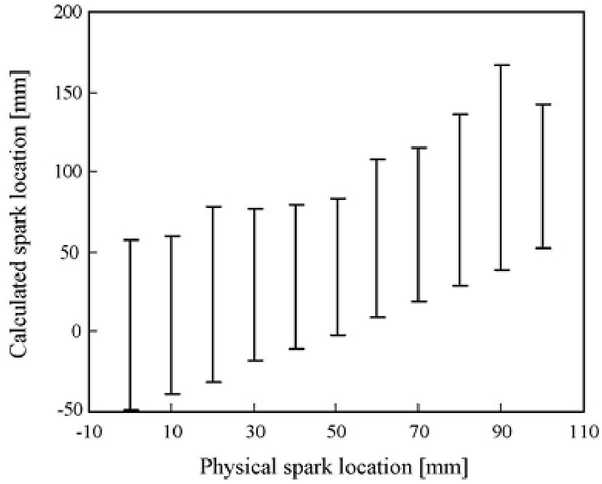

Figure 2.4: Calculated spark location using beginning signal voltage [17].

The noise present at the end of the signal varies relatively much less between the two branches resulting in a better accuracy using the signal at the end of the discharge, as shown in Figure 2.5. The accuracy of this method is still approximately 10 mm or 10% of the total 100 mm workpiece length.

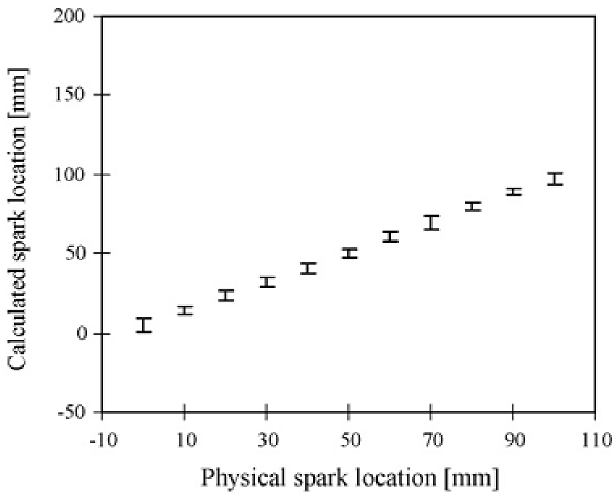

Figure 2.5: Calculated spark location using end signal voltage [17].

2.1.4 Electromagnetic Method

As discussed in Section 1.2.2, an electromagnetic wave occurs each time a discharge is produced. For most methods this is an unwanted interference that makes processing of data difficult, however some researchers [18] have experimented with discharge location via analysis of the produced electromagnetic signal. A Hall sensor is a device that is used to measure the magnetic field produced by a current passing through a conductor. By using two Hall sensors one can compare the magnetic flux intensity at each sensor to determine the location of the source between the two sensors. An issue with using Hall sensors is that they are "limited to shorter displacement ranges for strongly non-linear decrease of the magnetic field strength with distance from the field source" [19]. The distance from the source that the Hall sensor can detect effectively is approximately 20 mm [20] and is dependent on the magnitude of the source electromagnetic field. Due to this small sensing range, the sensors are most often used in conjunction with a magnetic field concentrator. A concentrator is made of a magnetic material, most often ferrite, and can magnify the flux density by a factor between 20 and 70 [21].

Experimental tests of this method involved surrounding a 140 mm x 140 mm workpiece with a magnetic flux concentrator and embedding a hall sensor in the concentrator at the midpoint of each edge. This setup allows for detection along two axes to locate a discharge in two dimensions. Discharges were produced with a 1 mm diameter copper electrode at 10 mm increments on a 100 mm x 100 mm area on the workpiece as seen in Figure 2.6.

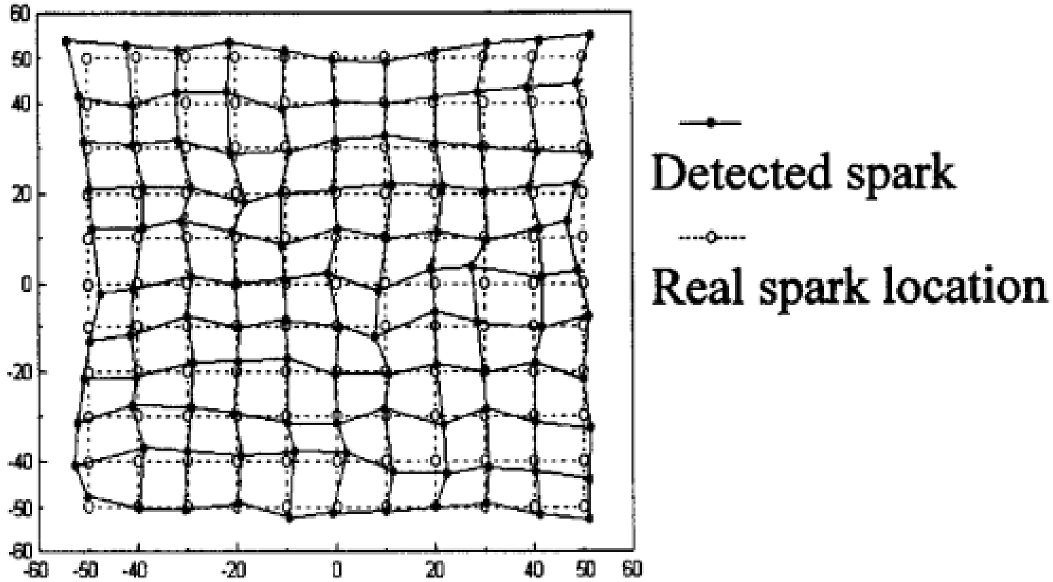

Figure 2.6: Spark location using Hall sensors [18].

It can be seen that the farther away from the center of the workpiece the dischargers occur, the worse the accuracy becomes even for a fairly small workpiece. Additional results using this method are limited, except that it has been noted that: "The error is several millimeters when the length of the workpiece is 80 mm" [14].

The experiments in this work used high sampling rates of 30 MHz for 4 channels in order to determine discharge location. Storage and transfer of this amount data is something that needs to be considered for real time monitoring. This author recommends that more tests should be performed using this method to test its feasibility for use in wire EDM.

2.1.5 Acoustic Emission Method

Currently, there has been little development in the use of acoustic emission sensors in the monitoring of the EDM process. Ydreskog and Novak [22] utilized a custom-made ultrasonic sensor to sense a spark location in a sinking EDM operation. It is termed an ultrasonic sensor because it has a 'resonance frequency about 5 MHz' and is used to detect higher frequency acoustic waves. A modified EDM die sinker and pulse generator were used to have control over sparks that are produced. This method involved a two stage approach; a calibration stage followed by machining. In the first stage a single spark is created at a known location and arrival times to an array of sensors are recorded and the speed of sound in the material is calculated. The next stage involved creating a discharge at an unknown location and using the calibrated speed of sound to determine the location.

By measuring the acoustic waves produced by single sparks, wave interference from a succession of discharges was not accounted for. The researchers also acknowledge "that two different types of interference, ground loop noise and electromagnetic interference (EMI), to a high extent affected the sensor signal" [22] yet make no mention as to how this was accounted for. Claims as to the expected 50 μm accuracy of the system are based on the time resolution as well as the speed of sound in the material. The time resolution is a function of sampling rate and is independent from the setup and sensor frequency range response. By using a sensor designed to detect the high speed longitudinal waves an increase in resolution is anticipated compared to the detection of other acoustic wave modes. Ultimately the authors [22] concede that they failed to reach the expected accuracy due to the issues of noise discussed above and the real experimental accuracy is not disclosed.

Muto et al. [23] also developed an acoustic emission sensor with a resonance frequency of 20 MHz in order to detect longitudinal waves. The sensor was attached to the end of the test workpiece with a Hall sensor used to trigger the data acquisition when a discharge occurred. The researchers perform a single spark experiment on the test workpiece, and show that as the acoustic emission sensor is placed farther and farther away from the point of discharge, the receiving time for the first incoming wave increases. Muto et al. state: “By calculating the time difference of transferring AE signals, it is possible to detect the location of a discharging point with a very high accuracy of 0.3 mm” [23]. This accuracy appears to be calculated based on the frequency characteristics of the sensor, as a maximum resolution of 6 mm is estimated for a sensor with a frequency characteristic of 1 MHz.

Due to the nature of single spark experiments, these researchers did not have to deal with interference caused by multiple acoustic emissions occurring rapidly. The researchers also do not describe the method used to determine the onset of the incoming acoustic wave and how signal noise might affect this determination. Determining the onset of the acoustic wave especially with background noise present is the biggest issue facing the use of acoustic emission sensors as a technique to determine discharge location, and up until this point has yet to be addressed and resolved.

2.2 Acoustic Emission Source Location in Other Media

Despite the lack of research that has been performed using acoustic emission sensors to monitor EDM, these sensors have been extensively used in source location in other processes. Acoustic emission sensors have been used to detect the sources of; leaks in long pipes, uneven events in conventional machining as well as partial discharges in power transformers. An examination of these techniques is important to ascertain the feasibility of acoustic emission discharge mapping in EDM. It is also a resource in terms of present signal analysis techniques for determining source locations from acoustic emissions that will be discussed later in Section 2.5.

2.2.1 Source Location of Leaks in Water Pipes

Acoustic emission sensors are used in the location determination of leaks in hidden pipes [24]. A pipe presents a one dimensional location problem with sensors affixed at either end.

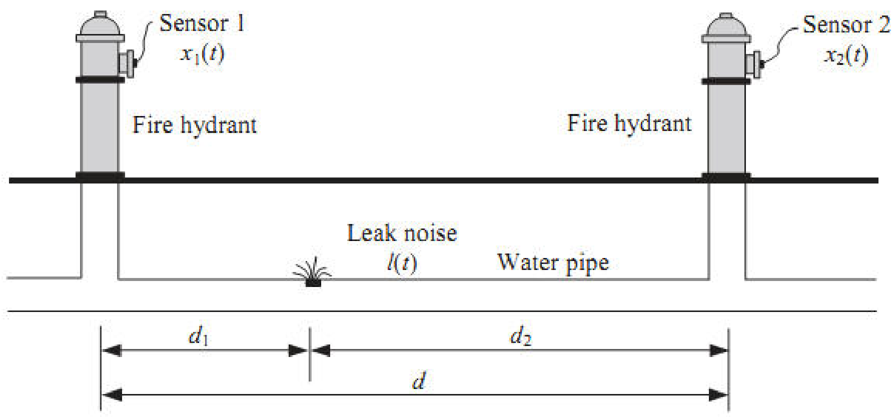

Figure 2.7: Acoustic emission leak detection in water pipes [24].

A leak in the pipe acts as a source of acoustic emission and various techniques have been used to determine this location. Of particular interest is the work of Ahadi and Bakhtiar [25], who used a Short Time Fourier Transform to note changes in the frequency content of the acoustic emission signal. Using this information, the researchers were able to detect a leakage based on frequency characteristics even in the midst of constant background noise.

2.2.2 Location of Uneven Events in Conventional Machining

Acoustic emission sensors are used as a process monitoring tool in conventional machining: grinding [26], turning, milling [27] and broaching [28], with much focus being on determining tool wear and other machine specific phenomena such as grinding burn [26]. This overall view of machining performance was expanded on by Axinte et al. [29] to: "locate, into three/two dimensional workspace of the workpiece, the acoustic sources that are related to the generation of uneven events". An uneven event refers to workpiece defects that occur during machining such as "surface scoring, tool material embedded in the workpiece, smearing, lapping, flaking, plucking" [29]. Researchers used a single edged broaching tool and a sample workpiece featuring machined slots. As the cutting edge entered and exited each slot, an acoustic emission signal was produced. Researchers were able to determine the slot position with a position error of 0.01 – 10.11 mm.

Researchers noticed some areas of concern in the accurate source location of uneven machining events. The material anisotropy can cause a variation in localized acoustic wave velocity in the workpiece. The researchers also noted that attenuation of the acoustic wave can cause decreased accuracy at farther distances from the sensors. Finally, sensor noise in more complex machining (eg. multiple cutting edges as opposed to a single cutting edge), as well as the triggering method to determine the start of an acoustic wave leads to decreased time delay estimation accuracies [29].

2.2.3 Location of Partial Discharges in Transformers

Acoustic emission sensors are often used to monitor the state of a power transformer. "A transformer is a static piece of apparatus used for transferring power from one circuit to another without change in frequency" [30]. A high voltage transformer is comprised of a conducting core immersed in dielectric oil, as well as a solid dielectric shielding the windings [31]. Through insulation breakdown whether due to aging or harmful events, it is possible for a partial discharge to occur. "A partial discharge can be defined as localized electrical discharge in insulating media which only partially bridges the insulation between conductors" [30]. This partial discharge occurs along the same mechanism as a discharge in the EDM process. It is necessary to examine the work performed using acoustic emissions and partial discharges in order to gain a better foundation for the present research.

Due to the complex inner core of a transformer, a partial discharge can occur between multiple geometries referring to the origin and terminus of the discharge; point-point, point-plane and surface [32]. There is also the possibility that multiple configuration of sparks can occur simultaneously; therefore researchers have focused on ways to differentiate between these discharges. Using a spectrogram based off of the Short Time Fourier Transform, researchers were able to show dominant frequency bands within the acoustic emission signals which corresponds to the different partial discharge forms. The detection of different simultaneous discharges is a useful starting point for solving the issue of interfering acoustic waves during EDM.

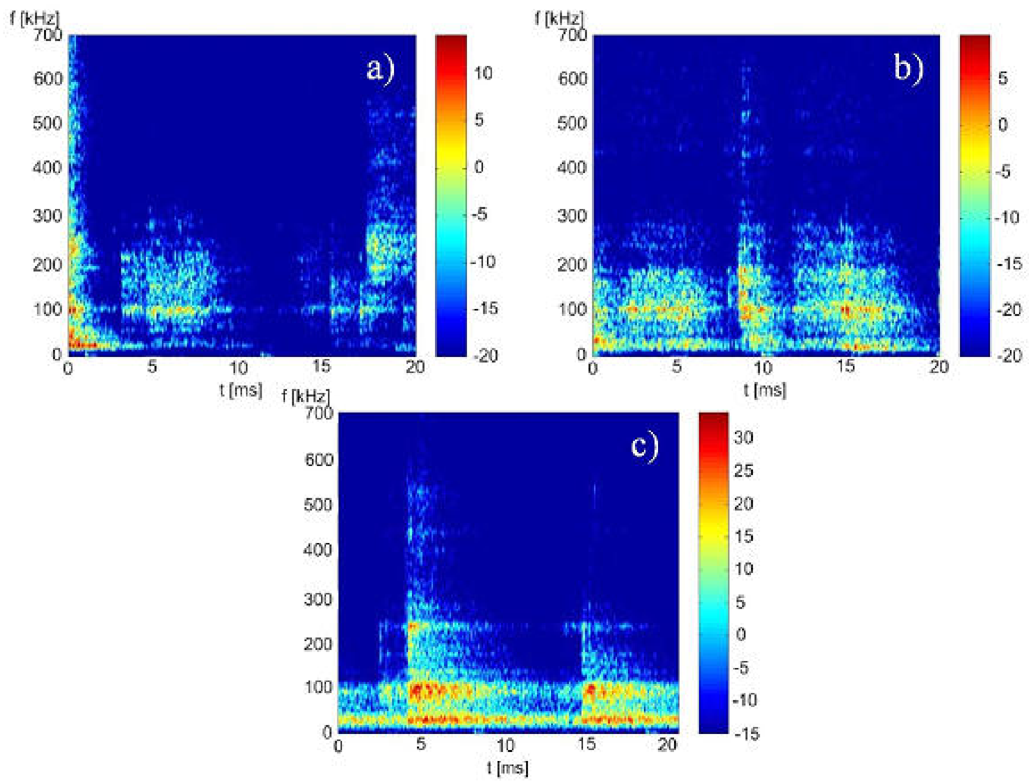

Figure 2.8: Spectrogram of multisource partial discharges: a) point-point and point plane, b) point-point and surface, c) point-plane and surface [32].

Through examination of the spectrograms shown in Figure 2.8, it was determined that a point-point discharge has a frequency band of 70-300 kHz, a point-plane occurs in 20-100 kHz and a surface discharge has the frequency characteristics in the 20-500 kHz range. Figure 2.8 c) shows the ability of the spectrogram to pick up the leading edge of the acoustic wave making it much more pronounced than the background noise.

Extending upon the ability to differentiate between sources of partial discharges, research has been performed to determine the partial discharge location. By being able to localize partial discharges, the ability to diagnose and fix issues becomes a much easier process. Howells et al. [33] used an iterative process in order to locate partial discharges in three dimensions with two sensors. With sensors placed on the outer tank, the sensor that is determined to lie farther away from the discharge (has a larger time delay), is moved closer to the other sensor. At the point in which the time difference is the same, the partial discharge is now known to be equidistant from both sensors on a plane. Repeating this process to determine another plane on which the partial discharge lies equidistant to both sensors can yield enough information as long as the two planes intersect. The intersection of these two planes is then where this partial discharge is occurring.

The researchers noted problems determining when the exact acoustic emission wave 'starts', as "this point can still sometimes be difficult to determine because severe attenuation tends to 'round' off the leading edge of the burst" [33].

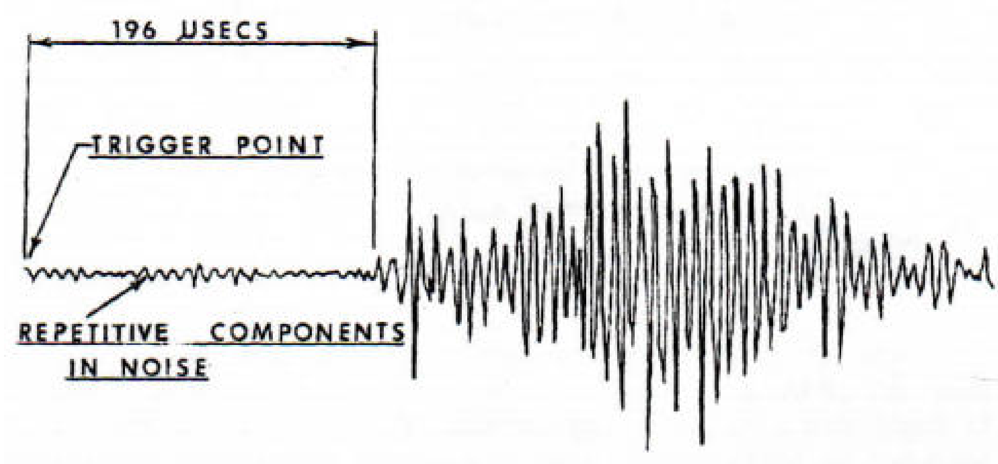

Figure 2.9: Triggering to determine start of acoustic emission [33].

It is easy to see in Figure 2.9 that if any more noise was present than already exists, determining the exact starting point of the acoustic wave becomes difficult.

In a laboratory setup knowing the exact speed of sound in the dielectric fluid, the researchers were able to detect the partial discharge source within +/- 5 mm from the real discharge location. However, when used in the field with unknown oil conditions the error in the location increases by an order of magnitude to +/- 5 cm [33]. Other research to determine spark location found an accuracy within 20 cm of the issue causing the partial discharges [34].

There are some main differences between the partial discharge location and spark location in the EDM, most notably being the scale. "The minimum distance of propagation will be the least distance between conductor to tank surface, which is found to be around 10 cm for a typical 5MVA, 33/11kV transformer… The maximum distance can be more than 1 m" [35]. Compared to the range of wire edm which is conservatively below 50 cm at its maximum [36]. Since the core of the transformer is comparatively large, accuracy is not as big of an issue as it is with EDM, instead it is only used to isolate a portion of the transformer on which to inspect closer. The time scale between the two processes is also vastly different. While sparks can occur in the EDM at a rate of 10^5 Hz, partial discharges in a transformer occur very sporadically and it may take minutes or hours "to collect sufficient data for unambiguous PD source location." [34].

An examination of applications which utilize acoustic emission as a means of source location for a variety of events has proved insightful. Before implementing acoustic emission sensors to develop a method for workpeice height identification and fast hole breakout detection it is pertinent to examine the state of the art in these areas.

2.3 Wire EDM Height Identification

Wire EDM productivity is limited by the strength of the wire used. Wire breakage is an important issue in wire EDM as it lowers productivity by interrupting machining in order to refeed the wire. Wire breakage can damage the surface, which in the case of a finishing process can lead to the whole part being scrapped. Wire breakage can also be a symptom of poor flushing causing discharge localization which also impairs the surface finish. As machining parameters are made more aggressive, machining speed is increased, however when made too aggressive wire breakage occurs. A main area of research in wire EDM is the detection of the onset of wire breakage in order to push machining parameters to the extreme without causing wire breakage. This is particularly important in situ as the instantaneous machining area (workpiece height) affects process stability. Since wire EDM is often employed to cut complex shapes as shown in Figure 2.10 with varying workpiece heights, the ability to detect machine stability in-process is paramount. Imported CAD models can be used to monitor workpiece heights during machining, though it is desirable to have a method that requires minimal changes from part-to-part as wire EDM is often used to machine custom one-off parts.

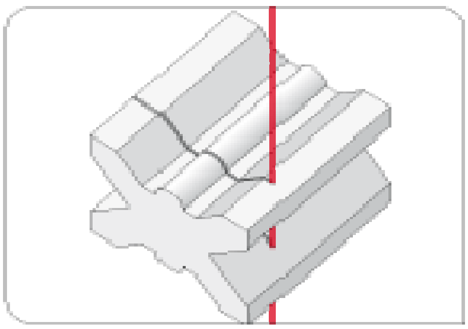

Figure 2.10: Wire EDM (in red) machining of complex part [36].

Figure 2.11 will be used to illustrate the effect of workpiece height on the wire EDM process. Machining parameters can be optimized for workpiece height in section 'A'.

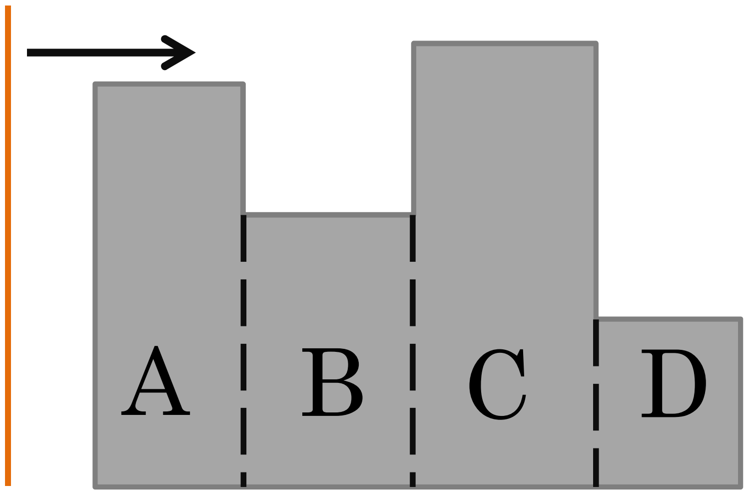

Figure 2.11: Effect of workpiece heights on wire EDM.

Machining occurs in section 'A' under optimal conditions, implying that machining is happening as fast as possible without wire breakage occurring. Once the wire reaches section 'B' and the workpiece height decreases, the machining is now overly aggressive, and while wire breakage may not occur, it is a distinct possibility. As the wire enters section 'C' which has a larger workpiece height than in section 'A', the discharges are now more spread out causing machining speed to decrease. In this scenario it would be possible to adjust the machining parameters to have more aggressive machining without causing wire rupture. Finally, when the wire machines a workpiece height significantly smaller than the height for which it is optimized such as in section 'D', wire breakage will occur due to the localization of discharges.

Currently the most common way of detecting workpiece height is by measuring the sparking frequency of the process [37]. Sparking frequency is, as the name suggests, a measure of the number of sparks per unit time. Traversing to a higher workpiece causes the sparking frequency to decrease. By monitoring this change in sparking frequency, the workpiece height can be estimated. The accuracy of this method is dependent on the control system used. Yan et al. [38] have developed an adaptive control system reportedly able to detect the workpiece height within 1.6 mm. In viewing their results in Figure 2.12, the system appears to respond better to a sudden increase in workpiece height than to a sudden decrease. There also appears to be a significant settling time (~1 min) for the estimated workpiece height to reach this 1.6 mm accuracy.

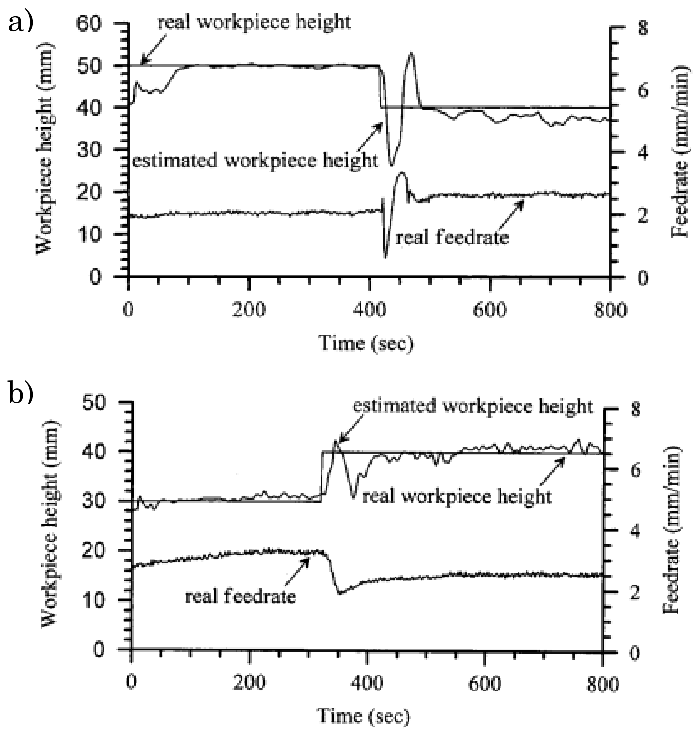

Figure 2.12: Workpiece height identification using adaptive control algorithm [38].

By developing a multiple input model accounting for average gap voltage, sparking frequency and cutting feed, Rajurkar et al. [39] were able to improve the accuracy in the transient period by 56% over a control algorithm based only on sparking frequency.

The problem with estimating workpiece height using sparking frequency is that "the machining state of the WEDM process may even become unstable without sparking frequency variation" [40]. Poor flushing can lead to localized arcs and shorts instead of stable sparking causing thermal damage to the wire and workpiece. As such it is beneficial to gain more detailed information of the discharging process, specifically **where** the sparks/shorts/arcs are discharging as opposed to an overall view of the situation that sparking frequency provides.

In 1983 a patent [41] was granted to detect the concentration of discharges through the use of inductance. By comparing the inductance from a fixed sensor due to multiple discharges, the detection of a concentration of discharges is possible if the values are approximately equal. The inventor does not discuss the accuracy of this method, nor do they make an attempt to convert these inductance values into workpiece heights, instead only working in relative values from one spark to another. This method appears to be an extension of the potential difference method discussed in Section 2.1.3 and might suffer from the implementation issues outlined in that section. This method could be useful in the situation described above where a localization of sparks can cause weakening of the wire and more experiments into the method are recommended by this author.

Another technique was patented in 1976 that measures the leakage current between the electrode and the workpiece [42]. In order to do this, the process must be momentarily halted, continuing machining until a stable gap distance is established. After a stable gap distance is established, the wire and workpiece will have a parasitic capacitance between them and subsequent leakage current will occur. This leakage current can be converted to a workpiece height value using a calculation based off of the resistance of the wire and dielectric, similar to the branched current method discussed in Section 2.1.2. Stopping the process in order to estimate workpiece height decreases productivity. The inventor does not discuss the accuracy of this method.

2.4 Fast Hole Machined Depth Detection

Process monitoring in fast hole EDM is important to provide stability for this micromachining process. Current process monitoring focus on detection of gap state [43], breakout detection [44] as well as depth monitoring [45]. Fast hole EDM is characterised by a higher tool wear rate than regular EDM [43]. Due to this, "tool plunge depth is affected by tool wear and does not always represent the true machined depth" [45]. The tool wears rapidly at the end which means that as the electrode is plunged into the workpiece it is not machining nearly as much as might be indicated. In some cases, the volume of material removed from the electrode could even be more than the volume removed from the workpiece [44]. The development of a method for detecting true electrode machined depth would be novel and beneficial.

Some research has been performed in attempting to determine the true machining depth of a fast hole electrode. Richardson et al. [45] used an antenna to detect electromagnetic waves emitted during fast hole machining of a workpiece created by electroplating 60 µm of copper onto a 100 µm thick stainless steel foil. A look at the signal intensity across a wide frequency range in Figure 2.13 shows a transition area between the steel and copper.

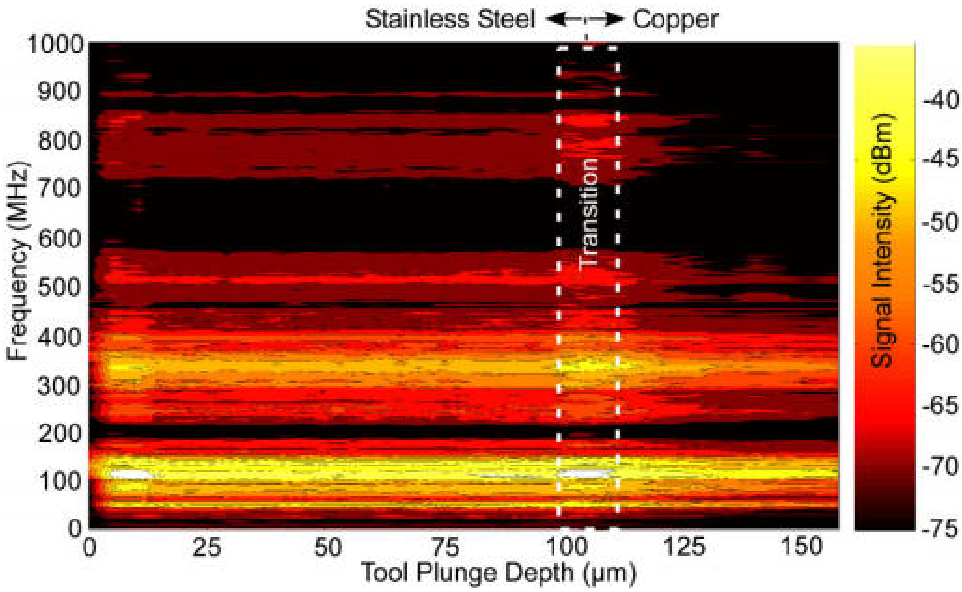

Figure 2.13: Signal intensity during fast hole EDM machining of multi-layered workpiece [45].

The researchers were only concerned with determining the location at which the fast hole electrode started to machine the copper underneath the stainless steel foil. In examining Figure 2.13, there does not appear to be any variation in the signal intensity, other than the transition area between stainless steel and copper, that would indicate the true tool plunge depth.

Technology also exists for breakout detection by measuring the back pressure of the dielectric fluid as it is used for flushing through the centre of the electrode. When the electrode breaks out on the other side of the workpiece, a drop in the back pressure as shown in Figure 2.14 is seen. Figure 2.15 shows the location of the electrode corresponding to this initial breakout condition [44].

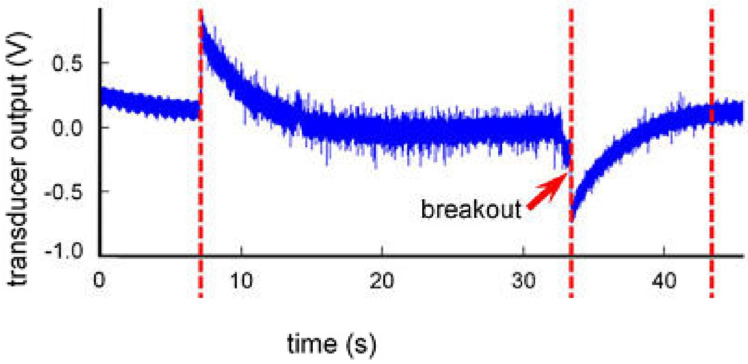

Figure 2.14: Method for detecting fast hole EDM breakout [44].

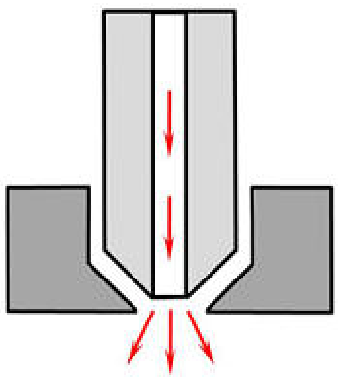

Figure 2.15: Location of electrode at breakout [44].

It is seen that due to the extreme wear a taper is formed at the end of the electrode. Due to this wear machining is continued despite the pneumatic sensor detecting a breakout. The researchers used the feed rate of the electrode as a measure to determine when a full breakout has occurred noting that "simultaneous monitoring of both pressure and displacement signals would enhance the robustness of the monitoring system" [44]. Having a method for determining true electrode plunge depth could be used in conjunction with this pneumatic method to further improve breakout detection.

A review of EDM source location methods, specifically for workpiece height identification and fast hole electrode depth measurement, demonstrate areas where possible improvement could occur. The use of acoustic emission sensors for determining source location in analogous processes leads one to believe that acoustic emission sensors could also be used during the EDM process. The only issue that remains is the processing of the acoustic signals from the EDM discharges to determine discharge locations. A review of data processing techniques used in time of arrival situations will now be performed.

2.5 Acoustic Emission Data Processing

The use of acoustic emission sensors are often used to determine source location based on a time of arrival method. When two sensors are used, the time lag between the sensors can be used to calculate the location, knowing the speed of sound in the media through which the acoustic wave travels. If the data is noise free it is easy to determine the onset of the acoustic wave, however with noise present this determination becomes difficult. This section discusses sophisticated techniques used for detecting the time lag between two acoustic emission waves.

2.5.1 Cross Correlation

Instead of measuring the time delay of each signal from a fixed reference point, the cross correlation method is often used in signal processing to measure the lag between two similar signals [46]. In simple terms, cross correlation is a measure of 'similarity' between two signals. A closer look at the cross correlation function is needed to determine how this similarity measurement is established. MATLAB has a cross correlation function (xcorr) that estimates the cross correlation as [47]:

$$\hat{R}_{xy}(m) = \begin{cases} \sum_{n=0}^{N-m-1} x_{n+m} y_n^*, & m \geq 0 \\ \hat{R}_{yx}(-m), & m < 0 \end{cases} \tag{2.4}$$

Where N is the length of the two vectors.

The function works by calculating the sum of the product of the two signals at lags ranging from –N to N. The reason this is considered a measure of similarity is that when peaks or valleys occur at the same point in the two signals the cross correlation will yield a positive result, while a peak and valley will give a negative value. The maximum value of the cross correlation function corresponds to the cell lag between the two signals which can be converted to a time lag with a knowledge of the sampling rate.

2.5.2 Wavelets

Another useful tool in signal processing is the use of wavelets. A wavelet "is a continuous and oscillating function of short duration" [48] and is written mathematically as:

$$\varphi_{a,b}(t) = \frac{1}{\sqrt{a}}\varphi\left(\frac{t-b}{a}\right) \quad a > 0, \quad -\infty < b < \infty \tag{2.5}$$

Key features of the wavelet are that it can be scaled with a, and translated in time with b. This scaling allows for the wavelet to assume a wide range of frequencies. Wavelets are commonly used in the wavelet transform and also as a tool for denoising a noisy signal.

The wavelet transform is similar in nature to the cross correlation function discussed in Section 2.5.1. For a signal $\boldsymbol{x(t)}$ and a wavelet $\boldsymbol{\varphi_{a,b}(t)}$ the wavelet transform is [25]:

$$WT_x(a,b) \triangleq \int x(t)\varphi_{a,b}(t)dt \tag{2.6}$$

Essentially the wavelet transform cross correlates the wavelet scaled to a range of frequencies with the source acoustic emission. This finds the time location in which the wavelet best matches the acoustic signal for a given frequency.

Ahadi et al. [25] used this method to detect leaks in water filled plastic pipes. After isolating a leakage frequency band the researchers examined the effect of different sized leaks. Of interest to this particular research is the ability to detect the time at which the leakage signal occurs. The researchers claimed to have started the leak after 100 ms, and this can clearly be seen in Figure 2.16.

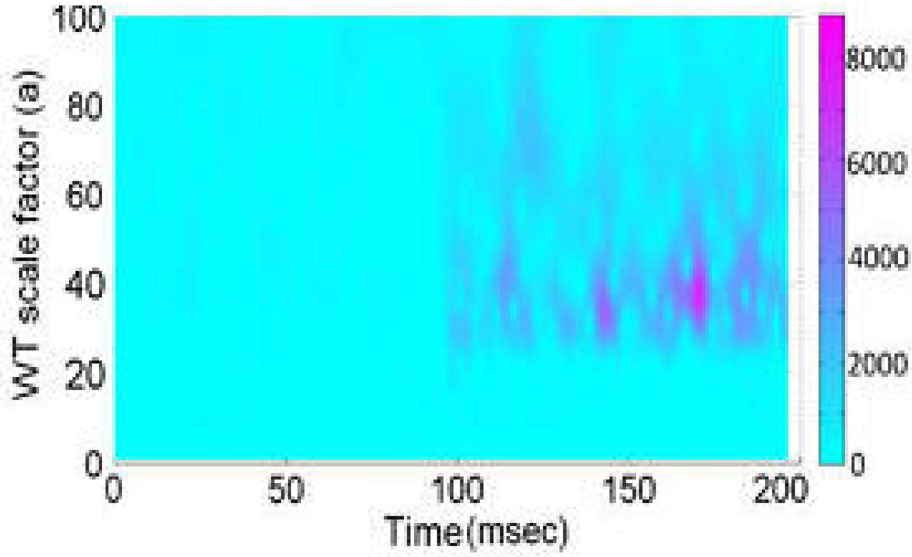

Figure 2.16: Wavelet transform of leak starting at 100 ms [25].

The choice of wavelets is extremely important, as the wavelet must be shaped as similarly to the acoustic wave as possible for best results.

Denoising with the use of wavelets is a way to remove some background noise from the signal. Wavelets are used to decompose the signal into two parts: a contracted wavelet transform extracts high frequency data, while a dilated wavelet transform extracts low frequency data. The high frequency data is termed ‘detail’, and the low frequency data is termed ‘approximation’ [48]. The decomposition occurs on the approximation data repeatedly for a number of levels.

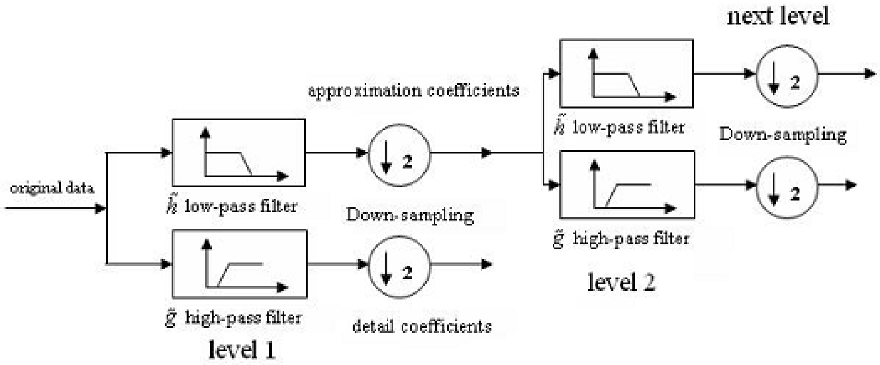

Figure 2.17: Wavelet decomposition tree [49]

Once the decomposition is completed, one approximation and several levels of details remain as shown in Figure 2.18. To finish denoising, thresholds are set on the details to limit unwanted frequency ranges of data. The signal can then be reconstructed, though care must be taken not to remove signal components during the thresholding process.

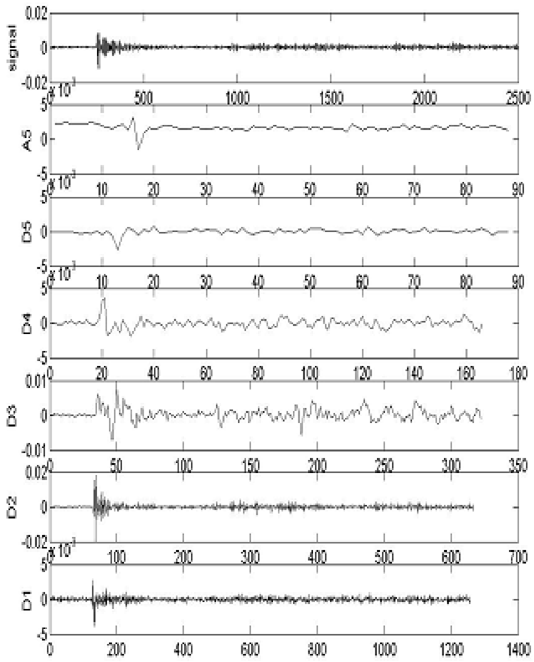

Figure 2.18: Wavelet decomposition through five levels [48].

2.5.3 Short Time Fourier Transform & Power Spectral Density

As discussed previously, analysis of the frequency content of acoustic emission waves is a useful technique for differentiating acoustic signals from background noise [26,33]. A Short Time Fourier Transform (STFT) performs a Fourier transform over a small window on the data, detailing the frequency content at that point in time. By sliding the window along the data it is possible to examine how the frequency content of the signal changes over time, as shown in Figure 2.19.

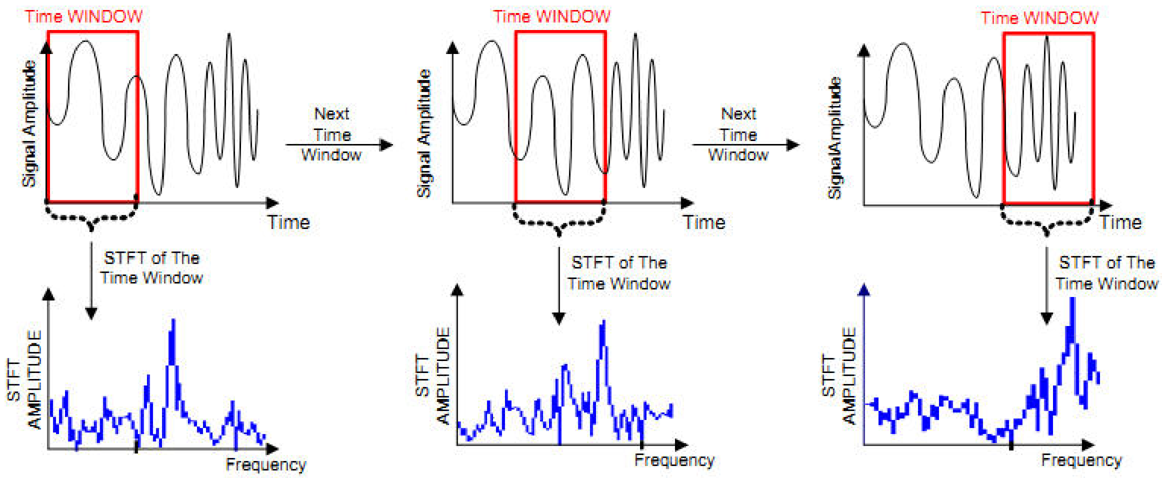

Figure 2.19: Short Time Fourier Transform [25].

Power spectral density is then calculated by squaring the magnitude of the STFT [50]. Power spectral density is a measure of the energy associated with each frequency over the STFT window. A spectrogram is a way of displaying this power spectral density for each instance along the acoustic emission signal and for a given frequency range. This gives a three dimensional surface representation of the power spectral density as seen in Figure 2.8, where it is possible to determine dominant frequencies and frequency trends through time in the acoustic emission signals.

Currently, there exists many methods for determining discharge locations during EDM machining ranging from the basic divided electrode method to the use of Hall sensors to detect electromagnetic waves resulting from discharges. Each method has implementation issues whether it be the need to use graphite electrodes in the branched current method or the range limitations of the electromagnetic method. Present discharge location accuracy is currently on the order of several millimeters which leaves room for improvement.

Discharge location calculations based on the propagation of acoustic waves remains an area with minimal research having been conducted to date. The research performed does show promise with sub millimeter accuracies being reported for single discharge tests. Further review of analogous processes utilizing acoustic emission sensors such as pipe leakage detection and partial discharge localization in transformers indicate that the development of a method for mapping EDM discharges is promising.

The main issue surrounding the use of acoustic emission sensors with electrical discharge machining is the fact that the discharges are occurring at such a fast rate (~10^5 Hz) that extreme interference between signals is present. For this reason, it was necessary to examine various data processing techniques to be used to handle such data. Cross correlation, wavelets, STFT and power spectral densities were identified as useful tools in time of arrival determinations and data processing in situations where extensive noise was present.

This thesis intends to focus on two specific applications for discharge mapping through acoustic emission signals. The first application being the workpiece height identification during the wire EDM process. Currently, the methods for estimating the workpiece height are based on sparking frequency which as discussed is not a parameter that is only dependent on workpiece height. The development of an AE method to detect true workpiece heights and optimize parameters accordingly would be beneficial in preventing wire breakage. Finally, due to a high amount of electrode wear in fast hole EDM there are problems determining true machining depth and the full breakout of the electrode. By determining the exact location of the discharges, these problems could be minimized and the fast hole EDM process could be improved.

Chapter 3

Experimental

A variety of experiments will be performed to develop the method for discharge mapping through the use of acoustic emission sensors. Using a ram-type EDM, a suitable setup will be created to perform experiments that simulate both a wire or fast hole EDM process. By altering the time between successive discharges, the accuracy of the developed method can be determined for both ideal single discharges and for conditions that are representative of those that one would find in industry.

3.1 Experimental Setup

Experiments were performed in the Machining Systems Laboratory (MSL) at McMaster University. These experiments were performed on an AGIETRON Impact 2 Ram-type EDM. Since the experiments were performed on a ram type machine, a setup was created to simulate a wire EDM configuration as shown in Figure 3.1. Since the fast hole EDM electrodes are of the same diameter as the wire used in the wire EDM experiments, the same setup can be used in the fast hole EDM configuration as well as will be discussed.

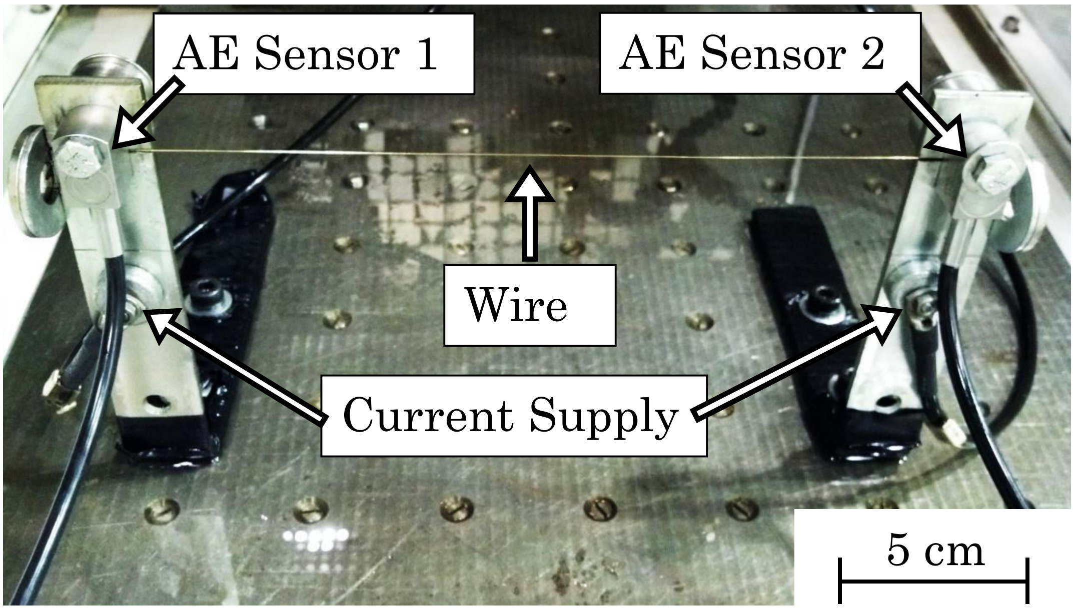

Figure 3.1: Wire EDM setup.

Slotted brackets were affixed to the table and the wire was held across both, or alternatively a fast hole electrode in just one. The acoustic emission sensor was bolted to the bracket such that the sensor is in direct contact with the wire in the slot. This is extremely important as it allows for the best transmission of the sound wave between wire and sensor. If there is a layer of dielectric fluid between the sensor and wire it affects the quality of the signal. A copper electrode of various sizes can then be plunged into the wire or fast hole electrode creating discharges, the locations of which were measured. In this case the copper electrode acts as a normal wire EDM workpiece would.

AE data was collected using Kistler type 8152B211 acoustic emission sensors in a data acquisition program written in MATLAB. The data collection is performed by a National Instruments PCI-6115 S series data acquisition (DAQ) board. This particular DAQ features a maximum sampling rate of 10 MHz per channel. This was the sampling rate used and allows for a time resolution of 0.1 µs. Due to the high sampling rate a fast write speed is required which is accommodated by a series of hard drives in a RAID format. Another concern with such a high sampling rate is the memory limitations of the computer. In order to ensure the MATLAB acquisition program does not exceed the memory capabilities of the computer, the tests were collected in 0.2 s increments. A current sensor was added to the third channel of the DAQ and was used to determine the time at which the discharge occurs.

3.1.1 Wire EDM Setup

For these experiments the sensors were located 250 mm apart as shown in Figure 3.2. The measurement is taken from centre point to centre point of the sensors as the piezoelectric ceramic sensing element is centred within the housing of the sensor [51].

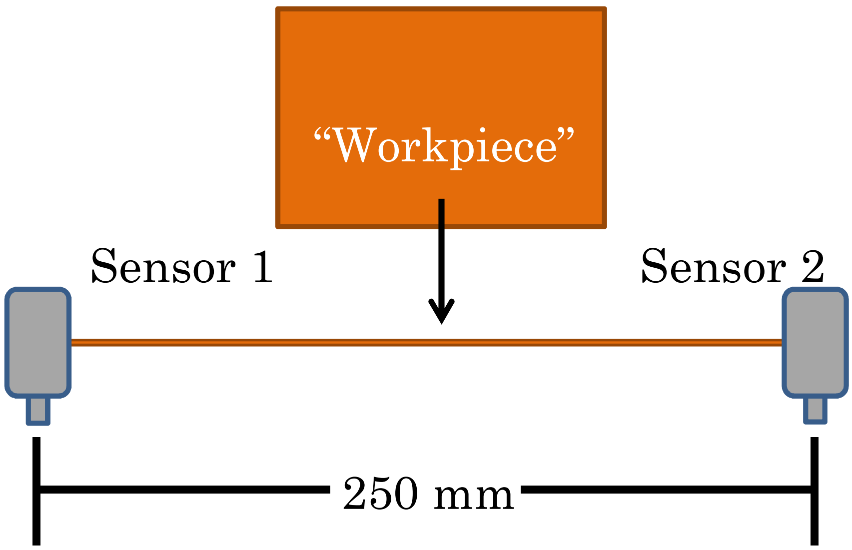

Figure 3.2: Schematic of wire experiments.

Two different types of wires were used in this experiment, with the majority of experiments using Initech brass 0.254 mm diameter EDM wire. For comparison purposes Thermocompact Thermo A 0.254 mm diameter wire was also investigated. This wire features a zinc coating on a brass core and was used to explore the effect this coating has on acoustic wave transmission. The workpieces used were made of copper and were 23 mm, 50 mm, and 90 mm in width. The workpieces were plunged into the wire as shown in Figure 3.2.

The tests were performed using slightly modified electrical parameters from the manual supplied with the EDM machine tool. The base parameters used will be those for copper – copper machining since no copper – brass parameters were available. The important parameters are tabulated in Table 3.1.

Table 3.1: Wire EDM test parameters.

On-Time	Off-Time	Discharge Voltage	Current	Polarity
1.12 μs	10-1000 μs	80 V	10 A	-

The on-time refers to amount of time the machine operator sets for the current to flow between the electrode and wire. Due to a time delay between the dielectric breakdown and the beginning of the current flow, the actual time the current has to flow between the electrode and wire is typically less than the set on-time. The off-time refers to the amount of time the machine allows the dielectric fluid to regain its dielectric strength before the next discharge is allowed to occur. The voltage refers to the voltage amplitude that is reached in the voltage waveform when the discharge occurs. A voltage of 80 V is relatively low and is used to ensure that wire breakage is not a problem during single spark tests. Current refers to the maximum amplitude of the current during the discharge. Finally, polarity is the definition of the electric charge on the electrode. In this case the polarity is negative which means that electrode is the anode. Throughout the tests, all parameters were held constant with the exception of off-time. The off-time was varied to create either a small or large separation between two subsequent discharges for purposes of investigating and resolving interfering acoustic waves.

3.1.2 Fast Hole EDM Setup

The fast hole electrode was supported by only one bracket and as such only one sensor was used during these discharge location tests. The setup and direction of workpiece movement is shown in Figure 3.3.

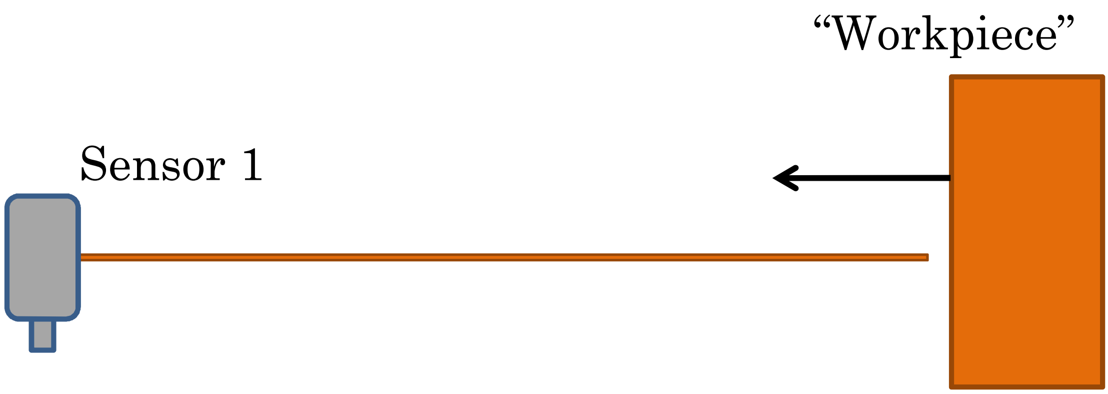

Figure 3.3: Fast hole experiment schematic.

For the fast hole experiments single channel brass electrodes with an outer diameter of 0.3 mm were used. The electrode length varied throughout the experiments ranging from 32.5 mm to 125.5 mm in order to determine the ability to detect various electrode lengths. As Figure 3.3 shows, the workpiece was used to machine the free end of the electrode.

The following parameters are typical for fast hole EDM machining with a 0.3 mm diameter electrode in industry and are therefore used for testing:

Table 3.2: Fast hole EDM test parameters.

On-Time	Off-Time	Voltage	Current	Polarity
12 μs	12 μs	80 V	13 A	-

3.2 Acoustic Emission Sensors

As previously mentioned the acoustic emission sensors used were Kistler type 8152B211 sensors. An important feature of these sensors is that they are hermetically sealed providing the ability to be operated fully submerged in the dielectric fluid. This sensor has a uniform sensitivity in the range of 100 kHz to 900 kHz as seen in Figure 3.4 (dotted line).

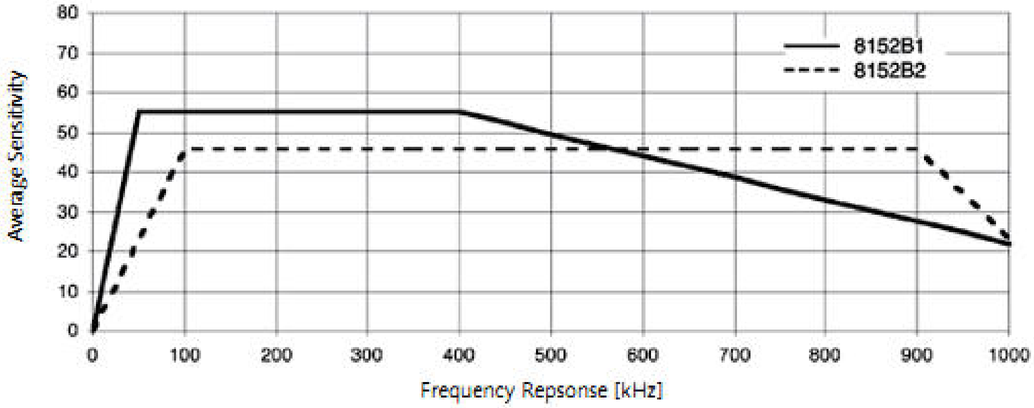

Figure 3.4: Average sensitivity for sensors across wide frequency band [51].

These sensors differ from the custom made ultrasonic sensors developed by Ydreskog and Novak [22] as well as Muto et al. [23] by being highly sensitive to the Rayleigh/Lamb surface waves [51] which as discussed in Section 1.2.1 carry the majority of the energy associated with the acoustic wave. By using commercially available sensors which operate at much lower frequencies the cost will be reduced and so will the computational load on the data acquisition hardware as much lower sampling rates can be used.

Before being connected to the DAQ the sensors were first connected to an amplifier which amplifies the signal by either a factor of 10 or 100. It has been seen that for the brass wire and experimental parameters a factor of 100 does not saturate the signal. It is important that saturation of the signal does not occur as it will affect later analysis. The preamplifier also comes equipped with a high pass filter of 50 kHz and a low pass filter of 1 MHz, which can be manually changed if needed. Since it is of interest to explore the entire frequency range of the sensors, these low and high pass filters are left as is for these tests.

Using the experimental setup outlined above, the following chapter will describe the development of the proposed method to use commercial acoustic emission sensors to determine discharge location. The experiments will begin by exploring the characteristics of individual acoustic emission waves and progress to the point where calculation of wire EDM workpiece height and fast hole electrode length are investigated.

Chapter 4

Results and Discussion

With an understanding of acoustic emission testing, present EDM discharge mapping techniques as well as various data processing methods, the development of an EDM discharge mapping method using acoustic emission sensors will now be presented. An examination of data processing techniques will be completed in order to determine the best method for obtaining accurate and repeatable time lags from acoustic emission signals. After obtaining these time lags and developing a relationship between discharge location and time lag, the issue of workpiece height identification and fast hole electrode length determination will be explored.

4.1 Examination of AE Signal from EDM Discharge

It is important to begin source location determination by examining single spark experiments to verify the suitability of various analysis methods under ideal conditions. Creating single sparks as opposed to a quick succession of discharges allows source location to occur without any interference from previous sparks. In order to create a single spark scenario, a “thin” electrode of 0.3 mm thickness was used to create a spark at a known location. The sparks are repeated at 1000 μs intervals allowing for the complete attenuation of any previous discharges.

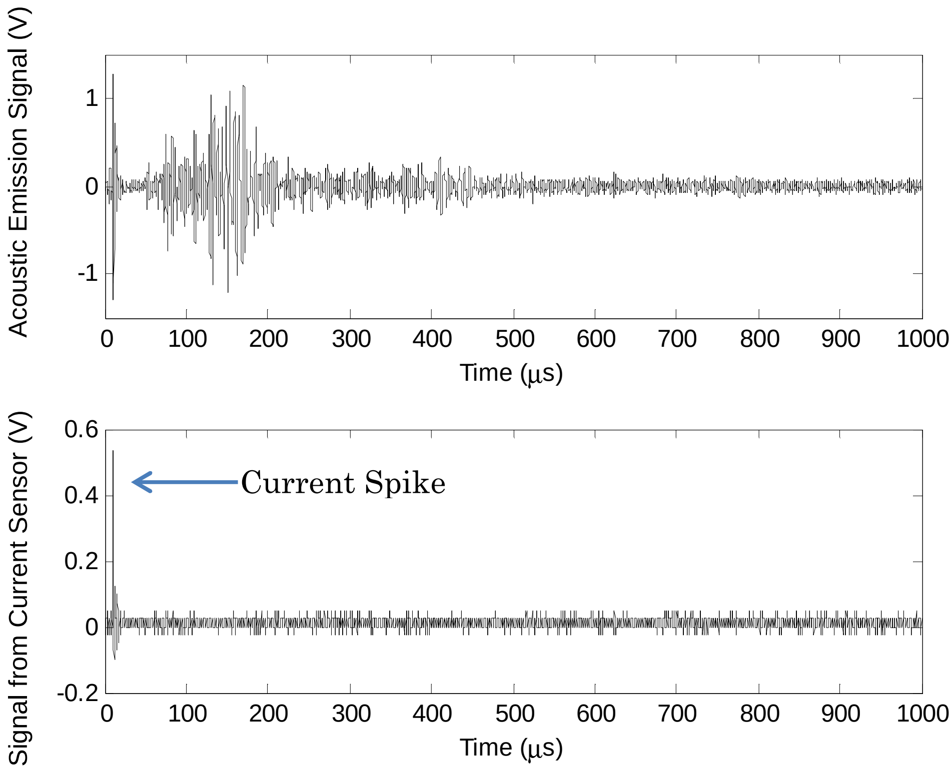

Figure 4.1 Output from acoustic emission sensor (top) and current sensor (bottom).

In Figure 4.1 we see a time delay of approximately 50 μs from the time the current is initialized to when the acoustic wave is received at the sensor. The bulk of the acoustic energy is then attenuated after approximately 250 μs, with low amplitude remnants of this acoustic wave still present for another 250 μs. It can be seen that for these tests 1000 μs is a sufficient amount of time to allow for the complete attenuation of acoustic waves between two discharges.

The most important information with regards to the determination of source location is contained in the first 200 μs where the bulk of the acoustic energy is present as seen in Figure 4.2. When analyzing the acoustic signal, it is only necessary to focus on the beginning of the signal where the bulk of the acoustic energy is seen. This reduces the amount of processing that is required, saving computational load and time.

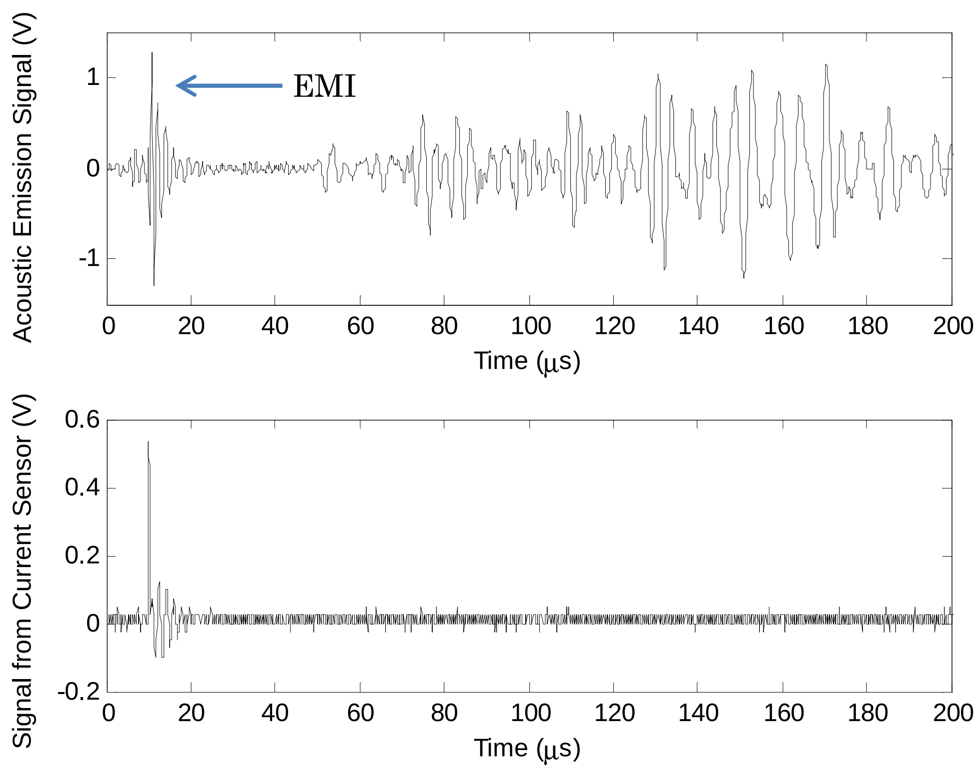

Figure 4.2: A look at the dominant segment of the acoustic wave.

The EMI generated by the process can be clearly seen in the raw AE signal shown in Figure 4.2. This agrees with results by other researchers [11,22] where an EMI signal occurring at the creation of the discharge is seen. In this case the EMI is larger in amplitude than the actual surface wave created by the discharge, which causes problems when a quick succession of sparks is created. For this reason, it is important that any analysis method used in the determination of acoustic wave arrival times must be robust against these high magnitude noise signals.

4.2 Arrival Time Analysis Methods

The applicability of several analysis methods will be discussed in this section. Initial analysis will be performed on 20 single spark acoustic waves at 7 known locations along the wire as shown in Figure 4.3. The order of the tests is randomized to ensure that the results are not susceptible to any trends resulting from unknown variables that may be a function of machining time.

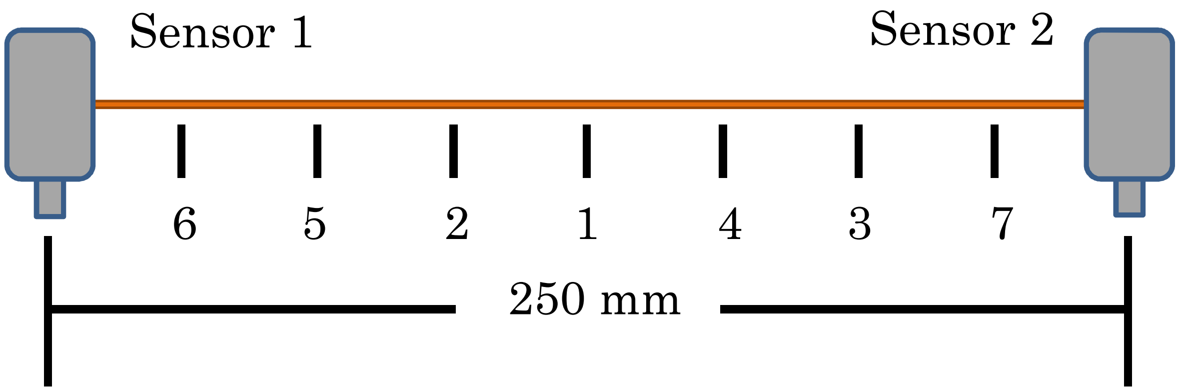

Figure 4.3: Single spark experimental setup.

For clarity sake the spark location will be measured from sensor 1 as shown in Figure 4.3. The distance between the two sensors was set to be 250 mm, and the tests will correspond to a spacing of 31.25 mm.

4.2.1 Cross Correlation Time Lag Determination

As discussed in Section 2.5.1, cross correlation measures the 'similarity' between two signals as the cross correlation coefficient. Throughout these experiments the signal from sensor 2 is used to determine time lags relative to the signal from sensor 1. This means that when the discharge is located closer to sensor 1 the lag will be negative. This is the scenario shown in Figure 4.4.

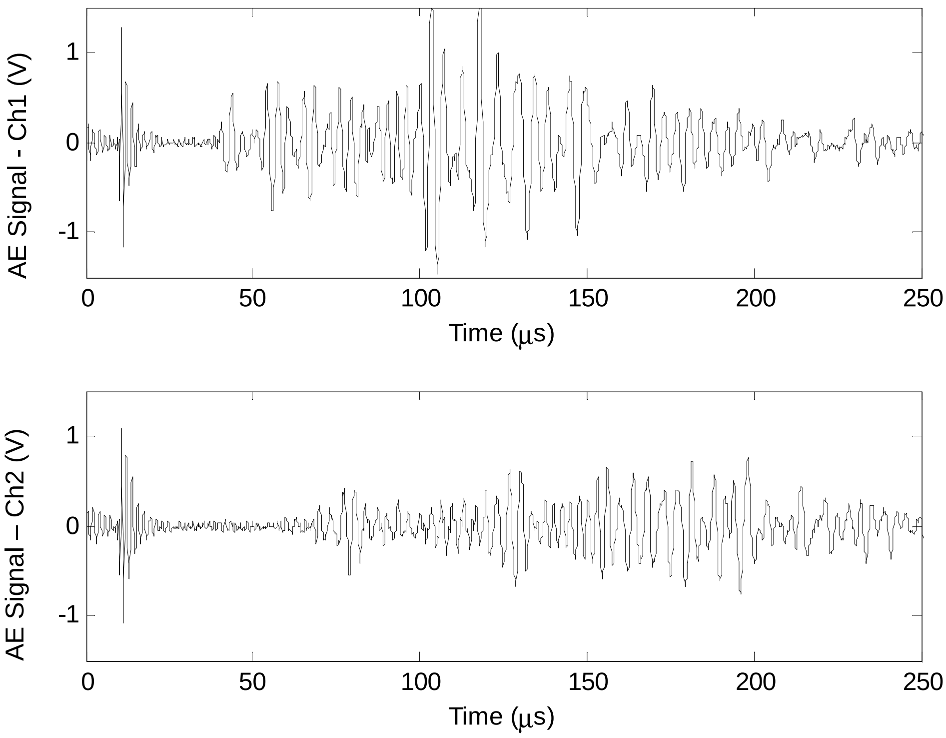

Figure 4.4: Acoustic emission signals showing discharge location to be closer to sensor 1.

The lag at which the cross correlation coefficient is maximized is deemed as the time lag between the two signals. The time lag between the signals shown in Figure 4.4 was determined by cross correlation in Figure 4.5 to be – 69.3 μs.

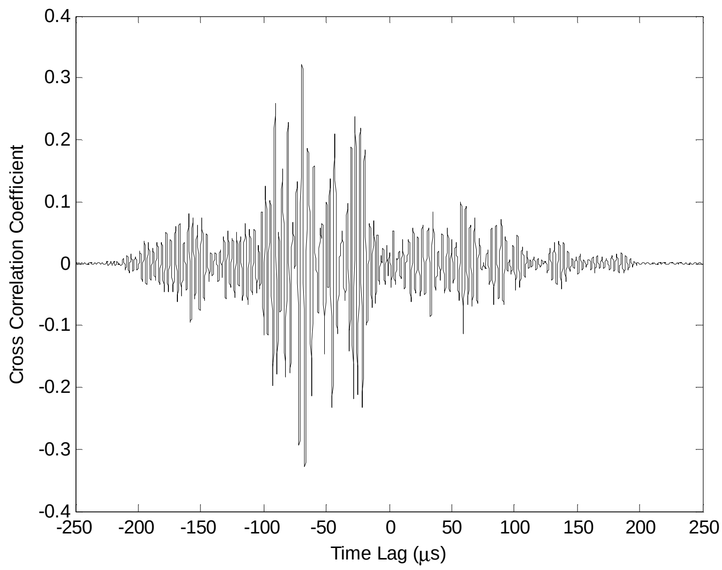

Figure 4.5: Output of cross correlation function for signals shown in Fig. 4.4.

By repeating this process for twenty signals at each location a relationship between time lags and real position was obtained through least squares fitting. The spark location exhibited a linear trend with respect to the time lag (Figure 4.6).

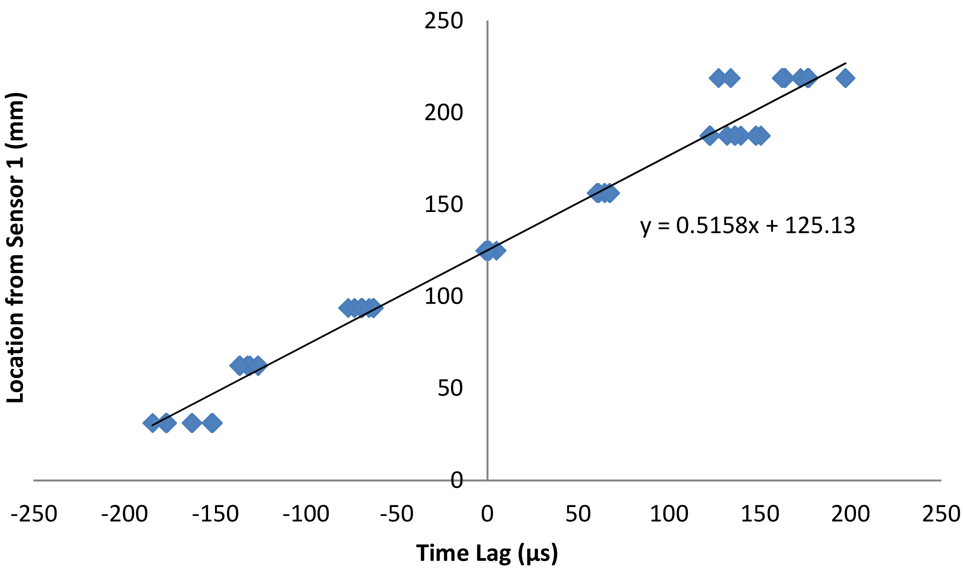

Figure 4.6: Location from sensor 1 vs. time lag obtained with cross correlation.

It can be seen that the range of time lags increases as the distance from the discharge to the midpoint between the two sensors increases. A box plot of the 25th and 75th percentiles of the error is shown in Figure 4.7. The error is calculated by converting all time lags into locations using the relationship Location = 0.5158*(Time Lag) + 125.13, subtracting this calculated location from the known location of the discharge and taking the absolute value of this difference.

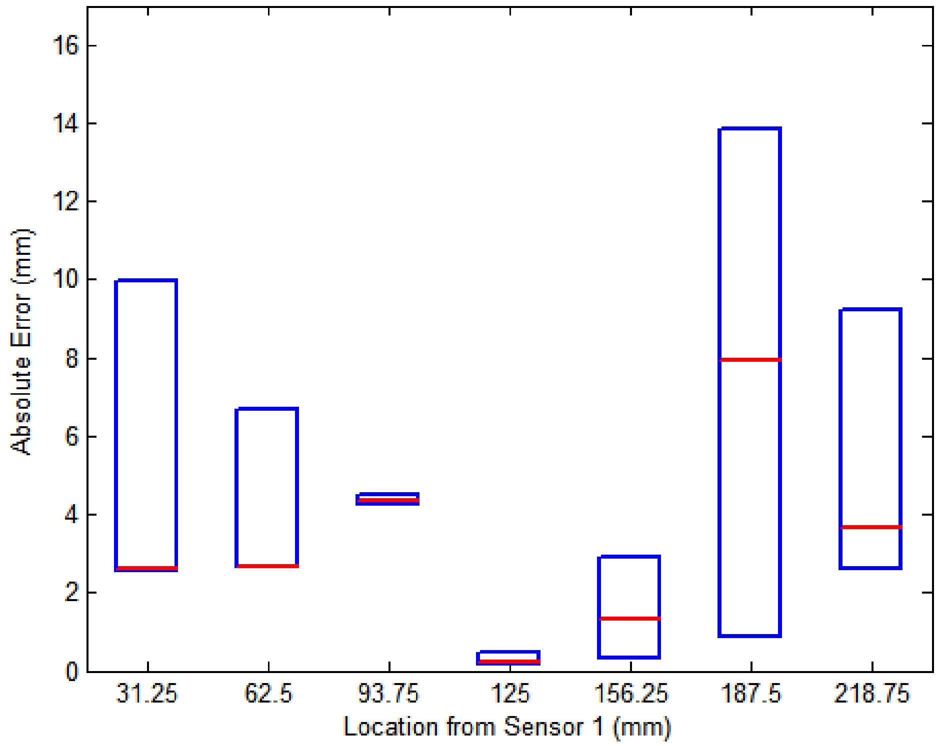

Figure 4.7: Box plot of location error with cross correlation method.

Using the 25th and 75th percentiles as a metric for examining the error it is seen that the error is minimized in the center of the setup with an error range of 0.18 mm – 0.45 mm. The increase in error is seen as the discharge location from the center increases, reaching a maximum range of 0.91 mm – 13.87 mm at a location 187.5 mm from sensor 1.

Figure 4.8 gives an insight as to the reasoning for the increase in error that is seen when the discharges are located closer to one sensor than the other. Due to attenuation of the acoustic signal along the wire, the wave that is detected by acoustic emission sensor 2 is much lower in amplitude than the signal picked up by sensor 1. Since the cross correlation takes the whole signal window into account during calculation, background noise has a much greater effect on the cross correlation when the signal to noise ratio of the signal from one sensor decreases.

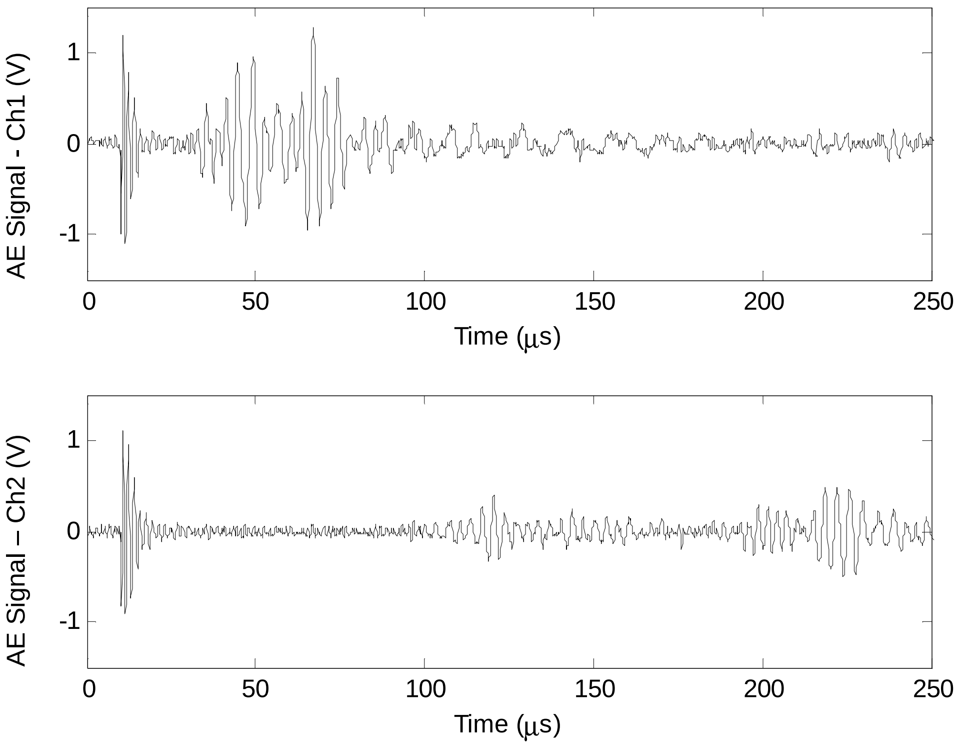

Figure 4.8: Spark discharged 31.25 mm from sensor 1, (218.75 mm from sensor 2).

4.2.2 Arrival Time from Threshold on AE Signal

Another method for determining the time of arrival of the acoustic wave is by measuring the time it takes from the beginning of the current discharge to when it first crosses a set threshold amplitude. An examination of the effect of this threshold magnitude is presented in this section. In order to take into account the negative values in the acoustic waves, the thresholds refer to the absolute value of the signal. Threshold values of 0.2 V, 0.3 V, 0.4 V, 0.5 V will be used to determine the effect of threshold amplitude on source location.

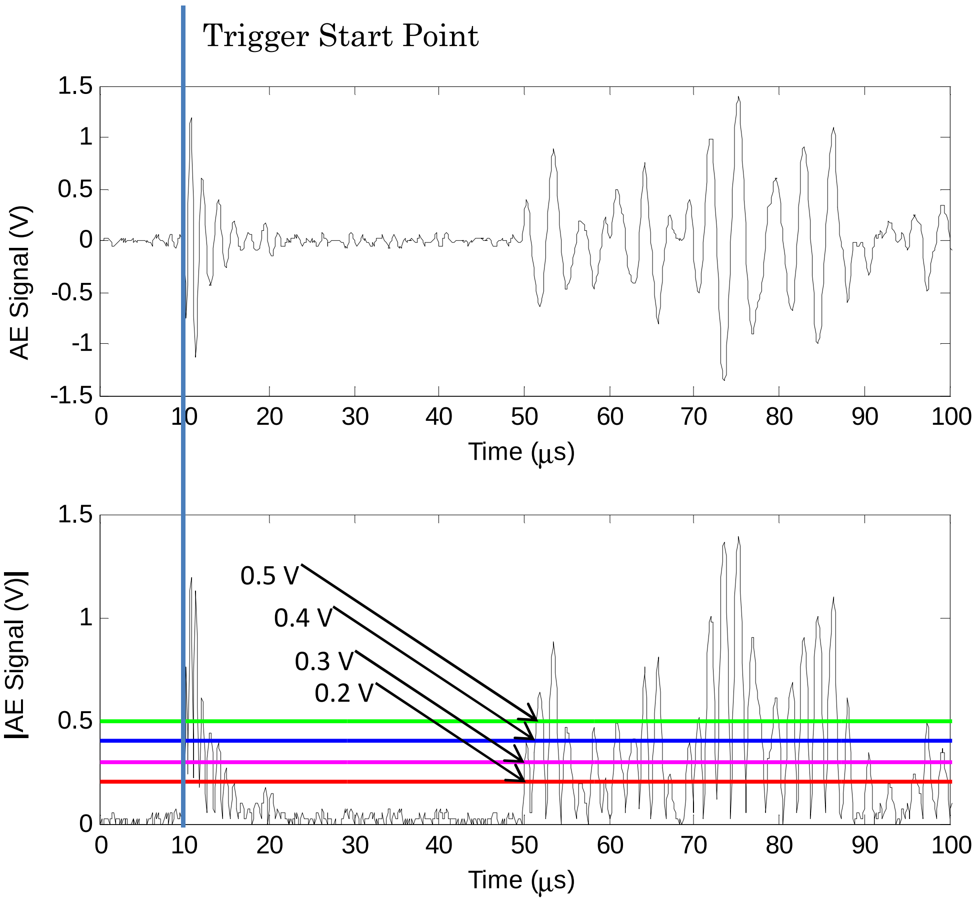

Figure 4.9: Threshold method for determining time lag; original signal (top) absolute value of signal with thresholds (bottom).

The main area of concern with the threshold method is the ability to provide repeatable time lag values for a single discharge location.

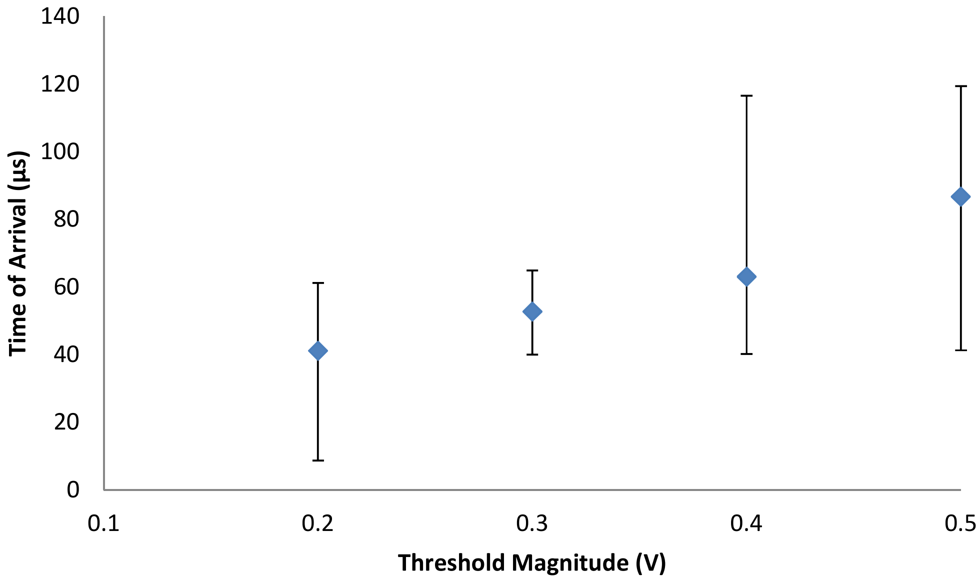

Figure 4.10: Time of arrival for discharges located 125 mm away from sensor, using threshold values.

Figure 4.10 shows the average time of arrival values for 20 discharge signals based on the various threshold levels, with error bars representing the maximum and minimum arrival times. While Figure 4.10 only shows results for discharges located 125 mm away from the sensor, results are similar for other locations and often showing an even greater range of arrival times. By using the average arrival time to determine speed of sound (Speed of sound $= \frac{125\text{ mm}}{\text{Arrival Time}}$) the error can then be expressed in terms of position by multiplying all arrival times by this speed of sound. The average arrival times ranges from 3040 m/s for a threshold voltage of 0.2 V, down to 1441 m/s for a threshold voltage of 0.4 V. A speed of sound of

3040 m/s is similar to what is expected for this configuration [10], while 1441 m/s is an extreme underestimate of the speed of sound in a brass wire.

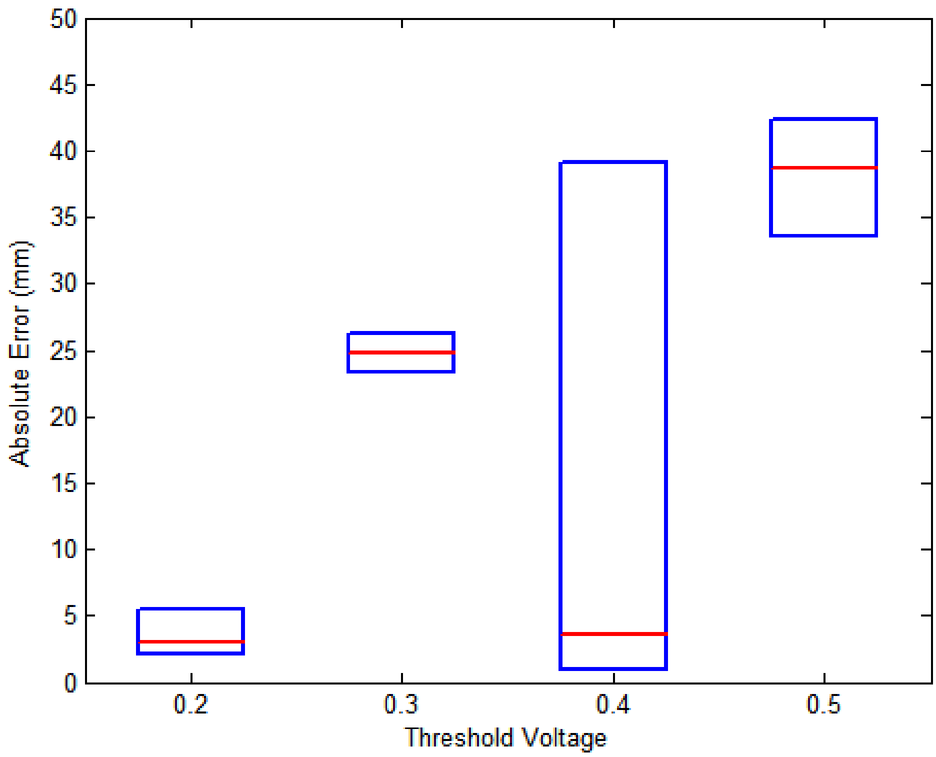

Figure 4.11: Error in location calculation with threshold method.

It can be seen in Figure 4.11 that as the threshold increases, the range of determined arrival times also increases owing to the fact that each acoustic wave is not created equal. More often than not, the lower threshold 0.2 V detects the first peak of the acoustic wave leading to its lower variability this is seen in a $25^{th}/75^{th}$ percentile error range of 2.07 mm – 4.81 mm. The 0.5 V threshold will detect a different peak for each signal leading to extensive error ranging from 33.6 mm – 41.88mm or approximately 25% of the real location. Referring to

Figure 4.9 it becomes clear as to why the 0.4 V threshold has such a large range in error. The first peak of the acoustic wave is approximately 0.4 V, this means that the threshold will detect this peak resulting in consistent arrival times and low error values, but at the same time will often barely miss this peak to create an extremely large error by detecting a completely different peak, the combination of extremely good and extremely poor detection leads to the large error range seen. It is important to note that decreasing threshold magnitude further does not necessarily decrease error in location detection as lower threshold values could refer to background noise as the onset of acoustic waves. Another issue with threshold time of arrival detection is that the amplitudes of the acoustic waves vary depending on their location due to attenuation. This makes choosing one threshold value which is suitable for a wide range of acoustic wave amplitudes rather difficult. It is clear that in order to accurately determine the arrival time a consistent fixed reference point on the acoustic wave is needed, which will be discussed in Section 4.2.3 following.

4.2.3 Arrival Time from Fixed Reference Point on AE Signal

Using a fixed reference point in order to determine the time of arrival of the acoustic wave can help ensure consistent results. The first fixed reference point to be investigated will be the onset of the acoustic wave. For the purposes of this discussion, the onset of the acoustic wave will be considered to be the first peak of the acoustic wave as seen in Figure 4.12. The background noise will be considered to be contained within a +/- 0.1 V boundary, meaning that the first peak of the acoustic wave will be the first peak of the AE signal once it has crossed this 0.1 V threshold.

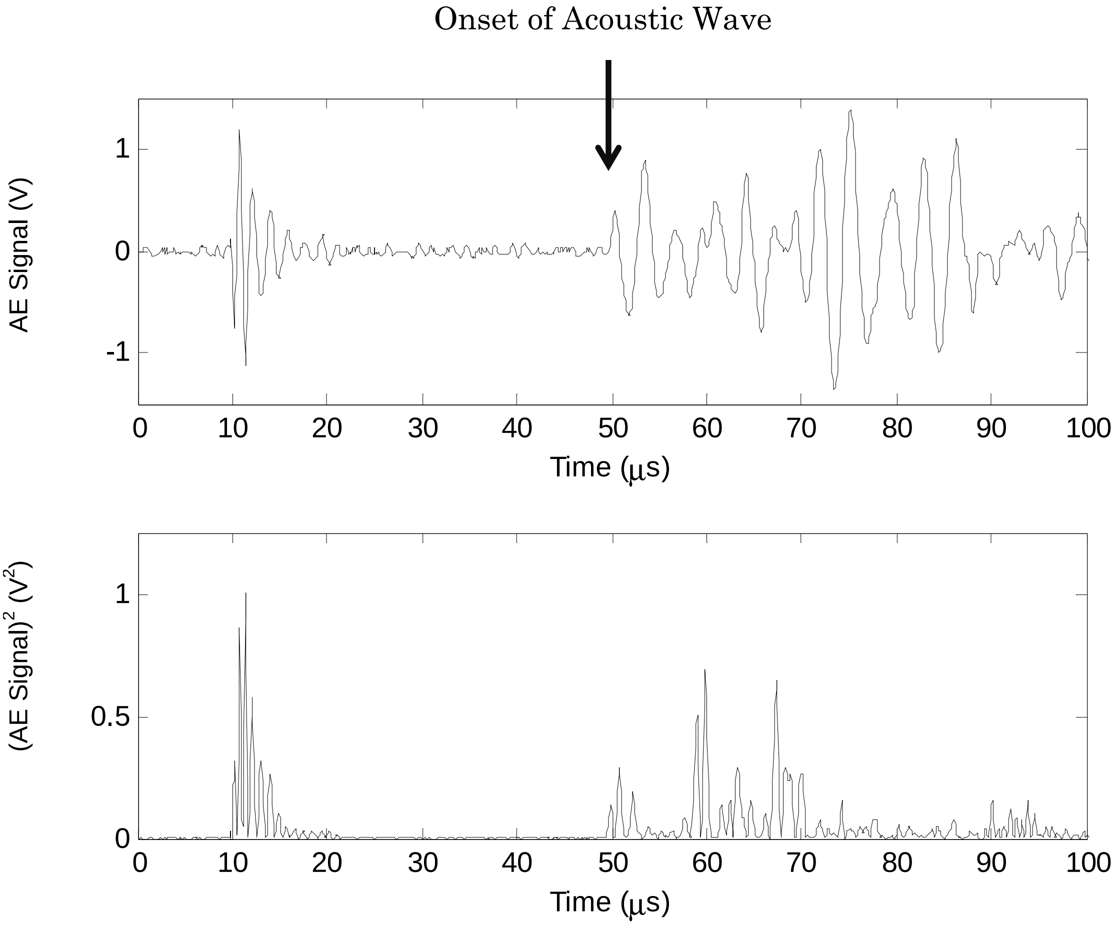

Figure 4.12 : Method for determining onset of AE wave using fixed reference; Original signal (top), Amplitude of signal squared (bottom).

Howells and Norton [33] noted that it is often useful to square the signal in order to help determine the onset of the acoustic wave when the signal to noise ratio is relatively low.

The average arrival times are plotted for each known sensor location, obtaining the relationship: $\text{Location} = 3.1669 * (\text{Arrival Time}) - 4.2412$. The slope of this line corresponds to the calculated speed of sound in the material as 3166.9 m/s. In thin rods, the three wave modes (longitudinal, shear, surface) combine together to produce a “thin rod velocity” [10]. Given the various possible compositions of brass, the calculated acoustic velocity in the brass wire of 3166.9 m/s is similar to reported values of 3500 m/s for brass [10].

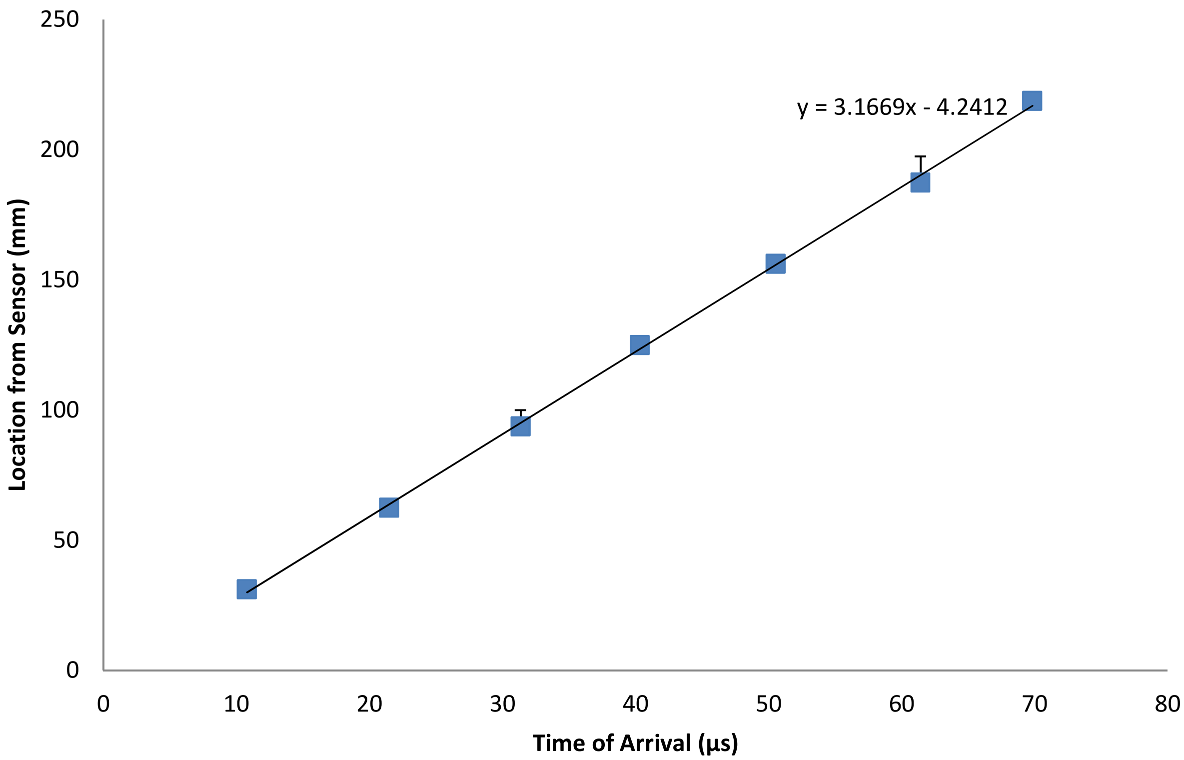

Figure 4.13: First peak determination of arrival time.

The relationship obtained in Figure 4.13 is used to determine the calculated location of all signals at each true location. Comparing the calculated locations to true locations yields an absolute error value. These error values are shown in Figure 4.14.

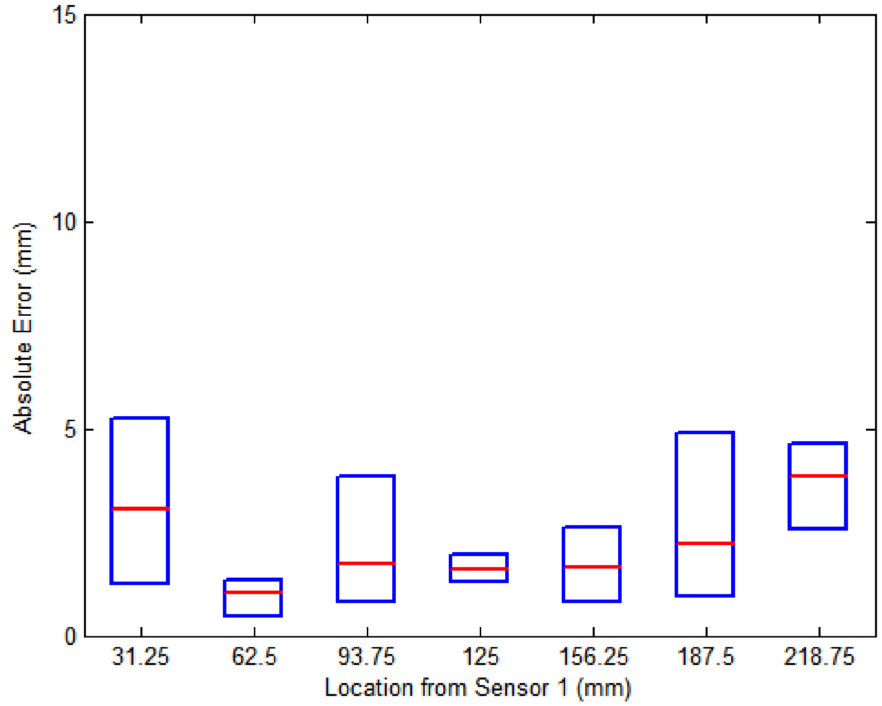

Figure 4.14: Location error with fixed reference method.

There is an improvement in overall error over both the cross correlation (Figure 4.7) and thresholding methods (Figure 4.11), with error for all locations falling within 0.51 mm - 5.17 mm. The cross correlation method for determining time lags still has the minimum error seen, but this only occurs at one specialized location (exact midpoint between sensors) and the fixed reference method is shown to minimize error at all other locations. The error in the fixed reference method was discussed in Section 2.2.3 (referring to Figure 2.9) with attenuation causing difficulties in determining the leading edge for acoustic waves that have travelled relatively long distances. Figure 4.15 shows a strong signal where it is easy to determine the first peak of the acoustic wave from both the acoustic signal and the squared amplitude of the signal. Alternatively, Figure 4.16 shows a lower amplitude signal where it is difficult to determine the first peak.

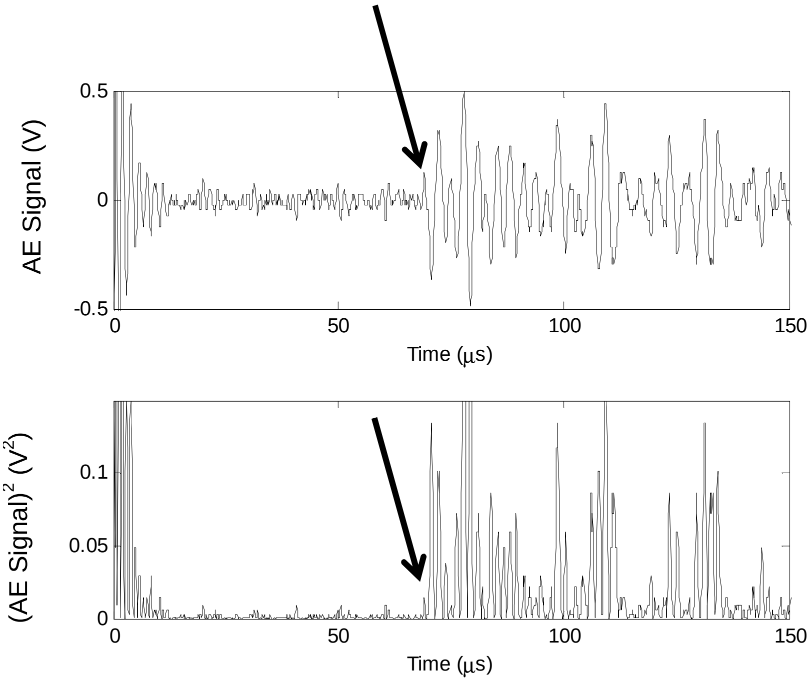

Figure 4.15: Example of an easy-to-determine first AE peak.

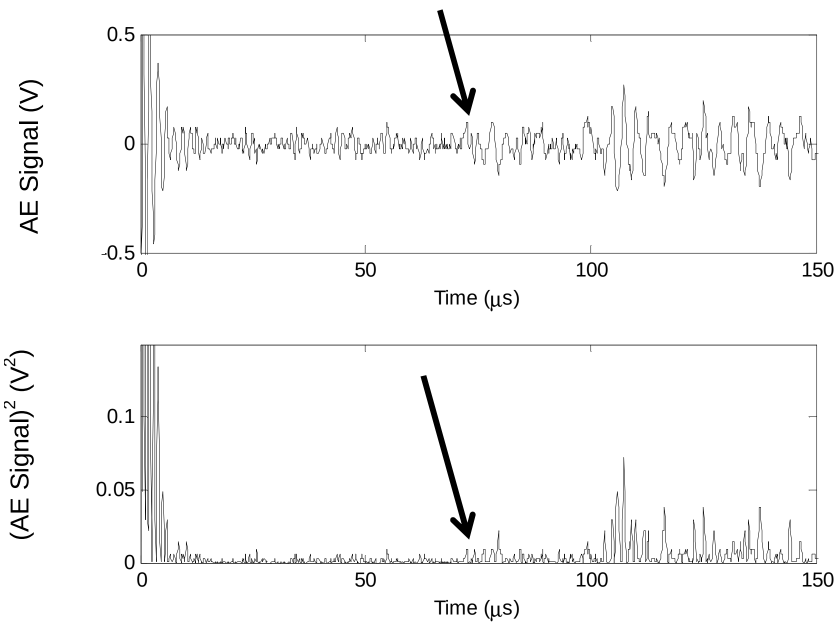

Figure 4.16: Example of a difficult-to-determine first AE peak.

A fixed reference method that is not affected by noise and attenuation will be discussed later in Section 4.4.3 as it is first appropriate to discuss signal interference.

4.3 Effect of Off-Time on Signal Analysis

As discussed, initial tests were performed on single sparks to show proof of concept. It was shown that the best results were achieved with the use of a fixed reference point, however using the first peak as a reference has some difficulties even on an ideal single spark. An off-time of 1000 μs is also unrealistic in EDM practice with much lower off-times used to ensure faster machining. Figures 4.17 through 4.19 show the effect of decreasing off-time on the signal in terms of the interference of two acoustic emission signals.

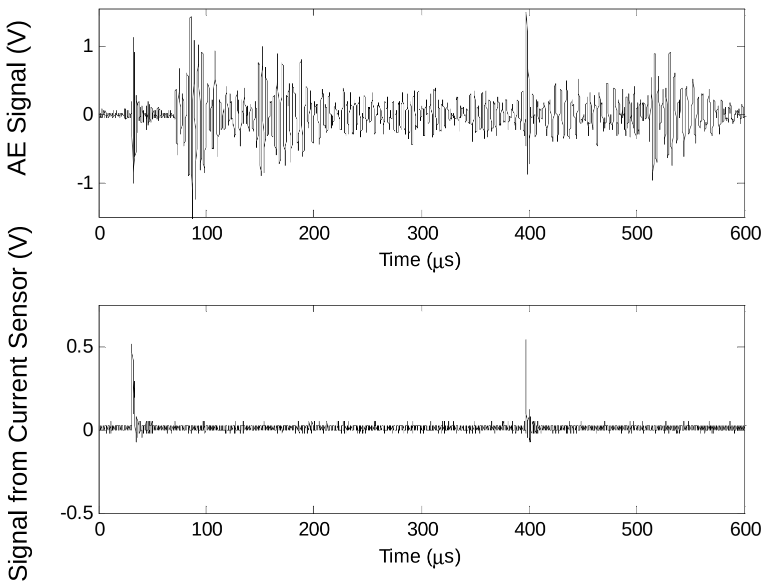

Figure 4.17: Consecutive discharges, 360 μs off-time.

Even at a relatively large off-time of 360 μs (Figure 4.17), the ability to discern the start of the second wave is compromised due to the interference from the previous acoustic wave.

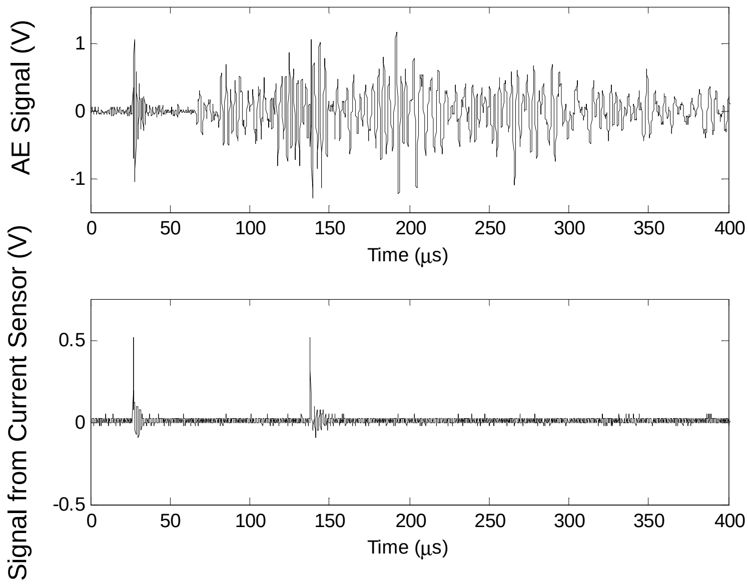

Figure 4.18: Consecutive discharges, 110 μs off-time.

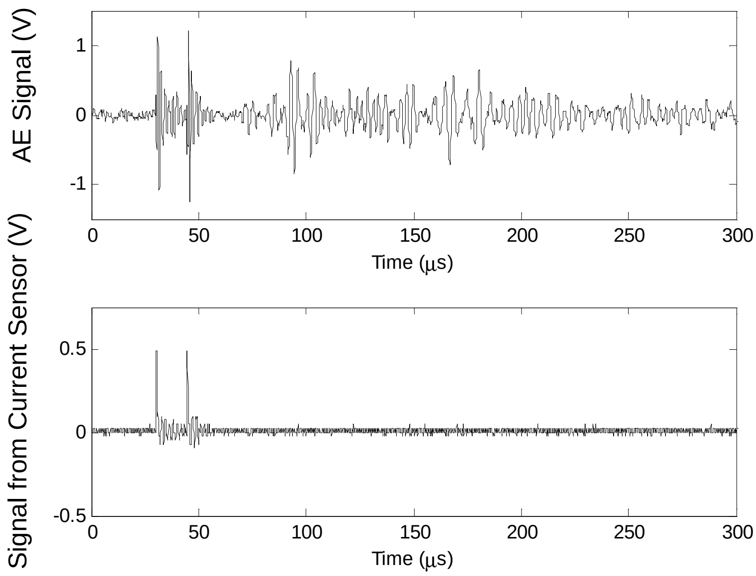

Figure 4.19: Consecutive discharges, 13 μs off-time.

As the off-time decreases further to 13 μs in Figure 4.19, it becomes hard to even differentiate the two signals to that of a single acoustic wave let alone determine the first peak of the second signal. It is hence necessary to determine a different characteristic feature on the acoustic wave rather than the first peak. Information gained from partial discharge and leak detection analysis, specifically the work of Ahadi, Bakhtiar and Cichon [26,33] make a more in-depth look into the frequency content of the acoustic waves the next logical step.

4.4 Frequency Content Analysis

There are two ways to explore the frequency content of the acoustic waves. First, a Fast Fourier Transform (FFT) will be used to give a broad overview of the dominant frequencies present in the signal. A more detailed examination of the progression of these frequencies through the use of a Short Time Fourier Transform (STFT) and a spectrogram will follow thereafter.

4.4.1 FFT Analysis of AE Signal

The raw AE signal of a typical discharge is shown in Figure 4.20a with the FFT of that signal being shown in Figure 4.20b. As seen by the FFT in Figure 4.20b there is a dominant frequency band from 150 kHz to 400 kHz with a peak occurring at approximately 300 kHz – 315 kHz. This range conforms with the findings of Cichon [32] on the frequency bands found in partial discharges. An FFT of the EMI will be performed separately from the sound wave in order to differentiate the frequency ranges of the two.

A closer look at the frequency spectrum of the EMI is seen in Figure 4.21, where it is seen that EMI has a characteristic frequency range above 500 kHz. As previously discussed, EMI is generated by a high frequency current oscillation caused by parasitic capacitance, as such it was expected that the EMI would be of higher frequency [12] and these results agree.

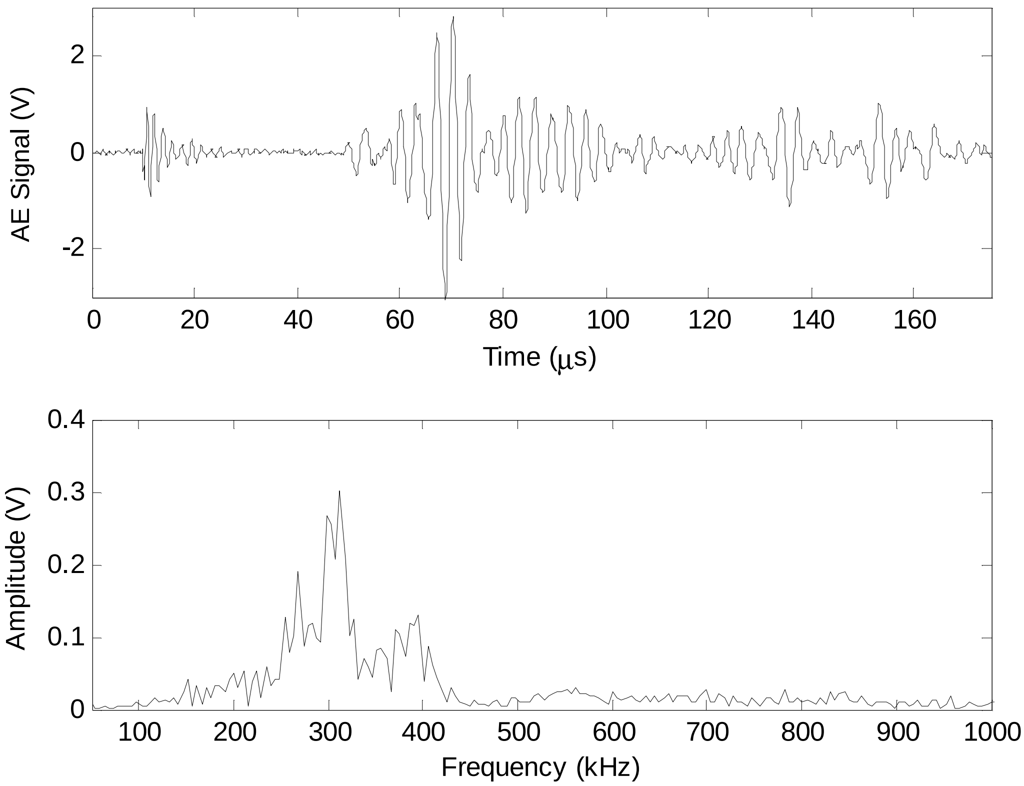

Figure 4.20: a) Raw AE signal including EMI, b) FFT of AE signal.

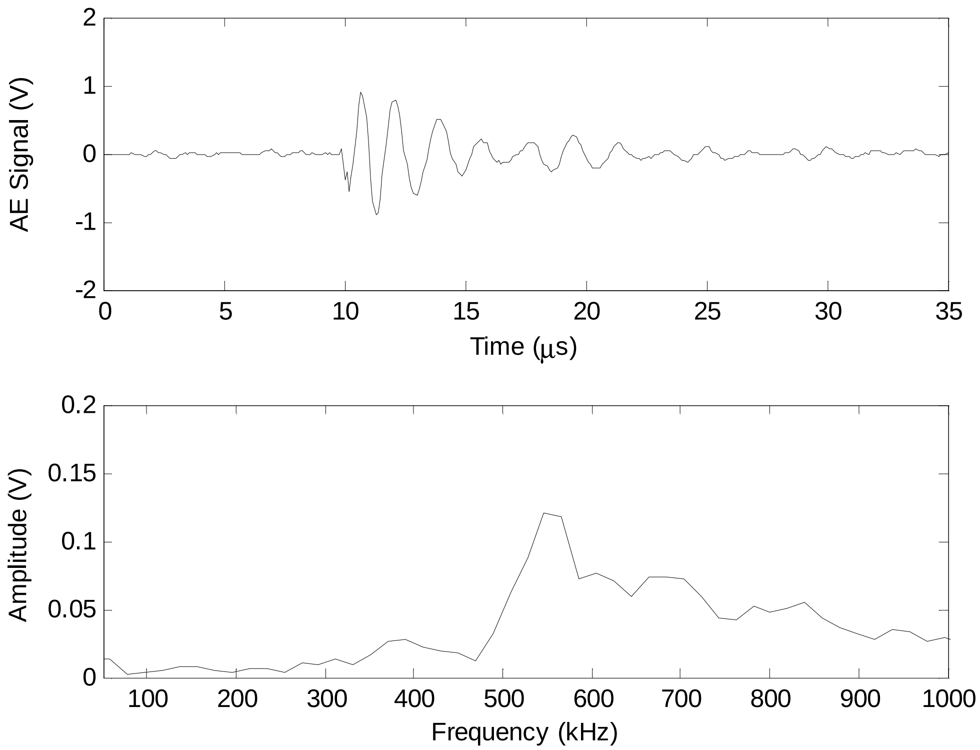

Figure 4.21: a) AE signal of isolated EMI, b) FFT of AE signal.

4.4.2 Fixed Reference Peak Determination using Spectrogram

The Fast Fourier Transform is useful in giving an understanding of the important frequencies in the acoustic emission signal; however it lacks the ability to show the evolution of these frequencies over the duration of the acoustic wave. In order to see how the frequencies progress over time a spectrogram is seen in Figure 4.22 of the acoustic wave shown in Figure 4.21a. As discussed, the spectrogram uses the Short Time Fourier Transform to calculate the power spectral density ($PSD = |STFT^2|$).

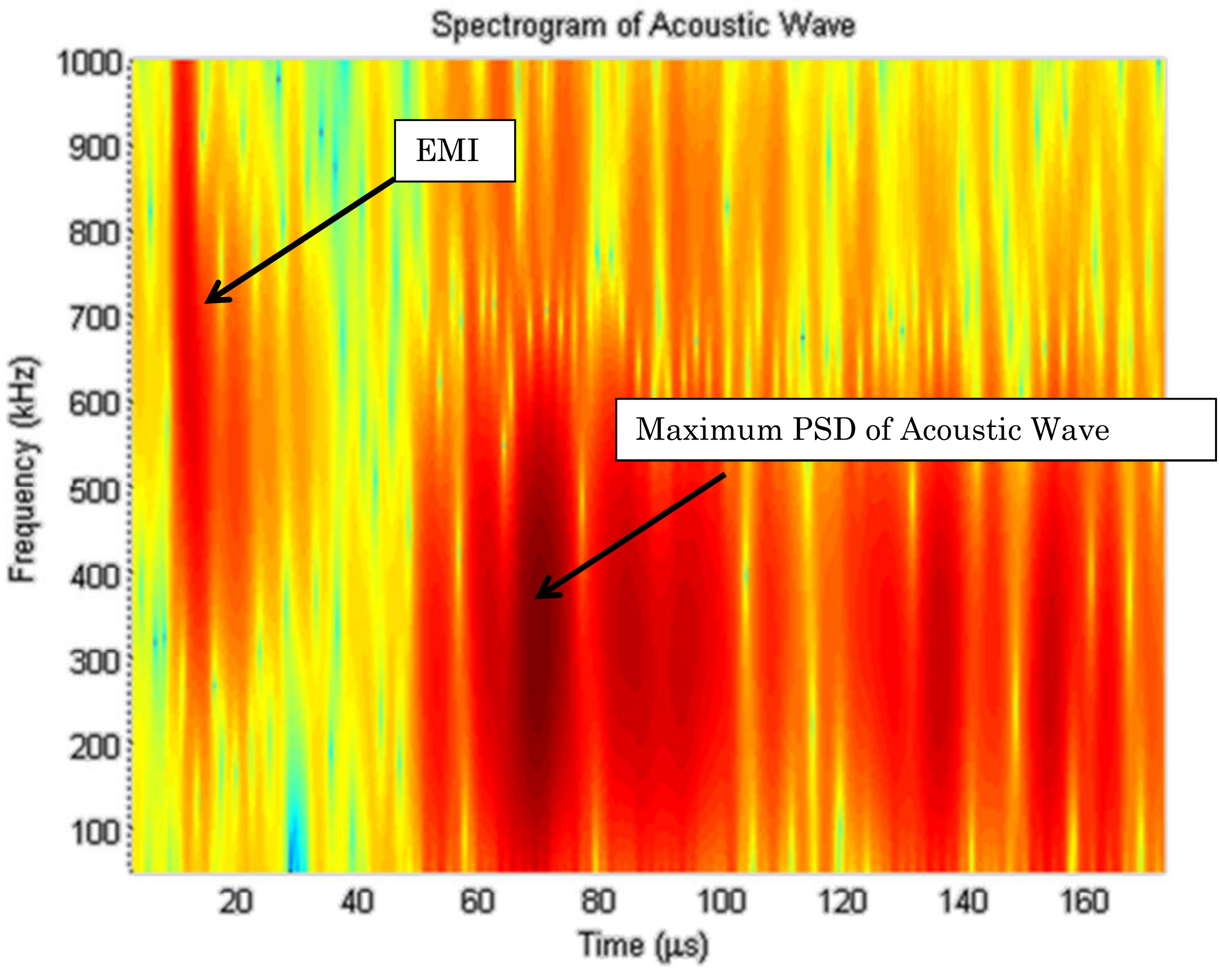

Figure 4.22: Spectrogram of acoustic wave.

The window used for the STFT was 5 µs with a 4.9 µs overlap to allow for a time resolution of 0.1 µs. The high frequency EMI is clearly seen at the 10 µs point of the signal, corresponding to the discharge. The acoustic wave starts roughly 40 µs after, with a peak in the spectrogram at approximately 70 µs. By taking a cross section of this surface at 300 kHz where the dominant frequency band occurs we can examine the power spectral density of the wave closer in Figure 4.23.

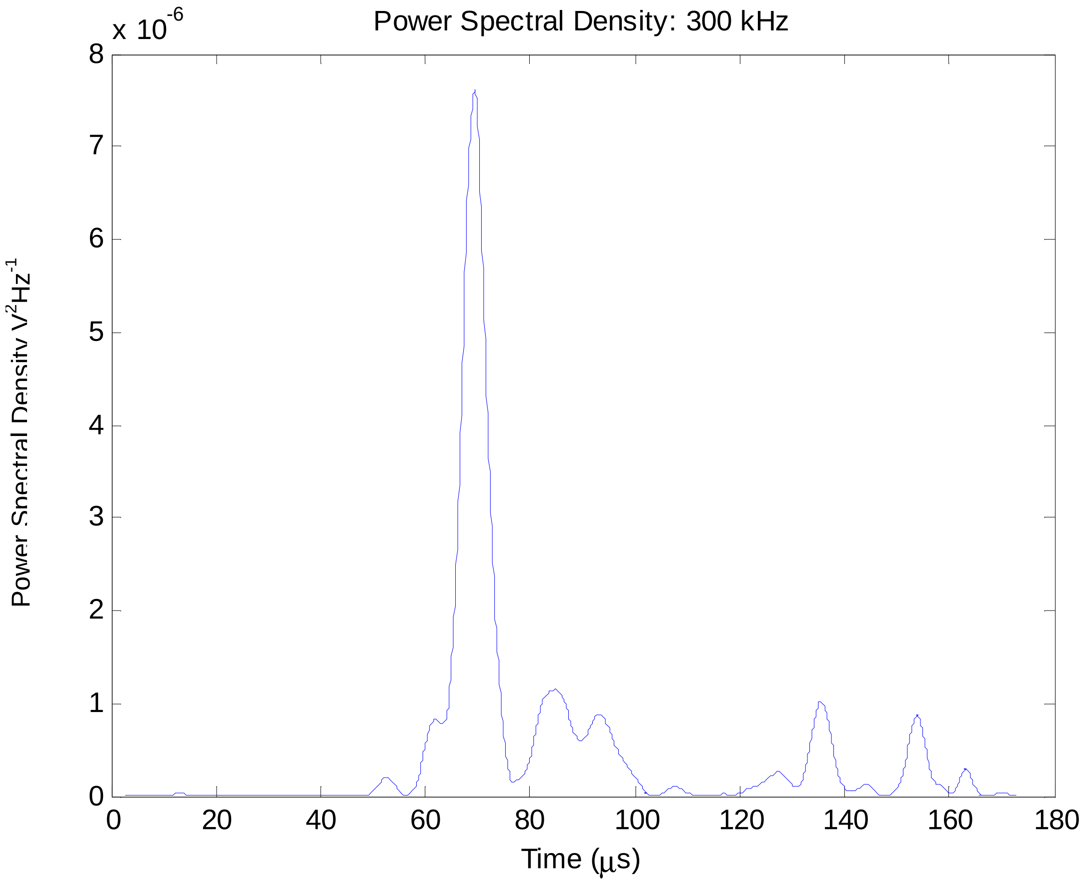

Figure 4.23: Power spectral density of acoustic wave at 300 kHz.

This examination method clearly shows the peak occurring at 69.4 μs, which is 59.4 μs from when the discharge occurred. Superimposing this information on the raw acoustic signal, Figure 4.24 shows that this peak occurs prior to the highest peak in the acoustic wave. This was observed to be consistent for each acoustic wave.

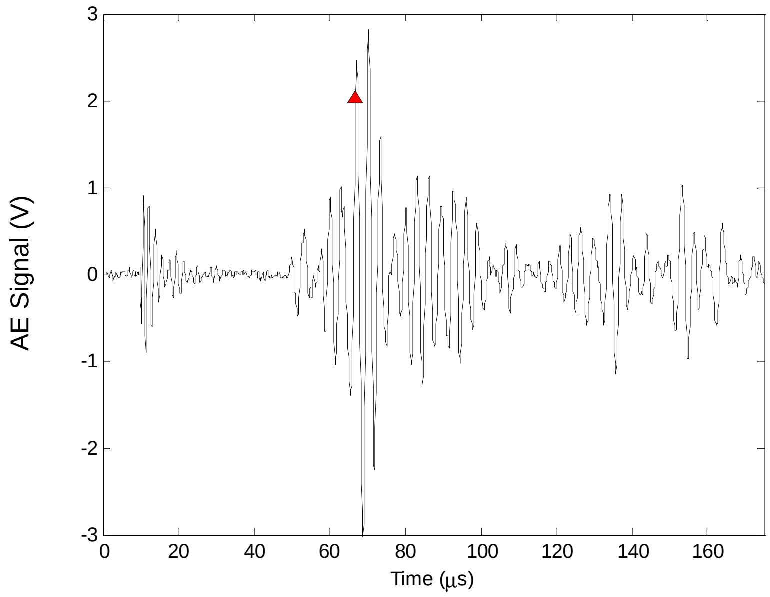

Figure 4.24: Location of PSD peak on AE signal.

Following the method for evaluating accuracy of previous methods presented in Section 4.2, the correlation between arrival time and real location is calculated on the basis of 20 signals at each location in Figure 4.25.

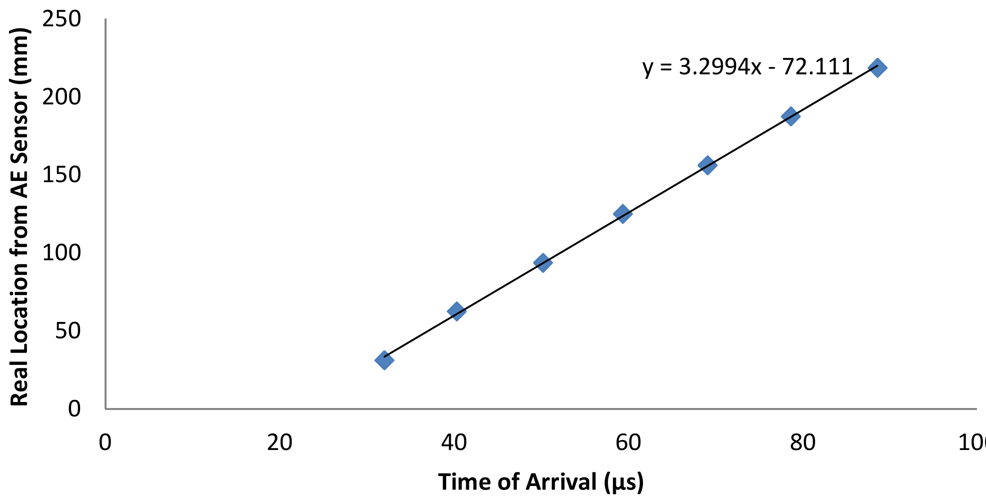

Figure 4.25: Calibration of time lags to real location from PSD method.

Note that according to the calibration equation seen in Figure 4.25, a time of arrival of zero does not correspond to a location calculation of zero millimeters away from sensor 1. This is due to the fact that the PSD method is detecting a point on the acoustic wave that is not at the very beginning of the wave. This adds a constant increase to all arrival time detections.

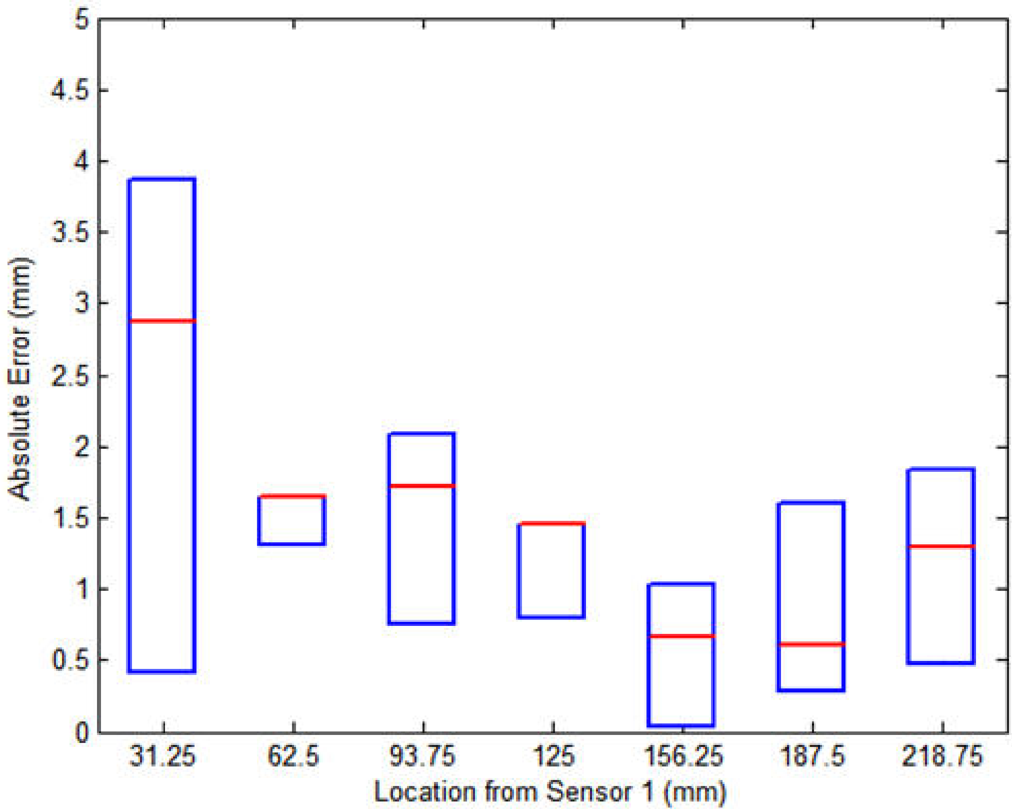

Figure 4.26: Location error with PSD method.

With the PSD method, aside from the location closest to sensor 1, the 75th percentile error is kept below 2 mm.

This method continues to work well as the time between subsequent discharges (off-time) decreases. Following the same method as above, the spectrogram in Figure 4.27 shows two EMI signals occurring prior to the onset of the acoustic wave. In this scenario the discharges were 32.2 μs apart.

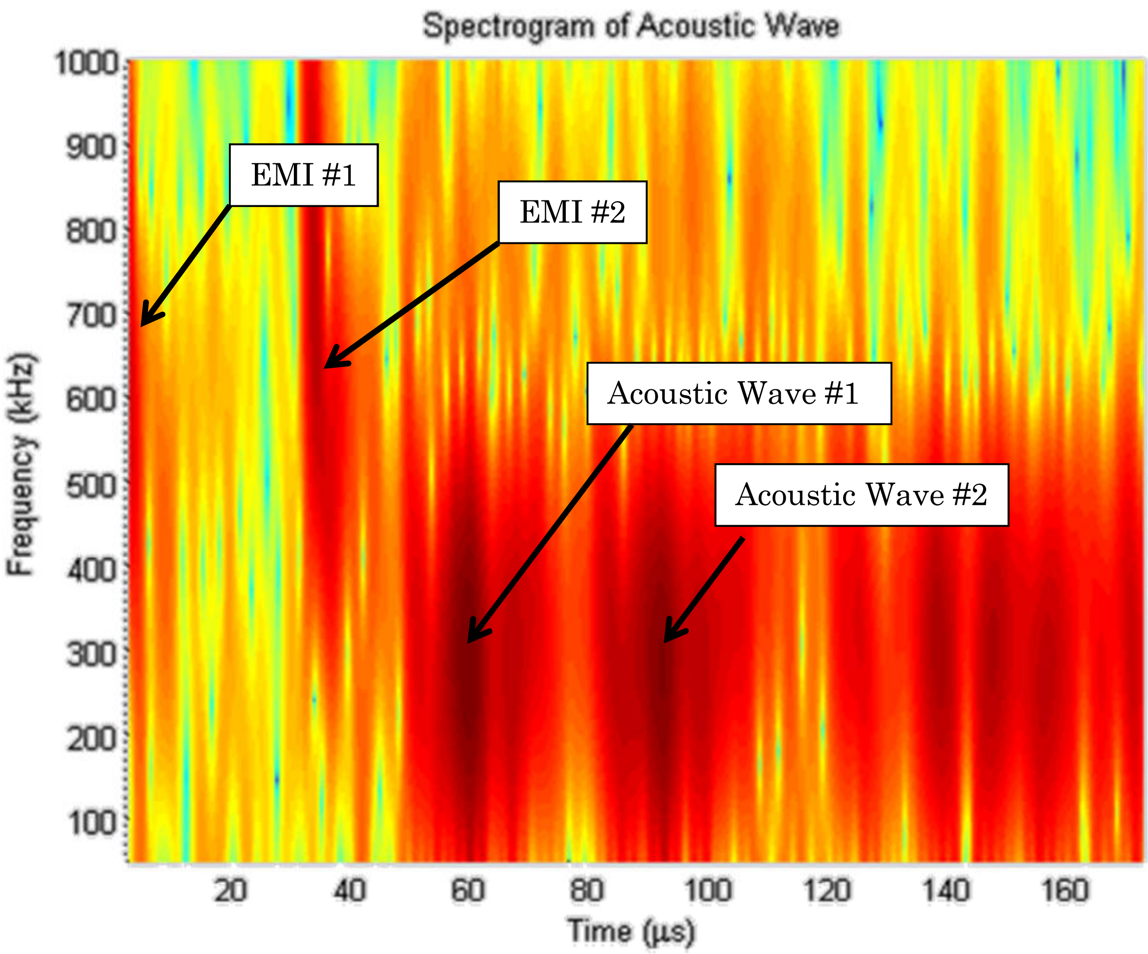

Figure 4.27: Spectrogram of two AE waves occurring 32.2 μs apart.

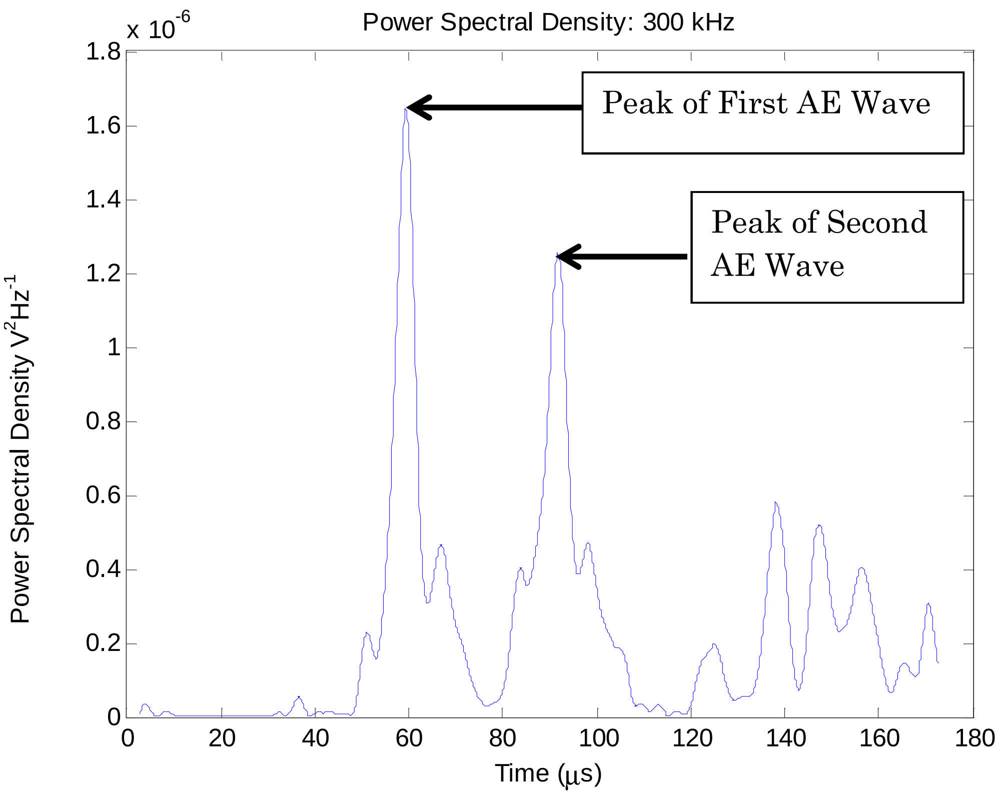

Figure 4.28: Power spectral density @ 300 kHz of two AE waves 32.2 μs apart.

The power spectral density at 300 kHz of the AE signal in Figure 4.29, shows two corresponding acoustic wave peaks occurring at 59.3 μs and 91.6 μs. This corresponds to a time difference of 32.3 μs between acoustic waves which is 0.1 μs more than the time between the two discharges and corresponds to a difference in expected location of the second discharge by approximately 0.033 mm. Figure 4.29 again shows the location determined from the PSD peak to occur at a consistent location just ahead of the main peak of the acoustic signal.

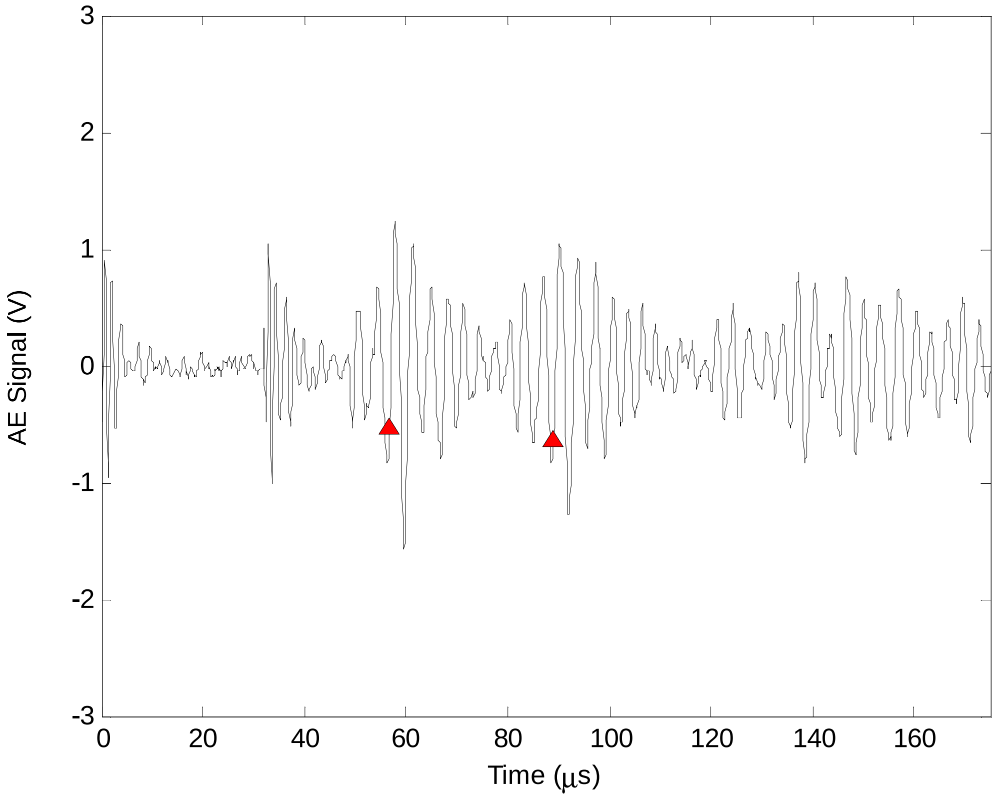

Figure 4.29: Location of PSD peaks on AE signal (32.2 μs apart).

Finally, a time difference of 12.9 μs between two discharges is used to test the method at low off-times. In Figure 4.30 and 4.31 we see the two characteristic peaks occurring 12.7 μs apart from each other with the first being initialized at 59.6 μs after the first current signal. This corresponds to a time difference of 0.2 μs between the measured time and actual time between discharges.

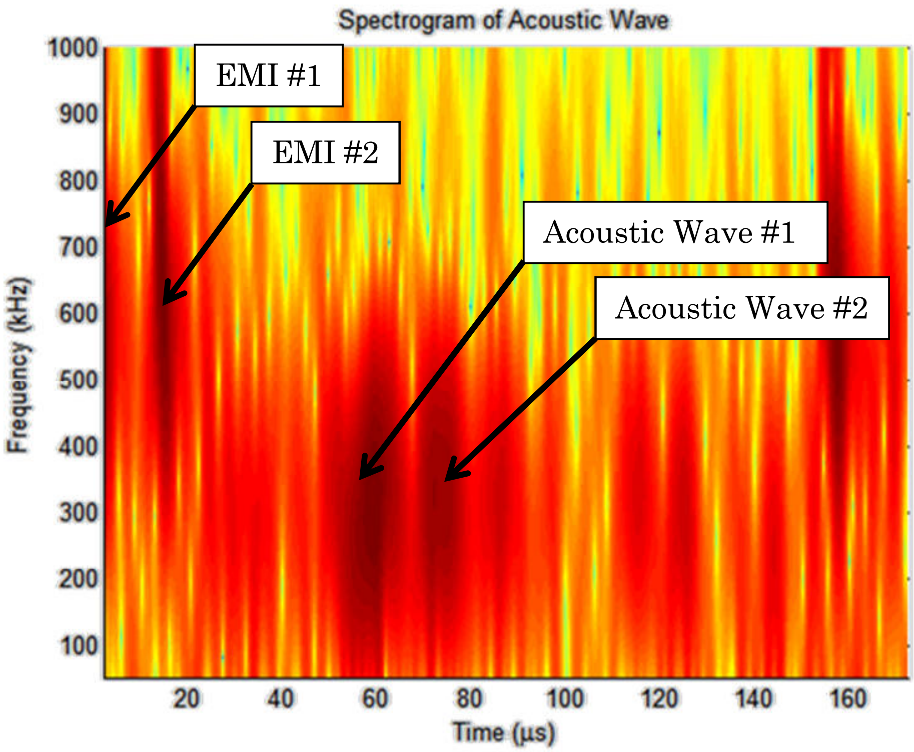

Figure 4.30: Spectrogram of two AE signals occurring 12.9 μs apart.

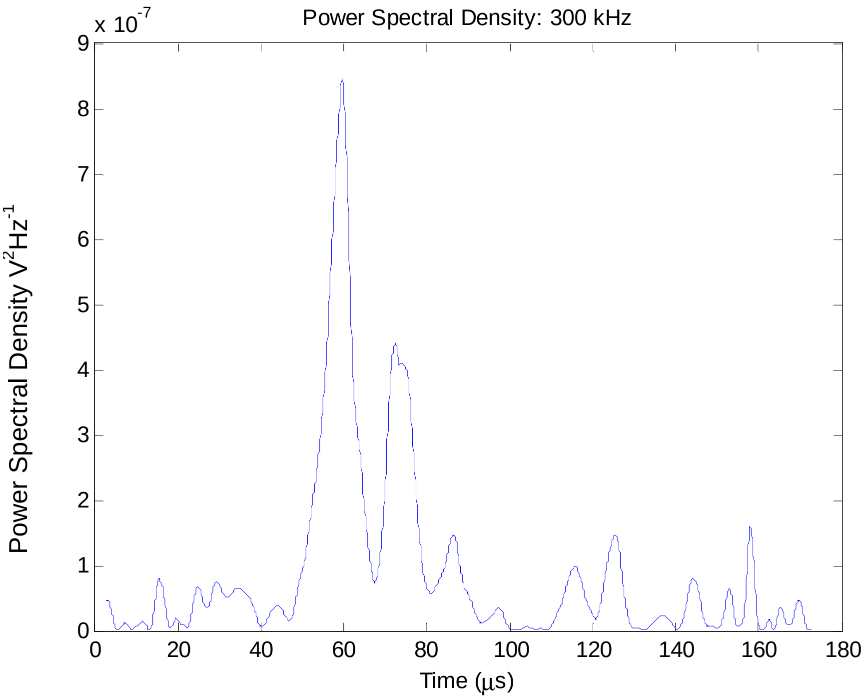

Figure 4.31: Power spectral density @ 300 kHz of two AE signals occurring 12.9 μs apart.

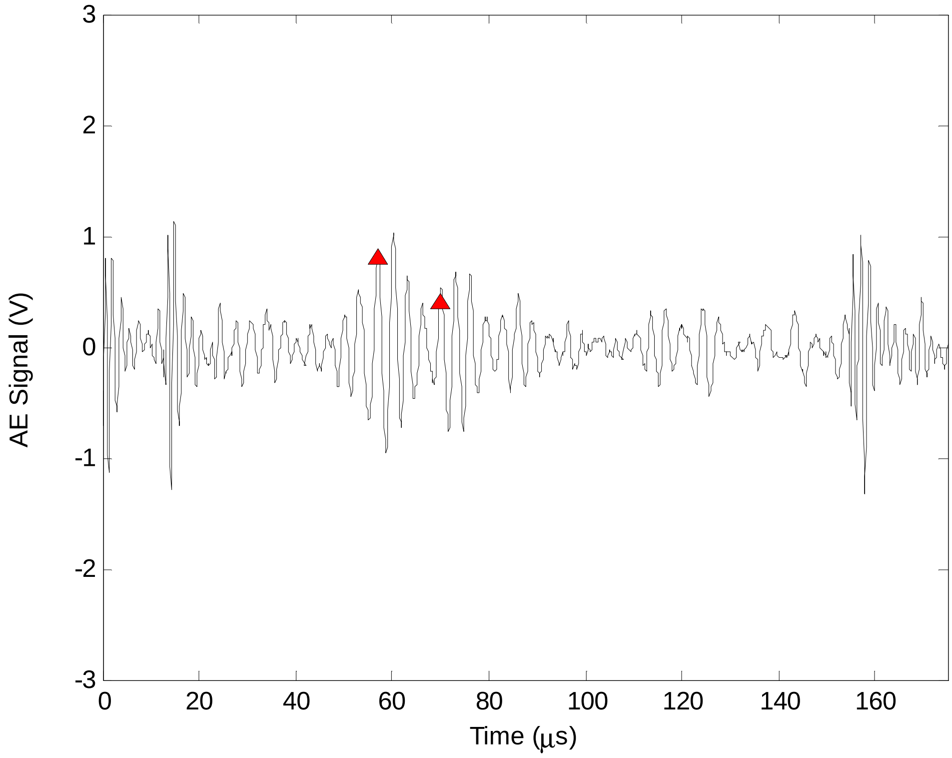

Figure 4.32: Location of PSD peaks on AE signal (12.9 μs apart).

By examining a variety of off-times it is seen that the PSD method has the ability to provide a constant reference point for multiple signals that are interfering with each other. This is of the utmost importance for any discharge mapping method utilizing the acoustic signals and until now is the key issue that has been interfering in the development of this technology. It is seen that even for low times between subsequent discharges, the PSD is able to accurately differentiate between two signals. No other method has shown the ability to handle this high level of interference to provide repeatable arrival time determinations.

4.4.3 Application of Wavelets

As discussed in Section 2.5.2, a wavelet is another commonly used signal processing tool. Recall that wavelets can be scaled (stretched or squished) and translated in time. A scalogram is a common representation of the wavelet transform on a signal, similar to a spectrogram. A scalogram allows the user to determine how well the wavelet transform matches the signal for a range of scales and times. The continuous wavelet transform function in MATLAB was used to output a scalogram using the daubechies order 8 (db8) wavelet and the signal seen in Figure 4.32 (12.9 μs time difference between discharges). The daubechies wavelet is chosen as it has been shown previously to work well in the analysis of partial discharges [49]. The daubechies wavlet of order 8 is shown in Figure 4.33 and the corresponding scalogram in Figure 4.34.

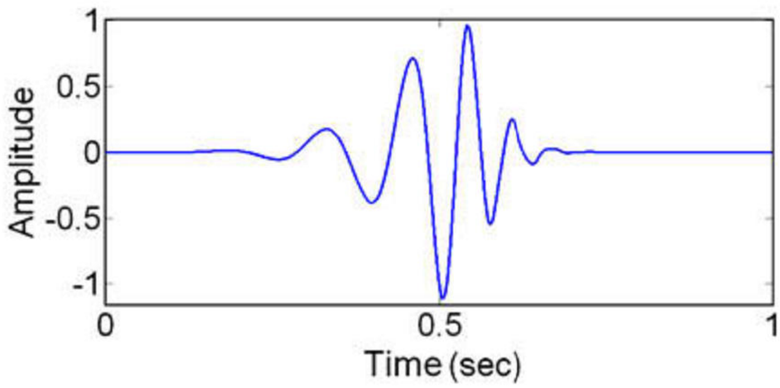

Figure 4.33: db8 wavelet [25].

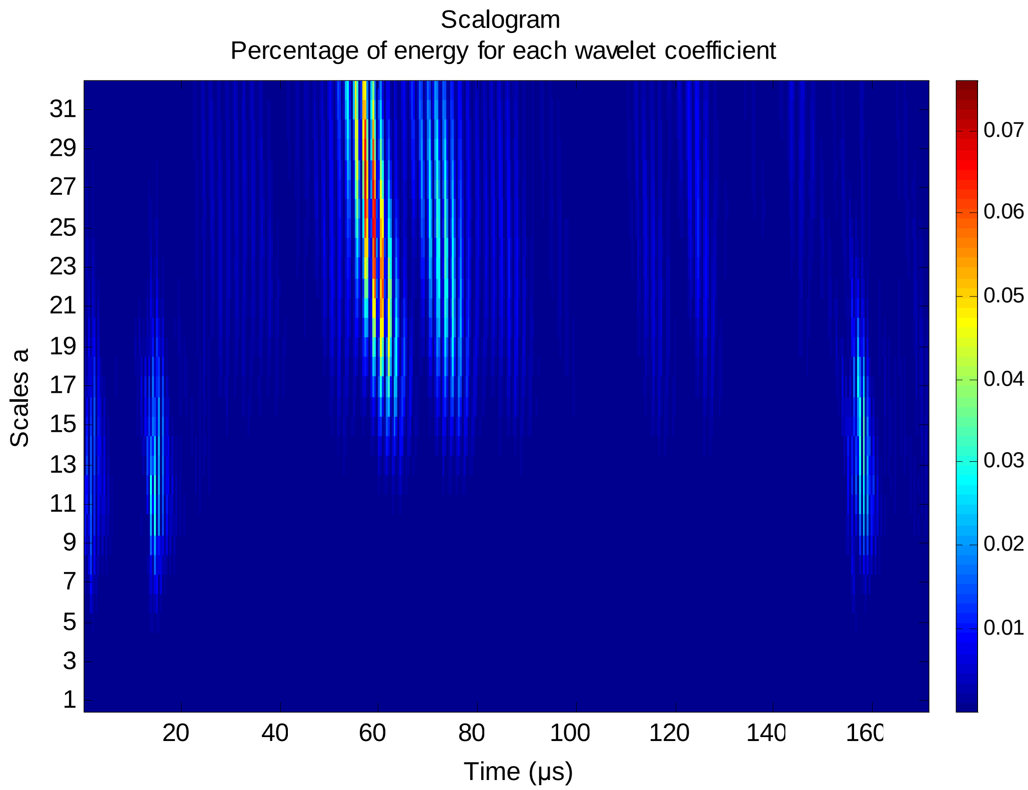

Figure 4.34: Scalogram of signal of two acoustic waves 12.9 μs apart.

Upon inspection, it can be seen that the scalogram does indeed show two distinct areas occurring where the two individual signals are expected. In a similar fashion to the PSD analysis, the scalogram amplitude at a scale of 24 is plotted in Figure 4.35. A scale of 24 is chosen as it approximates the 'db8' wavelet having a frequency of 303 kHz [52], which is in the dominant frequency range of the signal. The two peaks can be clearly seen and in fact the first peak corresponds to a time of 59.8 μs which agrees with the results found using the power spectral density in Figure 4.31. However, the second major peak of the scalogram amplitude is located at 74.2 μs which corresponds to a time difference of 14.4 μs. This is 1.5 μs larger than the real time difference of 12.9 μs. While it may not seem significant, such a time error can correspond to several millimeters of location error for high sound velocities.

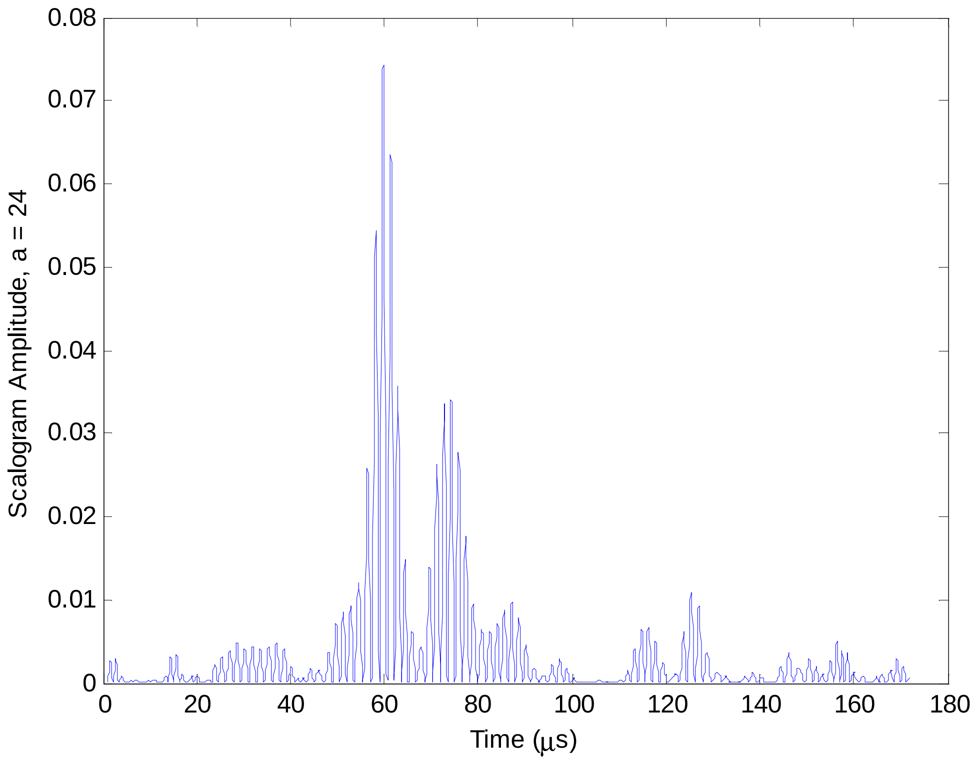

Figure 4.35: Scalogram amplitude at a scale of 24.

The use of wavelets remains an interesting analysis technique and continuing research using wavelet transforms and scalograms may prove to offer a second method for determining arrival times. However as the use of spectrograms and power spectral densities have been shown to accurately locate signals, it will be the main analysis method used throughout the remainder of this research.

4.5 Application to Wire EDM

The PSD method has now been shown to be capable of providing a fixed reference point for measuring time of arrival of the acoustic emission signal. This section continues to examine the use of the PSD method with the wire EDM setup previously described. Firstly, point source location is examined further with low off-times resulting in a high degree of interference between signals using the "thin" electrode. The effect of a wire coating on the time of arrival determination was also examined. The calibration between location and arrival time will then be used to estimate the workpiece height and location of an unknown "wide" electrode.

4.5.1 Point Source Location

In Section 4.4.2 spectrograms and power spectral densities were used to develop a calibration equation between arrival time and location for single sparks (1000 μs off-time). It was also shown that a spectrogram was able to differentiate between two signals with a low off-time (<12 μs off-time). Figure 4.36 shows the calculated location using the calibration relationship developed from the single spark tests applied to multiple discharges that occur within 10-15 μs of each other.

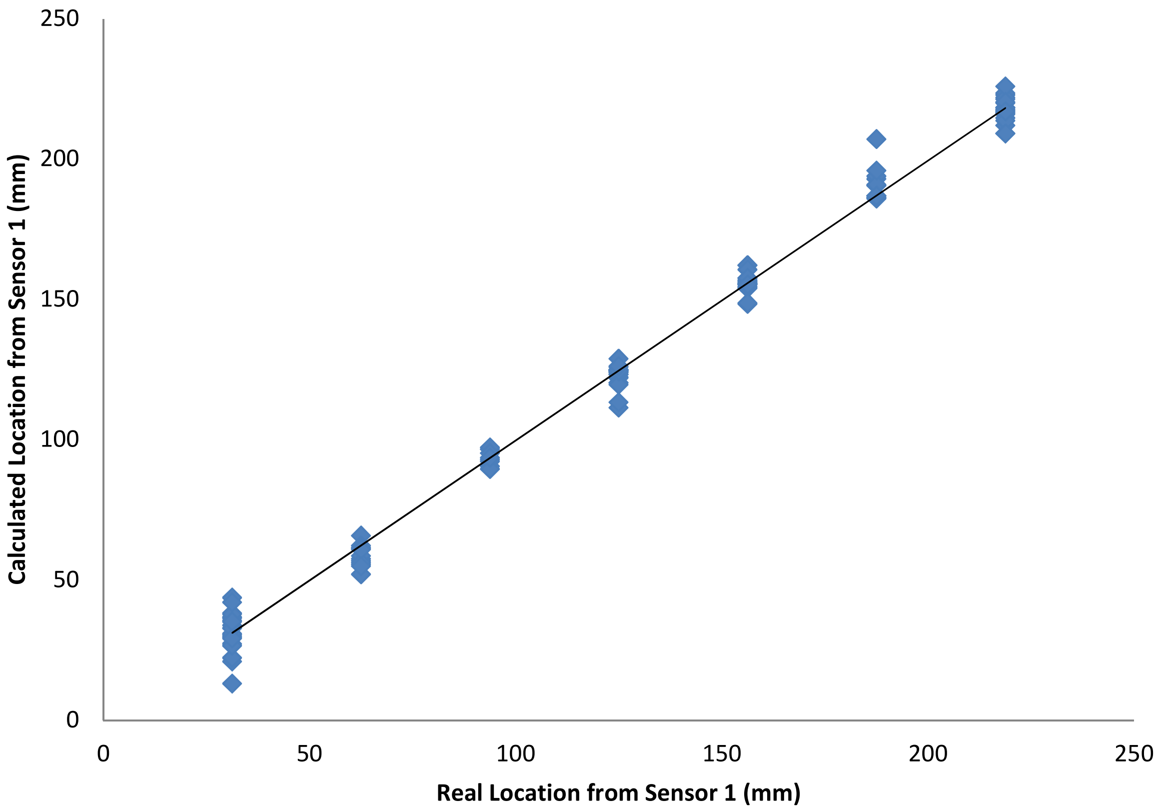

Figure 4.36: Calculated locations vs. real locations for a rapid succession of sparks.

A closer examination of the distribution of these locations is presented in Figure 4.37. The 25th and 75th percentile of the location errors are shown and it can be seen that the 25th percentile remains between 0.5 and 2 mm. The 75th percentile of the error is significant when located close to either sensor and is minimized to less than 3 mm when located in the center between the sensors.

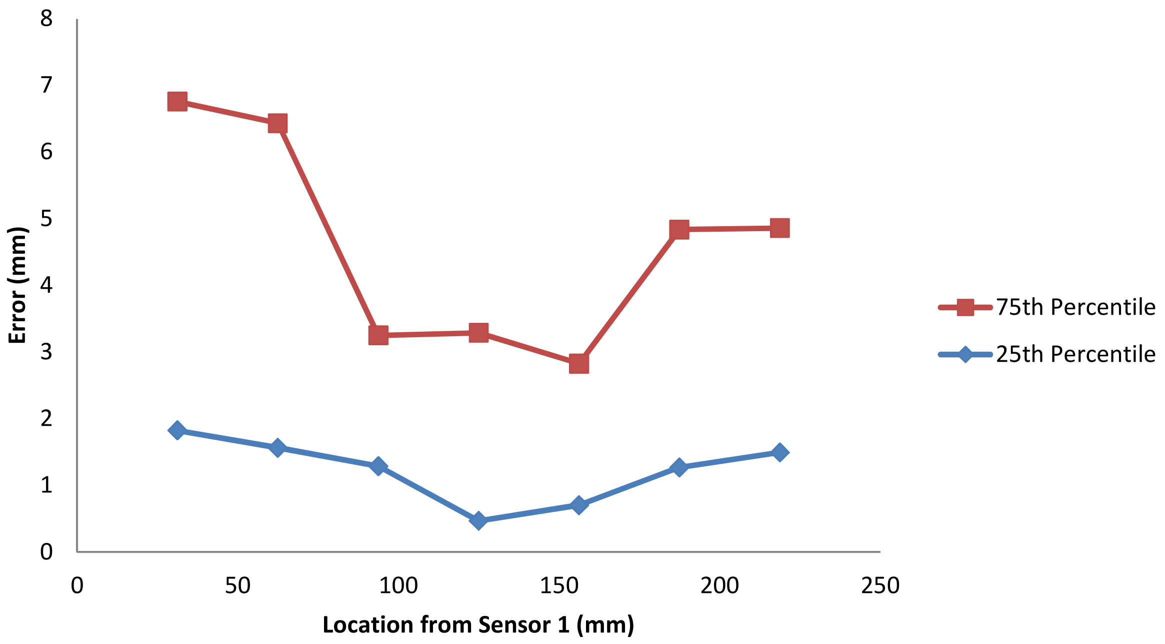

Figure 4.37: 25th/75th percentile for calculated errors of low off-time signals.

As previously discussed, EDM wire is often coated with a thin layer of zinc in order to allow for increased machining speeds. Since the acoustic waves that are being examined are surface waves it is of interest to determine the effect this zinc coating has, if any, on the location determination. Using Thermocompact Thermo A zinc coated EDM wire, point spark tests were performed using the 0.3 mm thick copper electrode as before. The off-time is set to 1000 µs to provide single sparks and the peak of the spectrogram is then used to determine the time of arrival.

Figure 4.38 shows the calibration of location with respect to arrival time. In the case of the zinc coating we find the calibration equation to be Location = 3.4525*(Arrival Time) – 76.608. Comparing the slope of 3452.5 m/s with the slope of the bare brass calibration 3299.4 m/s we see that the zinc causes a slight increase in the speed of sound. This increase in the speed of sound makes sense when we consider that the thin rod velocity of brass is approximately 3500 m/s, while the thin rod velocity of zinc is slightly higher at 3800 m/s [16]. It stands to reason that the addition of a zinc layer with a higher sound velocity will lead to an overall increase in the speed of sound in the wire.

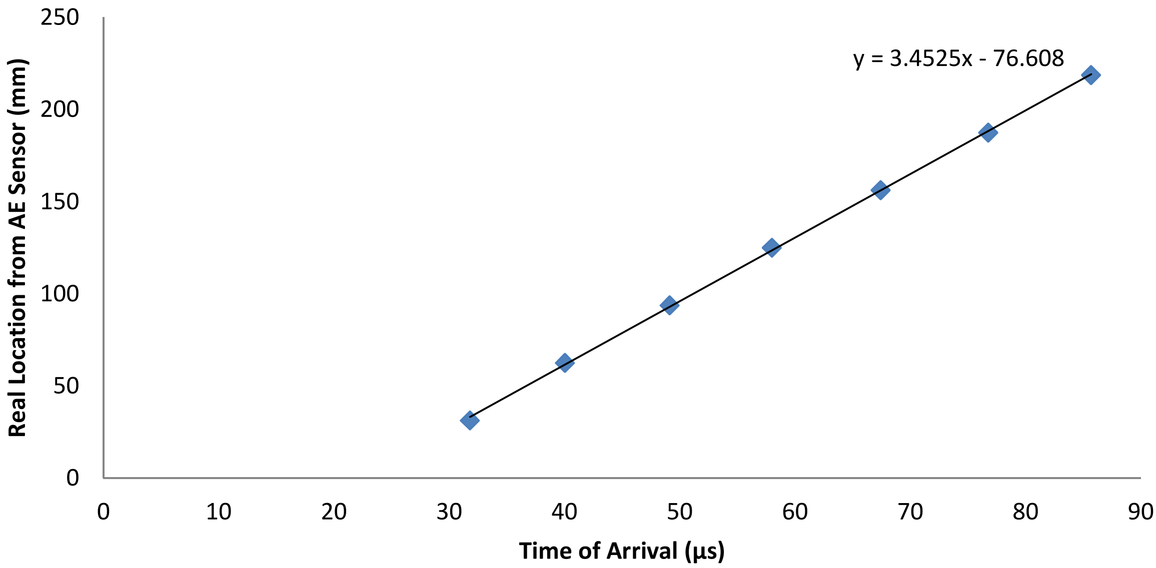

Figure 4.38: Zinc coating location calibration.

4.5.2 Discharge Mapping: Unknown Location (Wide Electrode)

Previous tests have shown the validity of the PSD method for determining source location by utilizing knowledge of the actual location. With knowledge of the exact source location it is possible to use only one sensor to determine whether or not the tests yield good results. However, this is not useful in practice as the whole reasoning behind the development of this method is to be able to determine discharge locations with as little prior knowledge of the workpiece as possible. For small off-times (<100 μs) multiple sparks are generated before the acoustic emission from the first spark reaches the sensor. Each of these current signals represent a possible source for the detected AE signal in time of arrival determinations. It is therefore necessary to utilize the second sensor to determine the source location as a method for ensuring the correct current pulse is considered when determining arrival times.

4.5.2.1 Methodology for Arrival Time Determination

With two sensors the only information needed are: a) the distance between sensors (250 mm) and b) the relationship between arrival time and location (Location = 3.2994*(Arrival Time) - 72.111). To provide a method for determining the location with two sensors we will momentarily continue with the knowledge of the real location of the electrode.

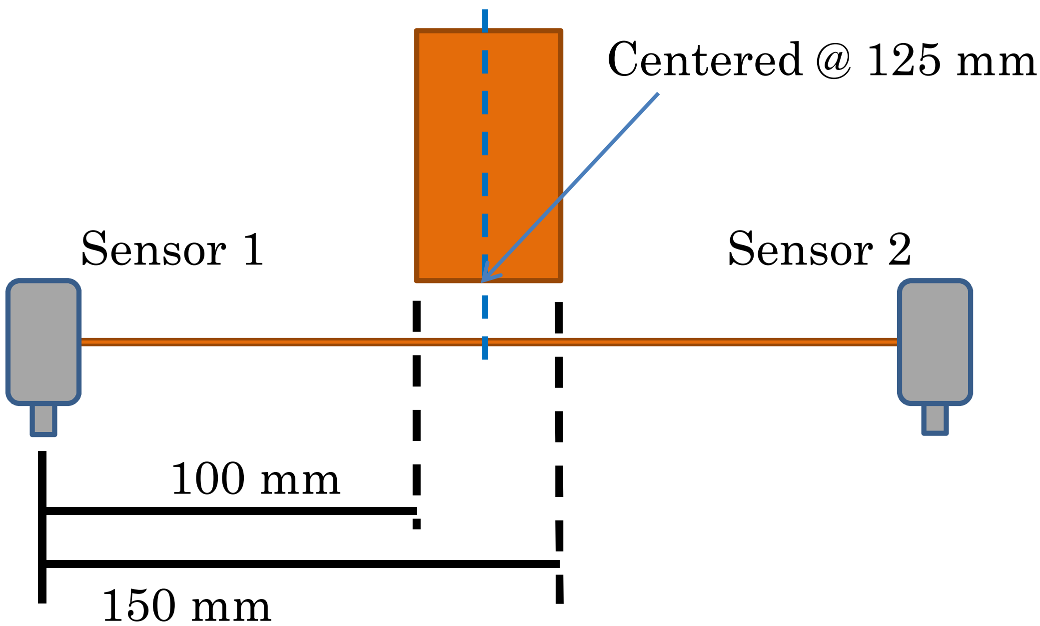

Figure 4.39: Schematic of experiment used to develop methodology for arrival time determination.

Figure 4.39 shows the setup that will be used to generate the acoustic emission signal shown in Figure 4.40. A 50 mm wide electrode is centered 125 mm away from sensor 1, meaning that the spark is generated within the range of 100 - 150 mm from sensor 1. STFT analysis on a 300 μs envelope surrounding the acoustic emission is performed and the location of the obtained PSD peaks are denoted by the triangular markers. Examination of the current signals show 10 current signals occurring ahead of the PSD peak, each having the potential to be the source of that particular acoustic emission.

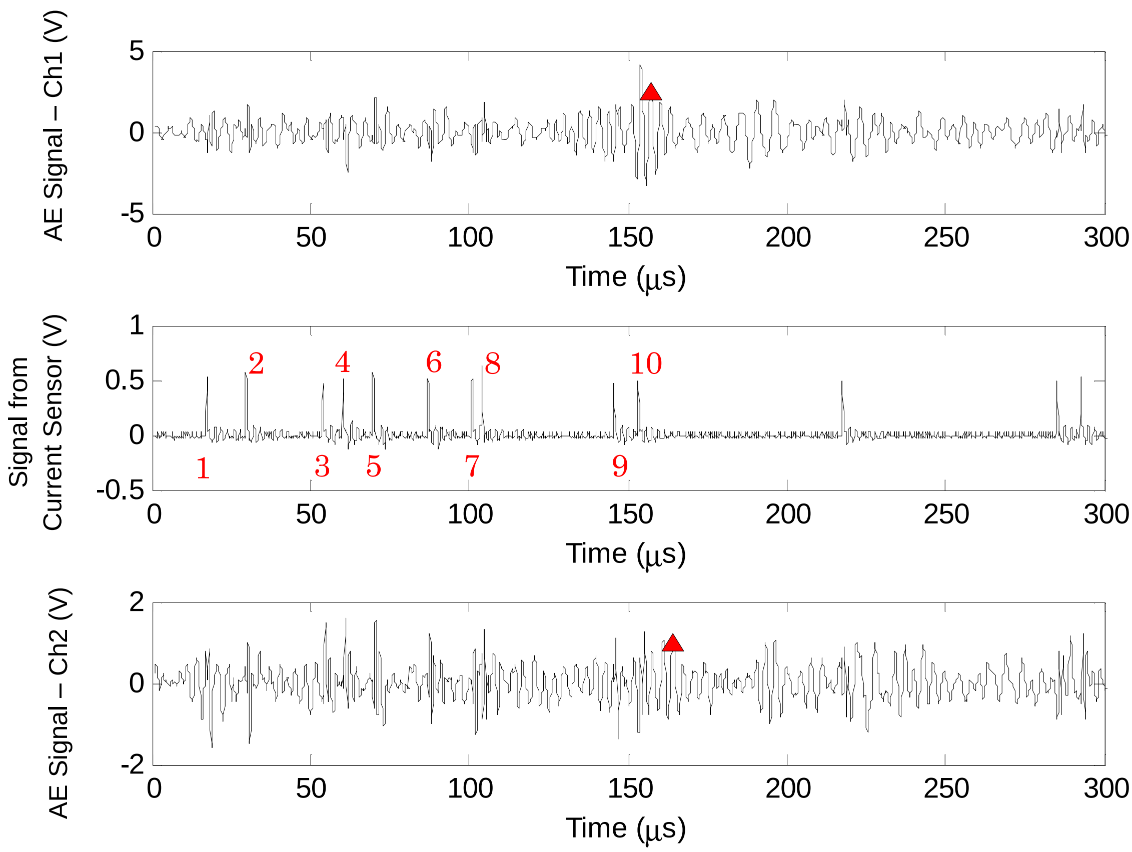

Figure 4.40: Use of two sensors to determine proper location.

If only sensor 1 is used, it is possible that a valid location (between 0 mm and 250 mm) could be calculated for multiple current signals. By calculating the location with sensor 2 as well, we are able to determine exactly which current pulse generated the acoustic emission by comparing the two calculated locations. The two calculated locations can be found using the following relationships:

$$\text{Location}_{[\text{Sensor 1}]} = 3.2994*(\text{Arrival Time}_{[\text{Sensor 1}]}) - 72.111 \tag{4.1}$$

$$\text{Location}_{[\text{Sensor 2}]} = 250 - (3.2994*(\text{Arrival Time}_{[\text{Sensor 2}]}) - 72.111) \tag{4.2}$$

Equation 4.1 gives the relationship between the calculated arrival time to sensor 1 and the location of that discharge from sensor 1. This was the relationship developed from single spark tests. *Arrival Time* $_{[Sensor\ 1]}$ refers to the time difference between the peak of the power spectral density at 300 kHz, and the time from which a current discharge signal occurs. Equation 4.2 is the same relationship for sensor 2, however in order to ensure that all location measurements are taken with sensor 1 as a reference, the calculated location must be subtracted from 250 mm (distance between sensors) or else it would be expressed as the location from sensor 2. With both sensors providing locations from the same reference point, they are easily compared to one another to see which current pulse provides the best correspondence for the initialization of each acoustic wave.

Table 4.1: Determining best acoustic emission to current pulse correspondence.

Current #	Location using AE1 (mm)	Location using AE2 (mm)	Error (AE1-AE2) (mm)
1	388.82	-162.57	551.39
2	348.23	-121.99	470.22
3	268.06	-41.81	309.87
4	246.94	-20.70	267.64
5	216.92	9.33	207.59
6	159.18	67.07	92.11
7	**112.99**	**113.26**	**-0.27**
8	103.09	123.16	-20.07
9	-33.84	260.08	-293.92
10	-59.24	285.49	-344.73

Table 4.1 shows the calculated locations of both sensors for the 10 current pulses shown in Figure 4.40. It can be determined immediately that current #'s 1-4 & 9,10 (shaded red) are not suitable candidates for location measurement as they are locations outside the range of the sensors. Focusing solely on current #'s 5-8 it can be seen that current signal 7 (shaded yellow) has a minimal difference between the two calculated locations and as such current signal 7 corresponds to the generation of the acoustic wave being considered.

Before continuing, it is important to determine the error between the two calculated locations that will provide the best results. Initially, MATLAB was programmed to return locations that have an absolute error less than 1 mm between the calculated locations from sensor 1 and 2. This is merely a starting point for determining the threshold of this error that produces the best results. Figure 4.41 shows the 25th and 75th percentile of calculated locations for all data inclusive to the error threshold. The dashed lines represent the true workpiece height of the electrode. It is found that the 25th and 75th percentiles best match the real workpiece height when only locations with an error less than 0.4 mm are used. This is the value that retains enough calculations for meaningful analysis, but removes the locations with the most error associated with them.

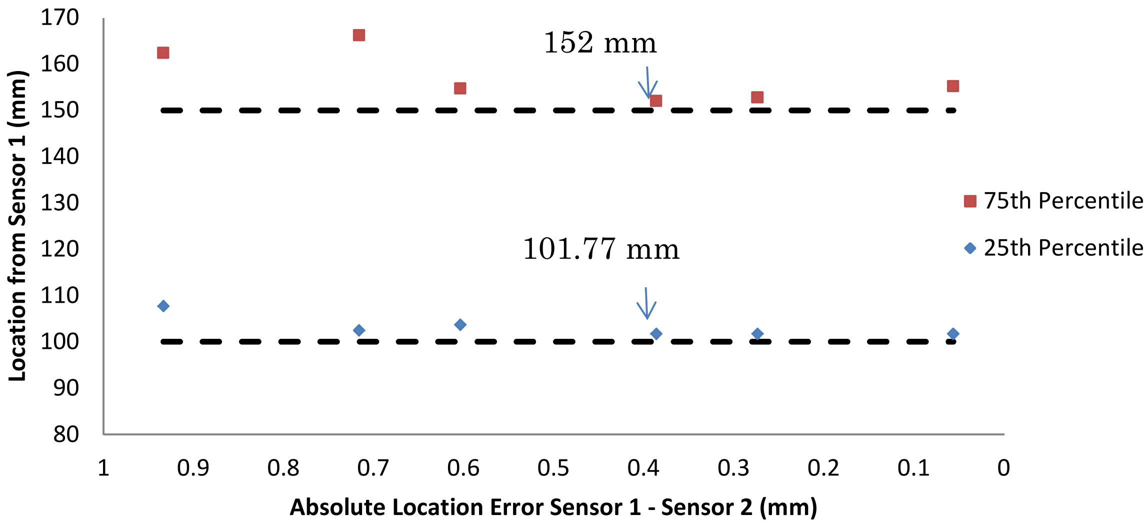

Figure 4.41: Determination of location error threshold.

One more piece of knowledge that can be useful for differentiating between an acceptable location determination and an unacceptable one is the knowledge of attenuation. As the acoustic wave travels its amplitude decreases due to attenuation in the material. Examining Figures 4.28 & 4.29 it is clear that there is a relationship between the amplitude of the PSD peak to the magnitude of the received acoustic emission. Meaning that the farther the acoustic wave had to travel the lower the PSD peak will be.

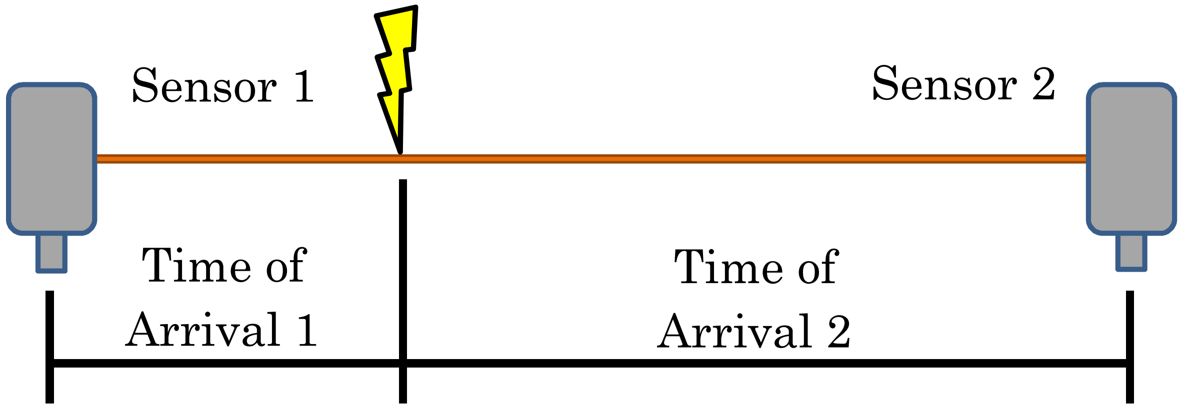

Figure 4.42: Representation of spark arrival times at both sensors.

Using Figure 4.42 as a reference it is clear that for the two scenarios of a discharge occurring off center the time of arrival and PSD peak relationship can be described as follows:

Discharge Closer to Sensor 1	Discharge Closer to Sensor 2
Time of Arrival 1 < Time of Arrival 2 PSD peak 1 > PSD peak 2	Time of Arrival 1 > Time of Arrival 2 PSD Peak 1 < PSD Peak 2

This means that the product of:

$$(\text{Time of Arrival 1} - \text{Time of Arrival 2})*(\text{PSD Peak 1} - \text{PSD Peak 2}) \qquad (4.3)$$

should always be negative. For the case of a discharge occurring in the exact center the product should be 0, meaning that discharge locations yielding a positive product can be ignored. A positive product would indicate that one of the acoustic waves used in the location calculation was actually generated by a different current signal and therefore did not experience the attenuation that was expected.

With these selection methods developed we can now investigate the application of the PSD method on an unknown electrode at an unknown location.

The acoustic signals will be separated into 100 μs increments, with the PSD peak being calculated for each 100 μs window. The PSD peaks will then be expressed in absolute time and each peak for both channels will be used in conjunction with **every** current signal to determine appropriate arrival times for both channels using the methodology outlined above. This method will allow us to only use the strongest PSD peaks and best location matches. Despite ignoring a lot of good determinations, for this research it is appropriate to sacrifice quantity of signal over quality of arrival times considering the amount of current signals at our disposal (>5000 current samples/second).

4.5.2.2 Workpiece Location Determination

A constant workpiece width will be used to examine the accuracy of using PSD peaks when determining the location of the electrode. The workpiece of width 50 mm was centered at 62.5 mm, 125 mm, and 187.5 mm. Throughout the experiments, the workpiece width and locations were considered unknown with true values only used after-the-fact to determine the accuracy of the estimations. Again a box plot is used to show the 25th and 75th percentiles of the locations. A comparison to the true location of the workpieces is also shown in Figure 4.43. The box plots are computed by using 40 calculated locations for a real location of 62.5 mm, 42 calculated locations for a real location of 125 mm, and 45 locations for a real location of 187.5 mm.

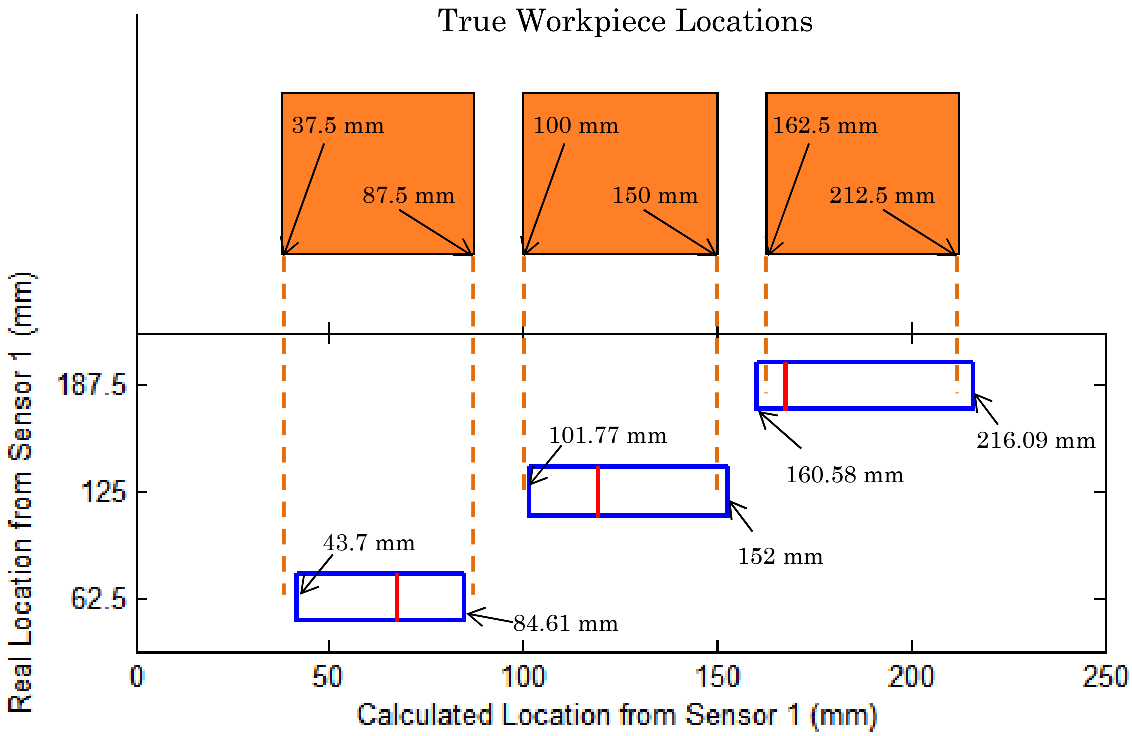

Figure 4.43: Location determination of 50 mm wide workpiece at three different locations.

It is seen that the calculated locations agree well with the real location range. This is especially true in the center of the setup with a location error under 2 mm. The error increases at the extreme ends of the test at locations 37.5 mm and 212.5 mm from sensor 1. The maximum error at these two ends still fall within the range of error that was seen in single spark tests.

It is possible that the distribution of discharges is skewing the results around the edges. In the case of the electrode located from 37.5 mm to 87.5 mm, we find that the median of the data falling within the interquartile range is 69.45 mm. This means that the data is preferentially located farther away from sensor 1. This information could potentially serve as another tool for monitoring spark localization within a workpiece height. If the discharges are becoming localized, the median would be drawn toward that area.

4.5.2.3 Workpiece Height Identification

Experiments were next performed at a constant location (125 mm from sensor 1) and varying workpiece heights to determine the ability to use power spectral densities to estimate the workpiece height. Workpiece heights of 23 mm, 50 mm, and 90 mm was used. Figure 4.44 shows the 25^{th} and 75^{th} percentile for these three workpiece heights and the results are tabulated in Table 4.2 to give calculated values to compare to the real workpiece heights. To compute the box plots; 48 calculated locations were used for the 23 mm high workpiece, 42 calculated locations for the 50 mm high workpiece, and 53 calculated locations for the 90 mm high workpiece.

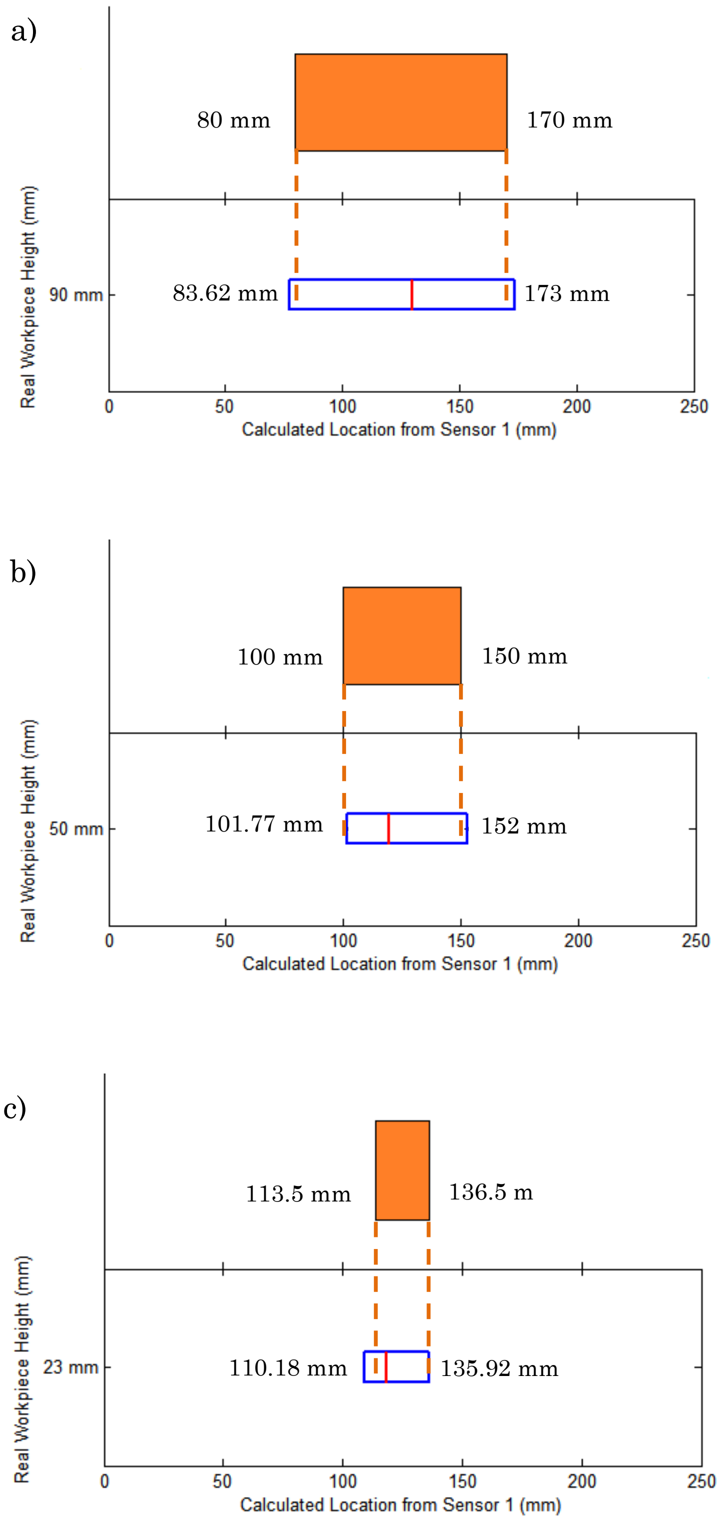

Figure 4.44: Workpiece height identification a) 90 mm high workpiece, b) 50 mm high workpiece, c) 23 mm high workpiece.

The largest error in the workpiece height is observed for the 23 mm wide workpiece which is overestimated at 25.74 mm. The other two workpiece heights are estimated to sub 1 mm values, 50.23 mm compared to 50 mm and 89.38 mm compared to 90 mm. There is an associated location error with these estimated workpiece heights of 2 to 3 mm as was seen previously, however accuracy in the workpiece height is valued over location measurement.

Table 4.2: Determination of workpiece height.

Real Workpiece Height (mm)	Calculated Height (mm)
23	135.92 – 110.18 = 25.74
50	152 – 101.77 = 50.23
90	173 – 83.62 = 89.38

It is also interesting to note the changes in the overall frequency characteristics of the signals for the different workpiece heights. In Figure 4.45, four sample FFTs are plotted for each workpiece height. Paying particular attention to the 150 kHz – 200 kHz frequency range (red box) this peak seems to decrease as the workpiece width increases. For the 50 mm wide workpiece a peak at approximately 320 kHz (green box) is much higher in magnitude than in the other two workpieces. Finally, the 90 mm wide workpiece is characterized by a significant peak at 300 kHz (blue box), a secondary peak at 400 kHz (orange box) and low amplitude frequencies elsewhere.

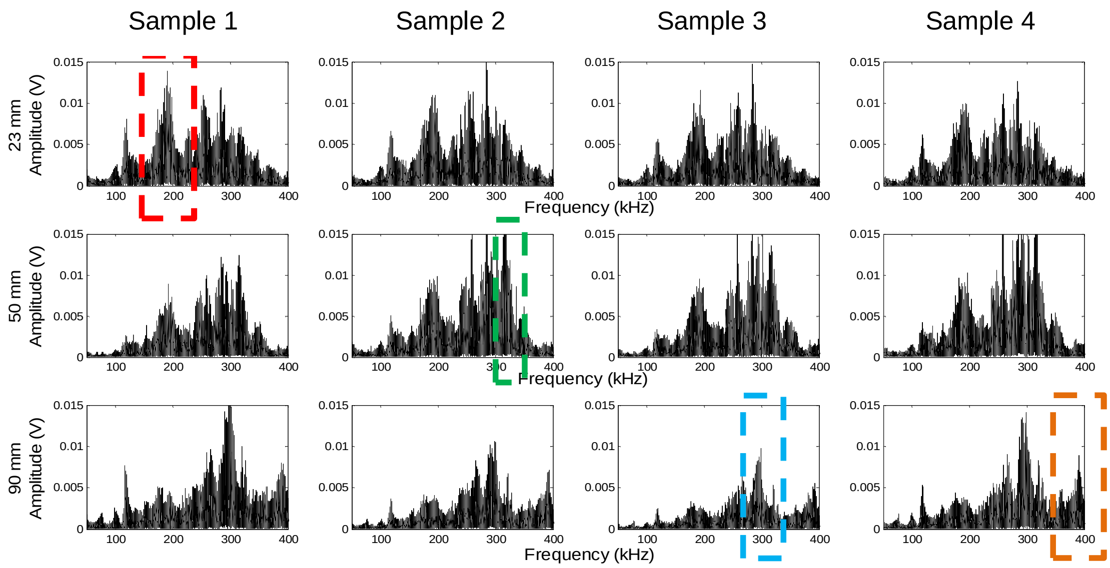

Figure 4.45: A comparison of 4 FFT samples for three workpiece heights.

Further study of these frequency peaks is recommended even if these specific frequency peaks are setup related (wire material, diameter etc.) it still shows a response to a change in workpiece width. If these various frequencies correspond to the acoustic emissions generated by different types of discharges (sparks, arcs, normal) this would be another beneficial tool to use in the monitoring of the process state.

Using power spectral densities as a tool for arrival time determination it is possible to estimate the workpiece height and location within an accuracy of 3 mm. It is possible to estimate these workpiece heights with only knowledge of the distance between sensors and the calibration of arrival time to location based on single spark tests. It is also able to make these estimates under real machining conditions with low off-times (~10 μs) between signals. A brief examination of fast hole electrode length determination now follows.

4.6 Application to Fast Hole EDM

It is also of interest to determine the applicability of this proposed method for use with the fast hole EDM process. Knowledge of the true fast hole electrode length would aid in better breakout detection during machining. There are a few key differences between fast hole and wire EDM. A fast hole EDM is plunged into the workpiece to machine fine holes, meaning that sensors can only be placed on one end of a fast hole setup. While fast hole electrodes are of comparable diameter to the wire used in the wire EDM process, they are characterized by having one or more channels running through the center of them to provide stiffness. Finally, the timing parameters that are used in fast hole EDM are generally higher than those of wire EDM, even reaching a total machining time (on + off) of close to 100 μs. The increase in the total machining time leads to less interference between subsequent signals and could make it possible to utilize only one sensor in the time of arrival determination. In the cases when two sensors are needed, the setup proposed in Figure 4.46 would provide a difference in time lags between the two signals in order to determine correct arrival times.

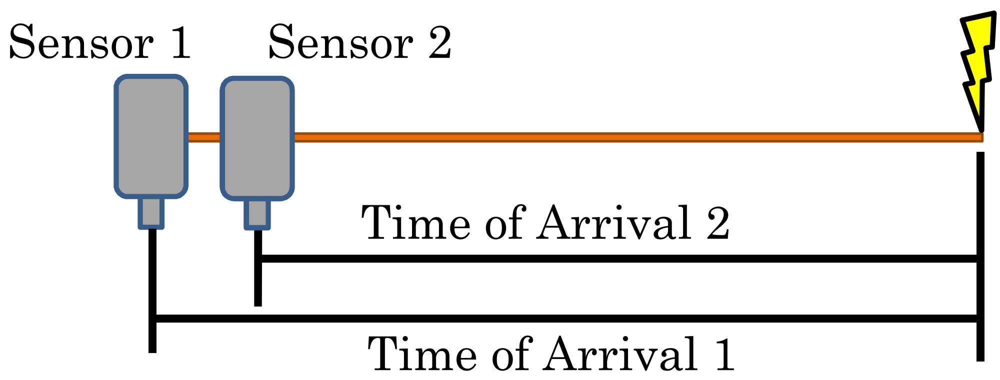

Figure 4.46: Possible 2 sensor fast hole setup (Note: Setup not used for these tests).

The channels that run through the fast hole electrode, do not only provide an increased stiffness for the electrode but are also used for through flushing of the process. Through flushing is important to maintain stable machining conditions. Unfortunately, as the EDM being used for this research is not configured for a fast hole process, it is difficult to provide through flushing and ensure stable machining during these tests. For this reason, an examination will only be performed on single spark tests. A sample single spark generated during fast hole EDM machining is seen in Figure 4.47. A notable difference from the wire EDM tests can be seen in the current signal where the current pulse has an on-time of 12 μs opposed to the 1.12 μs on-times that were used in the wire EDM experiments. If the single spark tests yield good results it is expected that stable machining results would be similar to those achieved in the wire EDM tests.

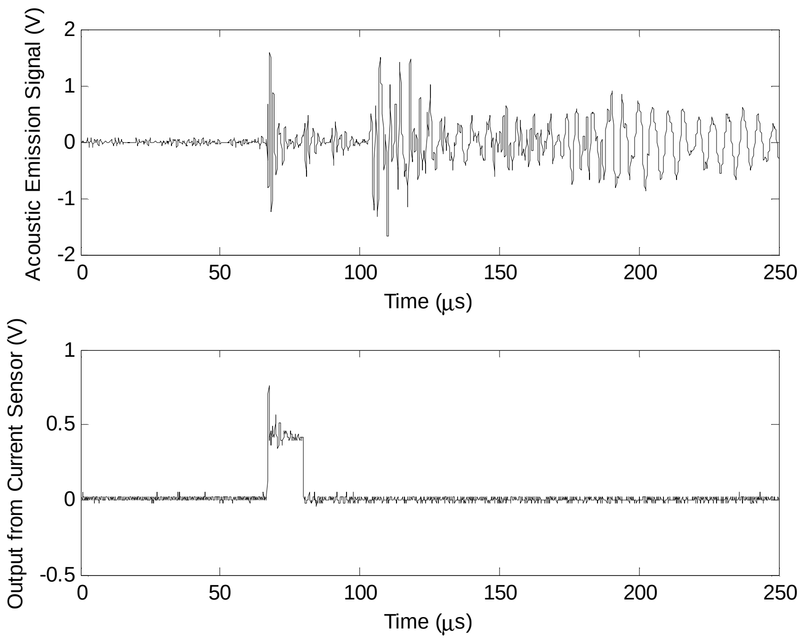

Figure 4.47: Sample single spark during fast hole experiments.

A series of 12 tests are performed on a 125.5 mm long x 0.3 mm diameter brass fast hole electrode. Each test is comprised of 20 arrival times obtained by finding the time from current signal to the PSD peak of the incoming acoustic wave. Over the duration of the tests the electrode length is decreased from 125.5 mm to 32.5 mm. The decrease in length is non-uniform and in some cases the difference between two test lengths is as little as 1.2 mm in order to test the ability to detect minute changes in length. This is important if this method is to be used in real time to monitor a fast hole machining process. Of the 12 tests; 4 tests will be used to develop a calibration equation in a similar fashion to single spark wire EDM tests. This calibration equation will then be used on the remaining 8 tests to see how well the calculated location matches the true location.

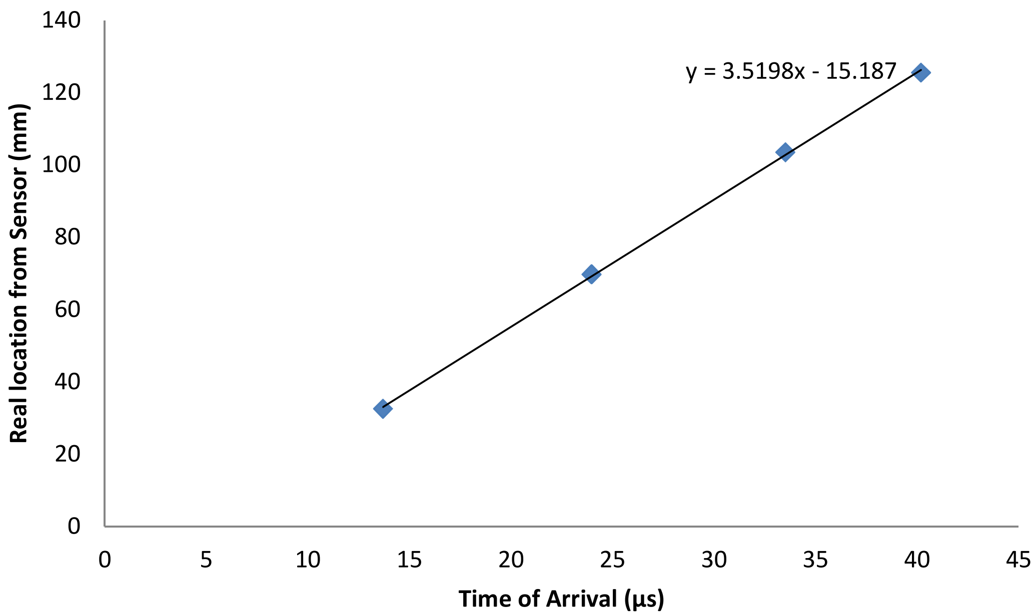

Figure 4.48: Calibration of arrival time to real location – fast hole.

Using the average arrival time values at each location we are able to develop the relationship of Location = 3.5198*(Arrival Time) – 15.187, which again gives us a speed of sound of 3519.8 m/s which is similar to what was seen during the wire EDM tests and the expected speed of sound in brass. In Figure 4.49 below this relationship is used to calculate the locations for each individual arrival times. The tests used in the development of the calibration equation are denoted as blue diamonds termed "Calibration Development" and the rest of the tests are denoted as red x's and termed "Calibration Verification". Examination of the plot clearly show the 12 distinct test groupings, even when the difference between two tests is minimal such as the case of the 86.7 mm and 85.5 mm lengths.

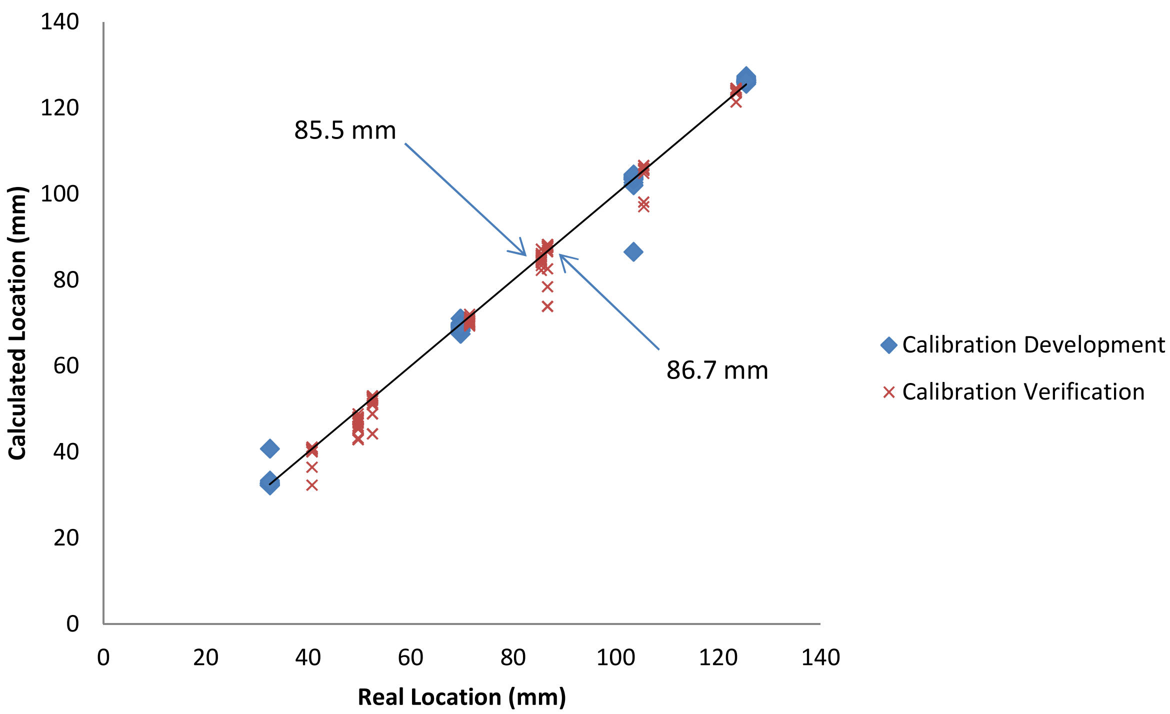

Figure 4.49: Calculated locations vs. real locations – fast hole.

As before, the 25th and 75th percentiles of the location errors will be examined to give a better understanding of the error seen in the calculated locations above. Figure 4.50 shows that 11 out of 12 of the tests have a 75th percentile of the location error under 1.5 mm. The lone exception being the case at a 49.7 mm length which has an error ranging from approximately 2mm to 4.25 mm. Using the proposed PSD method for detecting arrival times works well for detecting true electrode length in the fast hole EDM process.

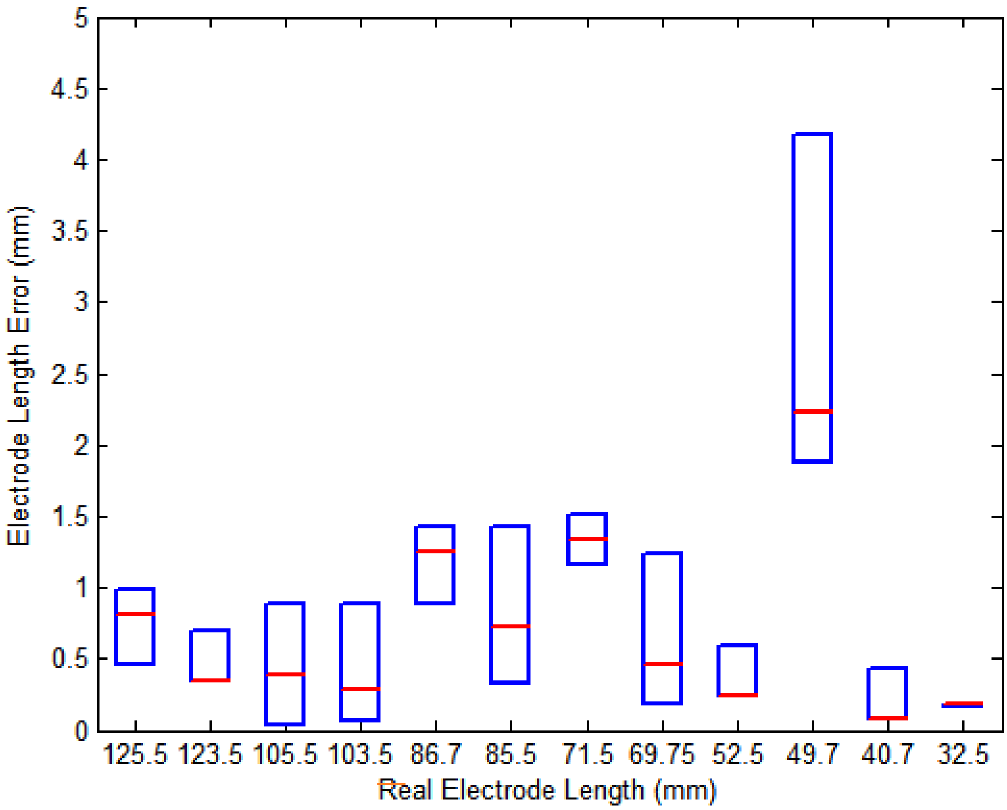

Figure 4.50: Location error for fast hole tests.

In the development of a technique to map discharges of an EDM process by using acoustic emission sensors, it has been shown that analysis of the frequency content of the generated acoustic emission wave is useful. A dominant frequency band around 300 kHz was seen and by analyzing the power spectral density of the signal at this frequency a fixed reference point on the acoustic wave is seen. A fixed reference point is important in time of arrival calculations to provide repeatable arrival times with which to generate calibration relationships. The power spectral density has the ability to provide a fixed reference point on the signal even when high levels of noise are present in the AE signals. With an arrival time – location relationship available it is possible to accurately map the discharges under real machining parameters to identify workpiece height as well as fast hole electrode length.

Chapter 5

Conclusions and Future Work

Applications utilizing acoustic emission sensing technology in the electrical discharge machining process have been presented. It is an area of process monitoring that has not been investigated extensively to this date and it is the hope of the author that this work will serve to advance research in this area. This chapter will summarize the conclusions of this thesis and discuss areas for continuing research.

5.1 Conclusions

With very little reference material available on the application of acoustic emission in electrical discharge machining, it was necessary to explore techniques used in other processes. Areas providing the most pertinent information were in the acoustic emission monitoring of partial discharges in electrical transformers, conventional machining as well as in detecting pipe leakages. Using this background information it was possible to expand upon the state of the art through this thesis. Below is a summary of the key results that have been explored in this research.

1. The interface between sensor and electrode is extremely important. To ensure the highest quality of signal, the sensor must always maintain contact with the electrode to provide the best transmission of the acoustic wave.

2. The most important aspect for maintaining a high accuracy in the time of arrival determinations is by using a fixed reference point on the acoustic wave. Since the speed of sounds that are being worked with are approximately 3300 m/s – 3500 m/s, an error of just 1 μs can lead to a 3.3 mm – 3.5 mm error in the location.

3. Due to the high interference between closely generated signals, a reference point selection based on the raw acoustic signal is not feasible. However, focusing on the frequency characteristics of the signal led to the use of power spectral densities to determine a fixed reference point on the signal. It has been shown that the PSD peak occurs at a constant location for a given signal, and that the PSD peak has the ability to differentiate between two signals occurring as little as 10 μs apart.

4. A calibration relationship can be developed using a thin electrode for given locations of the discharges. A methodology for utilizing this relationship with two sensors to select the best current signal to PSD peak correspondence was developed. Best results refer to the calculated location difference between the two sensors being under 0.4 mm and when attenuation of the acoustic wave was taken into account.

5. With only knowledge of sensor locations and a calibration relationship between location and time lags, it was possible to locate the workpiece spatially between the two sensors as well as identify the height of the workpiece. Location tests showed that error was minimized when the workpiece was kept as close to the midpoint between sensors as possible. Using the 25^{th} and 75^{th} percentiles of the calculated workpiece height measurements it was possible to identify the workpiece height to under 3 mm.

6. Promising results were also obtained when studying the fast hole EDM process. It was possible to differentiate between two electrode lengths differing by approximately 1 mm. The single spark tests performed lead to the expectation that similar results to that of wire EDM tests can be achieved given stable machining conditions.

Initial research into studying the frequency characteristics of acoustic emissions generated by EDM discharges has provided many results that can be further developed to improve process monitoring or help provide better insight into the process. Knowledge of workpiece height and location as well as true fast hole electrode length can be used to increase the efficiency of current EDM operations.

5.2 Future Work

This work should serve as a resource for further development in using acoustic emission sensors to monitor electrical discharge machining, not only in the identification of workpiece height and fast hole electrode length, but also in developing a better understanding of the EDM process itself. This section will now discuss key areas for continuing research.

5.2.1 Sensor Placement

The first issue that must be considered is the sensor placement on a dedicated wire or fast hole EDM. Tests should be performed on these machines to determine the location where the sensors give the strongest signals. Problems mounting the sensors could arise as current machines are not designed with acoustic emission sensors in mind. This may include the need to develop a mounting bracket with a waveguide in order to mount the sensor properly. A waveguide is a metallic connector between the sensor and the wire which allows for the transmission of sound waves from the wire to sensor. This would allow for the sensor to be mounted away from the wire.

As has already been discussed, two sensors placed on the same side of the fast hole electrode is a configuration that should be explored in order to provide two acoustic emission signals to determine fast hole electrode length at low off-times. It is not expected this would create a problem in location determination as the distance between sensors would still be known, and a common datum for measuring the arrival time could still be used. In fact this leads to the idea of a setup that could prove beneficial to the wire EDM process. A third sensor could be added to the system as shown in Figure 5.1.

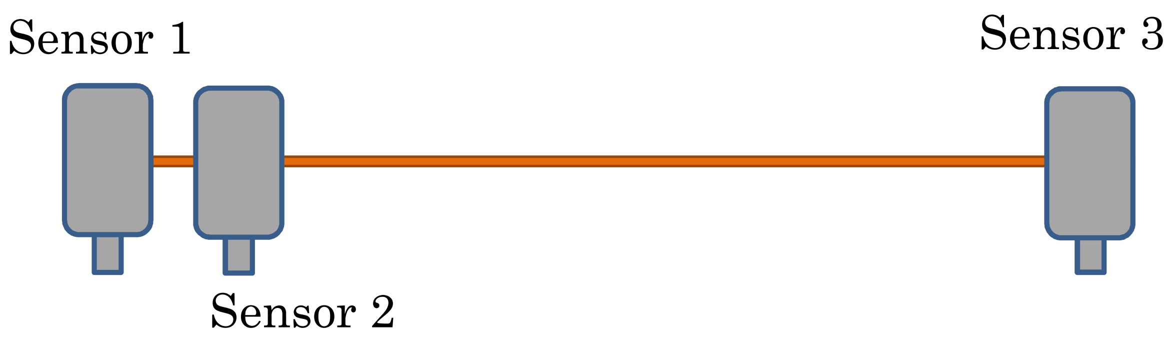

Figure 5.1: Proposed improved Wire EDM setup.

A setup of this nature would provide an extra time of arrival input in selection of “good” calculated locations. By requiring all three sensors to converge upon one value, it could help maintain good accuracy in real time.

Finally, one last area to consider is the use of three sensors on a plane to determine spark localization in a sink EDM process. By using at least 3 sensors enough information would be obtained to determine the discharge location on the plane. By mapping the discharge location in real time it would be possible to monitor the process for potential harmful discharges occurring in a localized spot. This spark localization affects the integrity of the workpiece surface and by utilizing real time monitoring there is potential for an adaptive flushing technique to be employed.

5.2.2 PSD Peak Characterization

Currently the method for determining the time of arrival only makes use of the strongest PSD peaks in order to obtain the best calculated locations. This means that a large amount of useful peaks and consequently calculated locations are ignored. Even though a large amount of data is available in only a short duration, it would be beneficial to develop methods for using as many PSD peaks as possible. Instead of focusing merely on the peaks of individual power spectral densities, it would be appropriate to investigate the characteristics of a single PSD peak as well as those around it. If a sequence of PSD peaks could be identified on both channels it could be used to determine a larger number of locations in a much shorter time. Determining these sequences automatically could prove difficult and may require the implementation of more elegant peak characterization methods.

Another possible area of investigation using power spectral densities would be to examine whether or not different discharge types have characteristic power spectral densities. If it was determined that a spark or arc type discharge could be identified from its power spectral density, it would improve the mapping of these harmful discharges. Since it has been discussed that these harmful discharges increase the likelihood of wire breakage, the ability to map a localization of harmful discharges would prove extremely beneficial.

5.2.3 General AE - EDM Development

This research has shown that acoustic emission sensors are a helpful tool in understanding electrical discharge machining. In the FFTs shown in Figure 4.45 characteristic frequencies were shown for three different workpiece heights. A better understanding of the correspondence between discharge and acoustic emission could prove useful in process optimization. Further research should focus on how electrical parameters affect acoustic emission signals. It should also focus on what other information acoustic emissions can provide us, whether it be machining stability or material removal rate.

References

[1] M. Kunieda, B. Lauwers, K.P. Rajurkar and B.M. Schumacher, "Advancing EDM through Fundamental Insight into the Process," *CIRP Annals – Manufacturing Technology*, vol. 54, pp. 64-87, 2005.

[2] M. Zahiruddin, M. Kunieda, "Comparison of energy and removal efficiencies between micro and macro EDM," *CIRP Annals – Manufacturing Technology*, vol. 61, pp. 187-190, 2012.

[3] Y.F. Luo, "An Evaluation of Spark Mobility in Electrical Discharge Machining," *IEEE Transactions on Plasma Science*, vol. 26, no. 3, pp. 1010-1016, 1998.

[4] A. Descoeudres, "Characterization of Electrical Discharge Machining Plasmas," *Ecole Polytechnique Federal de Lausanne, PhD Thesis No. 3542*, 2006.

[5] H. Kuroda et al., "Development of High Performance Coated Wire Electrodes for High-speed Cutting and Accurate Machining," *Hitachi Cable Review*, no. 22, pp. 51-56, 2003.

[6] C. Grosse, M Ohsu, *Acoustic Emission Testing: Basics for Research – Applications in Civil Engineering*, 1st ed, Berlin: Springer-Verlag, 2008.

[7] C.B. Seruby, "An introduction to acoustic emission," *Journal of Physics E: Scientific Instruments*, vol. 20, pp. 946-953, 1987.

[8] L. Braile, "Seismic Waves and the Slinky: A Guide for Teachers," *Purdue University*, http://web.ics.purdue.edu/~braile/edumod/slinky/slinky.htm, Retrieved 16/10/2012.

[9] NDT Resource Center, "Introduction to Ultrasonic Testing," www.ndt-ed.org/EducationResources/CommunityCollege/Ultrasonics/cc_ut_index.htm, Retrieved 16/10/2012.

[10] B. Muravin, "Acoustic Emission Wave Propagation and Source Location," *Acoustic Emission Presentations*, www.muravin.com, Retrieved 16/10/2012.

[11] M. Mahardika, K. Mitsui, Z. Taha, "Acoustic Emission signals in the micro-EDM of PCD," *Advanced Materials Research*, vol. 33-37, pp. 1181-1186, 2008.

[12] I. Takahashi, A. Ogata, H. Kanazawa, A. Hiruma, "Active EMI Filter for Switching Noise of High Frequency Inverters," *Proceedings of the Power Conversion Conference – Nagoka*, vol. 1, pp. 331-334, 1997.

[13] S.F. Yu, B.Y. Lee, W.S. Lin, "Waveform Monitoring of Electrical Discharge Machining by Wavelet Transform," *International Journal of Advanced Manufacturing Technology*, vol. 17, pp. 339-343, 2001.

[14] Y. Li, W. Zhao, X. Feng, H. Wei, "Research advancement on on-line detection of EDM spark locations," *Measurement*, vol. 22, pp. 29-35, 1997.

[15] M. Kunieda, H. Kojima, "On-Line Detection of EDM Spark Locations by Multiple Connection of Branched Electric Wires," *Annals of the CIRP*, vol. 39, pp. 171-174, 1990.

[16] D.R. Lide, R.C. Weast, *CRC Handbook of Chemistry and Physics*, 70th ed, CRC Press Inc: Boca Raton, Florida. 1989-1990.

[17] F. Han, P. Grangure, M. Kunieda, "Improvement in accuracy in potential method for detecting EDM spark locations," *Journal of Materials Processing Technology*, vol. 206, pp. 328-332, 2008.

[18] H. Qiang, H. Yongm Z. Wangsheng, "Research of two-dimension EDM spark locations detection using electromagnetic method," *Measurement*, vol. 31, pp. 117-122, 2002.

[19] X. Han, Q. Cao, "A Linear Hall Effect Displacement Sensor Using a Stationary Two-pair Coil System," *IEEE Instrumentation and Measurement Technology Conference,* pp. 1-4, 2011.

[20] Standex Meder Electronics, "Reed Sensors vs. Hall Effect Sensors," *Technical Papers*, www.meder.com/technical-documents4.html, Retrieved 2/8/2012.

[21] Infineon Technologies AG, "Current Sensing," *Linear Hall & Current Sensors*, www.infineon.com, Retrieved 2/8/2012.

[22] L. Ydreskog, A. Novak, "A Method for EDM Spark Location Detection," *Proc. Of ISEM-9*, pp. 297-300, 1989.

[23] K. Muto, Y. Shiota, S. Futamura, "Study on Observation of EDM Processing and Monitoring of Discharging Point with Acoustic Emission," *Proc. Of ISEM-9*, pp. 301-304, 1989.

[24] Y. Gao, M.J. Brennan, P.F. Joseph, J.M. Muggleton, O. Hunaidi, "On the selection of acoustic/vibration sensors for leak detection in plastic water pipes," *Journal of Sound and Vibration*, vol. 283, pp. 927-941, 2005.

[25] M. Ahadi, M.S. Bakhtiar, "Leak detection in water-filled plastic pipes through the application of tuned wavelet transforms to Acoustic Emission signals," *Applied Acoustics*, No. 71, pp. 634-639, 2010.

[26] J. Webster, I. Marinescu, R. Bennett, "Acoustic Emission for Process Control and Monitoring of Surface Integrity during Grinding," *Annals of the CIRP*, vol. 43, pp. 299-304, 1994.

[27] I. Inasaki, "Application of acoustic emission sensor for monitoring machining processes," *Ultrasonics*, vol. 36, pp. 273-281, 1998.

[28] D. Axinte, N. Gindy, "Tool condition monitoring in broaching," *Wear*, vol. 254, pp. 370-382, 2003.

[29] D. Axinte, D. Natarajan, N. Gindy, "An approach to use an array of three acoustic emission sensors to locate uneven events in machining – Part 1: Method and validation," *International Journal of Machine Tools & Manufacture*, vol. 45, pp. 1605-1613, 2005.

[30] Bharat Heavy Electricals Limited., *Transformers,* New York: McGraw-Hill, 2005.

[31] F. Connelly, *Transformers: their principles and design for light electrical engineers.* London: Pitman, 1950.

[32] A. Cichon, "The Application of the Selected Time-Frequency Descriptors Detection of the Acoustic Emission Signals Generated by Multisource Partial Discharges," *ACTA Physica Poloncia A*, vol. 116, pp. 290-293, 2009.

[33] E. Howells, E.T. Norton, "Location of Partial Discharge Sites in On-line Transformers," *IEEE Transactions on Power Apparatus and Systems*, vol. 100, pp. 158-162, 1981.

[34] P. M. Eleftherion, "Partial Discharge XXI: Acoustic Emission-Based PD Source Location in Transformers," *IEEE Electrical Insulation Magazine*, vol. 11, pp. 2-26, 1995.

[35] P. Kundu, N.K. Kishore, A.K. Sinha, "Frequency Domain Analysis of Acoustic Emission Signals for Classification of Partial Discharges," *Annual Report Conference on Electrical Insulation and Dielectric Phenomena*, pp. 146-149, 2007.

[36] GF AgieCharmilles, "Wire Cut EDM," www.gfac.com, Retrieved 2/8/2012.

[37] K.P. Rajurkar, W.M. Wang, J.A. McGeough, "WEDM Identification and Adaptive Control for Variable-Height Components," *Annals of the CIRP*, vol. 43, pp. 199-202, 1994.

[38] M.T. Yan, Y.S. Liao, C.C. Chang, "On-line Estimation of Workpiece Height by Using Neural Networks and Hierarchical Adaptive Control of WEDM," *International Journal of Advanced Manufacturing Technology*, vol. 18, pp 884-891, 2001.

[39] K.P. Rajurkar, W.M. Wang, W.S. Zhao, "WEDM-Adaptive Control with a Multiple Input Model for Identification of Workpiece Height," *Annals of the CIRP*, vol. 46, pp. 147-150, 1997.

[40] S. Kwon, M.Y. Yang, "The benefits of using instantaneous energy to monitor the transient state of the wire EDM process," *International Journal of Advanced Manufacturing Technology*, vol. 27, pp. 930-938, 2006.

[41] T. Itoh, "Wire EDM For Detecting Discharge Concentrations using Inductance," *US Patent 4559432*, 1985

[42] K. Inuoe, "Method of and apparatus for electrical-discharge machining with a traveling wire electrode," *US Patent 4052583*, 1977.

[43] Y. Jiang, W. Zhao, X. Xi and L. Gu, "Adaptive control for small-hole EDM process with wavelet transform detecting method," *Journal of Mechanical Science and Technology*, vol. 26, pp. 1885-1890, 2012.

[44] P. Koshy, M. Boroumand, Y. Ziada, "Breakout detection in fast hole electrical discharge machining," *International Journal of Machine Tools & Manufacture*, vol. 50, pp. 922-925, 2010.

[45] M. Richardson, Y Gianchandani, "Real-time wireless monitoring of workpiece material and debris characteristics in micro-electro-discharge machining," *IEEE 21st International Conference on Micro Electrical Systems*, pp. 379-382, 2008.

[46] C. Knapp, G. Carter, "The Generalized Correlation Method for Estimation of Time Delay," *IEEE Transactions on Acoustics, Speech, and Signal Processing*, vol. 24, pp. 320-327, 1976.

[47] MathWorks, "Cross-Correlation," *Matlab Signal Processing Toolbox*, www.mathworks.com/help/signal/ref/xcorr.html, Retrieved 16/10/2012.

[48] X. Song, C. Zhou, D. Hepburn, "An Algorithm for Identifying the Arrival Time of PD Pulses for PD Source Location," *2008 Annual Report Conference on Electrical Insulation Dielectric Phenomena*, pp. 379-382, 2008.

[49] P. Kundu, N.K. Kishore, A.K. Sinha, "Wavelet based Fractal Analyzing Method of Partial Discharge Acoustic Emission Signal," *Second International Conference on Industrial and Information Systems*, pp. 357-360, 2007.

[50] MathWorks, "Spectrogram using short-time Fourier transform," *Matlab Signal Processing Toolbox*, www.mathworks.com/help/signal/ref/spectrogram.html, Retrieved 16/10/2012.

[51] Kistler Instrument Corporation, Piezotron Sensor: Acoustic Emission Sensor, 2007.

[52] MathWorks, Scale to Frequency, *Matlab Wavelet Toolbox*, www.mathworks.com/help/wavelet/ref/scal2frq.html, Retrieved 16/10/2012.